

**Late Quaternary dynamics of an Arctic thermokarst landscape
indicated by deposits at Lake El'gene-Kyuele (Northern Siberia)**

Spätquartäre Dynamik einer arktischen Thermokarstlandschaft
an Hand von Ablagerungen am El'gene-Kyuele-See (Nordsibirien)

Masterarbeit

eingereicht am

Geographischen Institut der Universität Leipzig

Fakultät für Physik und Geowissenschaften

von

Philipp Schleusner

Matrikelnummer: 1062705

zur Begutachtung durch

Prof. Dr. habil. Christoph Zielhofer
Institut für Geographie, Universität Leipzig

apl. Prof. Dr. Bernhard Diekmann

Alfred-Wegener-Institut für Polar- und Meeresforschung, Forschungsstelle Potsdam



Leipzig, März 2013

Eidesstattliche Erklärung

Hiermit erkläre ich, dass ich die Masterarbeit selbstständig verfasst und keine anderen als die angegebenen Quellen und Hilfsmittel benutzt habe. Alle Stellen der Arbeit, die wörtlich oder sinngemäß aus Veröffentlichungen oder aus anderweitigen fremden Äußerungen entnommen wurden, sind als solche kenntlich gemacht. Ferner erkläre ich, dass die Arbeit noch nicht in einem anderen Studiengang als Prüfungsleistung verwendet wurde.

Ich bin einverstanden, dass die Arbeit nach positiver Begutachtung in der Universitätsbibliothek zur Verfügung steht.

Ort, Datum

Unterschrift

Table of contents

List of figures.....	iv
List of tables.....	v
Abbreviations.....	vi
Abstract.....	vii
Kurzfassung.....	viii
1 Introduction.....	1
1.1 Motivation and background.....	1
1.2 Reconstruction of Late Quaternary dynamics of North Siberian thermokarst landscapes – an overview.....	1
1.3 Research gaps and study objectives.....	2
2 Study area.....	4
2.1 Regional Setting.....	4
2.2 Environmental setting.....	5
2.2.1 Climate	5
2.2.2 Regional geology and relief.....	7
2.2.3 Soils.....	8
2.2.4 Vegetation.....	9
2.3 Periglacial environment.....	12
2.3.1 North Siberian permafrost	12
2.3.2 Ice Complex sediments.....	13
2.3.3 Thermokarst and lake formation.....	14
2.3.4 Ice-wedge polygons.....	16
2.4 The study site: Lake El'gene-Kyuele	16
3 Methods and material	20
3.1 GIS analysis and mapping.....	20
3.2 Field work	20
3.3 Laboratory analyses.....	21
3.3.1 Dating.....	22
3.3.2 Sedimentology.....	23
3.3.2.1 Freeze-drying and water content.....	23
3.3.2.2 Particle size analysis.....	23
3.3.2.3 Mineralogy.....	25
3.3.3 Biogeochemistry.....	25
3.3.3.1 Elemental analysis.....	25
3.3.3.2 Stable carbon isotopes.....	27
3.3.4 Plant macrofossil analysis.....	28
4 Results.....	30
4.1 Lithostratigraphy and geochronology.....	30
4.2 Sedimentology and mineralogy.....	32
4.3 Biogeochemistry.....	35
4.4 Plant macrofossils.....	36

5 Interpretation and discussion.....	43
5.1 Proxy interpretation and reconstruction of the past sedimentary processes.....	43
5.1.1 Allogenic clastic sediments.....	43
5.1.2 Authigenic clastic sediments.....	44
5.1.3 Biogenic input.....	45
5.1.4 The question of carbonate existence.....	49
5.1.5 Application of the radiocarbon ages.....	50
5.2 Vegetation reconstruction and palaeoenvironmental implications.....	51
5.3 Late Quaternary thermokarst basin evolution and relative lake level variability.....	59
6 Conclusions.....	67
References.....	69
Appendix.....	78
Determination of lake and river catchments using ArcGIS 10.1.....	79
Water content, grain-size, and mineralogy.....	80
CNS, TOC, and $\delta^{13}\text{C}$	81
Total plant macrofossil finds.....	82
Acknowledgements.....	85

List of figures

Fig. 1: Overview map of the study region.....	4
Fig. 2: Climographs of Tiksi and Dzhardzhan, Sakha Republic, Russia.....	6
Fig. 3: a) Circum-Arctic distribution of cryosols, b) microcracks in a grain due to cryogenic widening, c) exemplary cryosol.....	9
Fig. 4: Vegetation units of the study region.....	10
Fig. 5: a) Circumpolar distribution of permafrost in the northern hemisphere, b) permafrost depth in Yakutia/Russia.....	12
Fig. 6: a) Cyclic development of Yakutian alasses, b) exemplary aerial photograph of thermokarst lakes in the Lena Delta, c) aerial view of Lake El'gene-Kyuele.....	15
Fig. 7: Calculated watershed position of the river catchments of Lena and Olenyok, including the calculated catchment area of Lake El'gene-Kyuele.....	17

Fig. 8: a) Hydrochemical parameters of the surface waters of Lake El'gene-Kyuele, b) Interpolated bathymetric map of measured soundings.....	18
Fig. 9: Photographs of the study area.....	19
Fig. 10: Flow chart of the applied laboratory methods.....	21
Fig. 11: Selected objects for radiocarbon dating.....	22
Fig. 12: Depiction of the outcrop PG2038-1.....	30
Fig. 13: Results of water content, grain-size, and mineralogical laboratory analyses.....	32
Fig. 14: Grain size distribution of PG2038-1.....	33
Fig. 15: a) Box plot of the mean grain sizes of PG2038-1, b) lithological classes.....	34
Fig. 16: Results of the biogeochemical laboratory analyses.....	36
Fig. 17: Macrofossils indicative for taiga ecosystem.....	40
Fig. 18: Macrofossils indicative for Arctic and Subarctic wooden shrubs.....	41
Fig. 19: Plants indicative for moist or lacustrine environments.....	42
Fig. 20: Animal macrofossils.....	42
Fig. 21: Correlation of the TOC/N _{atomic} values with the $\delta^{13}\text{C}$ values of PG2038-1.....	46
Fig. 22: Distinction of lacustrine and terrigenous sediment input at PG2038-1.....	47
Fig. 23: Relocation procedures of plant remains into lakes in Arctic environments.....	52
Fig. 24: Late Quaternary occurrence of <i>Larix</i> and <i>Betula</i> trees in northern Eurasia.....	54
Fig. 25: Plant communities at Lake Elgene-Kyuele.....	57
Fig. 26: Panoramic view of the Ice Complex accumulation plain north of Lake El'gene-Kyuele.....	58
Fig. 27: Stages of Late Quaternary basin evolution, relative lake levels, and depositional environments at the eastern slope of Lake El'gene-Kyuele.....	61
Fig. 28: Aerial view of the eastern margin of the El'gene-Kyuele thermokarst basin.....	63
Fig. 29: Thermokarst depressions at the Lena-Olenyok watershed.....	65

List of tables

Tab. 1: Distinction of different particle sizes.....	24
Tab. 2: Results of the ^{14}C AMS dating.....	31
Tab. 3: Semiquantitative overview of the fossil material.....	37
Tab. 4: Overview of plant macrofossils and corresponding syntaxa.....	38
Tab. 5: Overview of sedimentological implications of the outcrop units of PG2038-1.....	49

Abbreviations

AD	anno domini
AMS	accelerator mass spectrometry
a.k.a.	also known as
a.s.l.	above the sea level
ASTER	advanced spaceborne thermal emission and reflection radiometer
AWI	Alfred Wegener Institute for Polar and Marine Research
BP	before present (before AD + 1950)
ca.	circa
cal.	calibrated
cf.	confer (compare)
CNS	carbon, nitrogen, sulfur
db	depth below the surface
DEM	digital elevation model
E	east
e.g.	exempli gratia (for instance)
et al.	et alii (and others)
etc.	et cetera (and more)
GIS	geographic information system
i.e.	id est (that is)
N	north
PDB	pee dee belemnite
sect.	section
s.l.	sensu lato (in the broad sense)
sp.	species
ssp.	subspecies
TI	total intensity
vol-%	volume percent
vs.	versus
wt-%	weight percent
XRD	X-ray diffraction
yr	year(s)

Abstract

Thermokarst lakes are a wide-spread feature of permafrost affected landscapes, of which highly dynamic geomorphological and environmental processes are closely connected with current and past climate variability. This study investigated Late Quaternary sedimentary dynamics, basin evolution, relative lake level variability, and environmental interrelations of the northern Siberian Lake El'gene-Kyuele (71°17'N, 125°34'E), which contains characteristics of an Arctic Ice Complex thaw-lake and of a Yakutian alas. The study area is characterized by an extreme continental Arctic climate, deep continuous permafrost, a topographically dissected terrain, and a current vegetation of arctic shrub tundra. For reconstruction of past thermokarst processes, the sediment archive PG2038-1 at the modern eastern shore was investigated by field observation, geochronology, sedimentology, biogeochemistry, and the analysis of plant macrofossils and was compared to preceding investigations of nearby archives. The results reveal two main sources for sediments in the lake basin: terrigenous diamicton provided by thermokarst slopes, and lacustrine detritus that has mainly settled in the deep lake basin. Lake El'gene-Kyuele and its adjacent thermokarst basin rapidly expanded during the Early Holocene/Holocene Thermal Maximum. This climatically warmer period was characterized by open woodlands composed of larch, birch trees, and shrubs, which were eventually affected by fire. The maximum lake depth, and the lowest limnic bioproductivity, at the modern eastern shore occurred as the longest period of about 7,000 yr throughout the progressively cooler Neoglaciation. Partial drainage and a westerly lake migration occurred ca. 1,000 cal. yr BP as a non-climate-driven thermokarst process.

Kurzfassung

Thermokarstseen sind eine weit verbreitete Oberflächenform in arktischen Permafrostlandschaften, deren hoch dynamischen geomorphologischen und landschaftlichen Prozesse eng an Klimavariabilität gekoppelt sind. Diese Arbeit untersucht die Sedimentdynamik, spätquartäre Beckengenese, relative Seespiegelschwankungen und Umwelt-Wechselwirkungen am nordsibirischen See El'gene-Kyuele (71°17'N, 125°34'E), welcher typische Merkmale eines arktischen Eiskomplex-Thermokarstsees und eines jakutischen Alasses enthält. Das Untersuchungsgebiet ist gekennzeichnet durch ein extrem kontinental-arktisches Klima, tiefen kontinuierlichen Permafrost, Strauchtundren-Vegetation und ein hügelig zerfurchtes Relief. Um vergangene Thermokarst-Prozesse zu rekonstruieren, wurde das Sedimentarchiv PG2038-1 am heutigen östlichen Seeufer mittels Feldbeobachtungen, Geochronologie, Sedimentologie, Biogeochemie und Pflanzenmakrorest-Analyse untersucht. An Hand dessen konnten zwei prinzipielle Quellen für Sedimenteintrag unterschieden und charakterisiert werden: terrigenes Diamikton, welches von Thermokarsthängen erodiert wurde und lakustrin-detritischer Sedimenteintrag im tieferen Seebecken. Der El'gene-Kyuele-See und dessen Thermokarstbecken expandierten schnell während des holozänen Klimaoptimums im Frühholozän. In dieser klimatisch wärmeren Phase herrschte lichter Taiga-Wald mit Lärchen, Baumbirken und Tundrensträuchern vor, welcher bisweilen von Bränden betroffen war. Ein längerer Zeitraum von ca. 7000 Jahren, welcher die klimatische Abkühlung des Neoglazials beinhaltet, war gekennzeichnet durch den Wasserhöchststand und die geringste limnische Bioproduktivität am gegenwärtigen Ostufer. Vor ca. 1000 cal. Jahren BP dränierte der See teilweise und migrierte westwärts in Folge von nicht klimatisch gesteuerter Thermokarstdynamik.

1 Introduction

1.1 Motivation and background

According to the phenomenon of Arctic amplification, climate variability and the consequent landscape dynamics are more intense than elsewhere in the northern hemisphere (Holland and Bitz, 2003; Serreze and Barry, 2011). In North Siberian lowlands, thermally induced permafrost degradation has widely caused thermokarst depressions, lakes, and thermal erosion (e.g. Grosse et al., 2006; Morgenstern, 2012; Romanovskii et al., 2000). Thermokarst lakes furthermore trigger positive feedbacks of climate warming by producing talik growth, by the higher thermal capacity of water, and by increasing microbial decomposition of stored organic carbon that increase greenhouse gas emissions to the atmosphere (Walter et al., 2006; Zimov et al., 2006). Therefore, thermokarst dynamics deserve special attention.

A large number of modern lakes in North Yakutia are of thermokarst origin. According to Morgenstern et al. (2008), the Lena Delta contains an amount of 58,700 lakes, which cover 12 % of the Delta area. However, lakes in elevated and dissected areas, such as the Lena Delta hinterland, are less frequent because lateral thermo-erosion predominates vertical permafrost down-wearing (Czudek and Demek, 1970). Besides the geomorphological processes, also environmental features, such as the vegetation composition, are closely connected with thermokarst activity due to their dependence on specific climatic and hydrological conditions (e.g. Kienast et al., 2008). A considerable part of present day thermokarst lakes are not a product of recent Arctic warming but developed at the Late Pleistocene - Early Holocene transition during a phase of global warming (Murton, 2001; Romanovskii et al., 2000). Thus, the reconstruction of the corresponding Late-Quaternary landscape dynamics can support a detailed understanding of the conditioning factors and the spatio-temporal features of thermokarst activity.

1.2 Reconstruction of Late Quaternary dynamics of North Siberian thermokarst landscapes – an overview

Hitherto, several studies provided a comprehensive understanding of thermokarst processes and landforms (Hopkins, 1949; Davies, 1969; Czudek and Demek, 1970;

Washburn, 1979; French, 2007; etc.). Moreover, miscellaneous investigative approaches were applied in order to obtain a detailed understanding of Arctic palaeoenvironmental dynamics as documented by Kaufman (2009) and Miller et al. (2010a). Bioindicators became suitable proxies for palaeoenvironmental reconstruction due to their sensitivity with respect to climate and environmental variability. For instance, the investigations of chironomids (Andreev et al., 2004), diatoms (e.g. Biskaborn et al., 2012), ostracods (e.g. Wetterich et al., 2008), and palynological data (e.g. Andreev et al., 2009; Werner et al., 2010) underlined several cold and warm stages during the Late Quaternary and their regional aspects. In addition, plant macrofossils served as useful proxies for reconstruction of local and regional landscape features and of the palaeoclimatic conditions, such as summer temperatures and continentality (e.g.: Kienast et al., 2001, 2005; Binney et al., 2009). Besides bioindicators, sedimentological and biogeochemical analyses were carried out for reconstruction of Late Quaternary landscape dynamics in Northern Siberia, as well (e.g.: Schirrmeister et al., 2003; Grosse et al., 2007; Schwamborn et al., 2012). Detailed sedimentological investigations of depositional structures and processes of thermokarst basins were carried out, e.g., in the Western Arctic by Murton (2001) and in Yakutia by Biskaborn et al. (in press), regarding the physical and geochemical parameters of lacustrine records. Lastly, the spatial distribution, shapes, and geomorphology of thermokarst structures were studied by means of remote sensing (Grosse et al., 2006; Morgenstern et al., 2008; Ulrich et al., 2009). In general, thermokarst studies in Siberia have focused on thaw lakes of the Arctic coastal lowlands (Romanovskii et al., 2000) and on large alas depressions in central Yakutia (Czudek and Demek, 1970).

1.3 Research gaps and study objectives

Despite the above mentioned studies of Arctic landscape dynamics, research gaps hinder a detailed understanding of thermokarst processes. From a geomorphological point of view, there exists merely a general idea of Holocene basin alterations and lake shoreline migration. To improve on that knowledge, the ubiquitous interrelation of geomorphological activity and the environmental background has to be considered. Thus, an essential contribution to knowledge about local environmental conditions can be provided by individual requirements of plant species.

North Siberia is interesting within the context of Late Quaternary thermokarst dynamics

because: It constitutes the transition zone of marine polar and extremely continental climate domains. It is characterized by different geological settings ranging from Precambrian to modern. Lastly, Northern Siberia is interesting for the environmental heterogeneity at the transition of taiga and tundra ecosystems. Varying landscape factors on a local scale underline the region's natural complexity and make thermokarst activity complicated to understand, as well.

Therefore, this study focuses on the Arctic thermokarst Lake El'gene-Kyuele in the Lena Delta hinterland with a complex environmental setting. The main objectives for this study are defined as follows:

- i. Reconstruction of sedimentary processes in the thermokarst lake basin
- ii. Reconstruction of Late Quaternary compositional variations in local vegetation and its implications on thermokarst processes and palaeoenvironmental conditions
- iii. Detection of Late Quaternary shoreline shifts and morphological alterations of the thermokarst basin

The study objectives are accomplished through an interdisciplinary approach. An outcrop at the eastern shore was investigated by methods of field observation, geochronology, sedimentology, biogeochemistry, and the investigation of plant macrofossils. In addition, the following questions arise: (a) Are shoreline sediments applicable for reconstruction of thermokarst variability? (b) How do thermokarst processes, sediment dynamics, and the vegetation composition interrelate? (c) Can the discovered environmental changes be ascribed to regional Late Quaternary climate variability?

2 Study area

2.1 Regional Setting

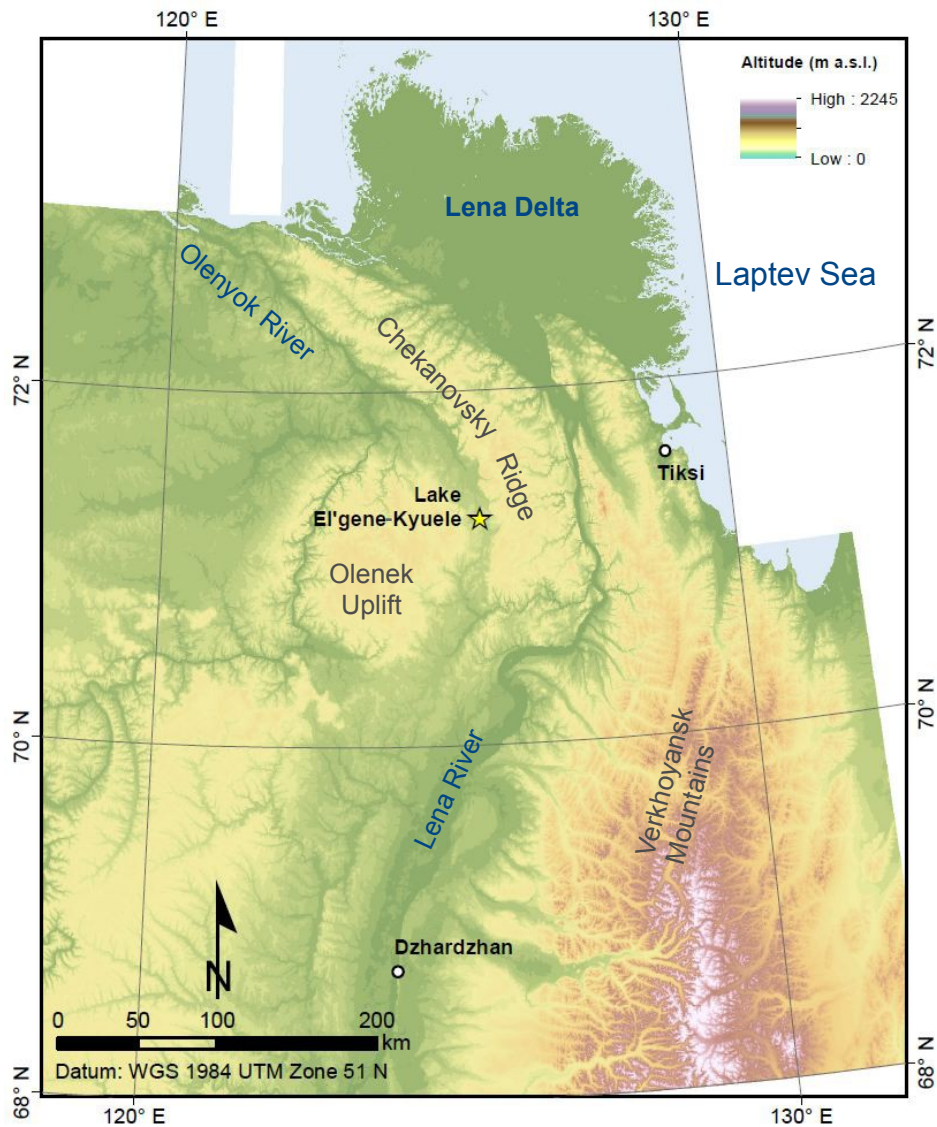


Fig. 1: Overview map of the study region; DEM data derived from Santoro and Strozzi (2012): Circumpolar digital elevation models (doi:10.1594/PANGAEA.779748, accessed: 24th January 2013), modified

The northern Siberian Lake El'gene-Kyuele (Эльгене-кюеле, a.k.a. 09-Tik-05 in former studies) and its surrounding thermokarst basin are located in the northern part of Yakutia (Sakha Republic, Russia) at 71°17'N and 125°34'E. The study area is located about 120 km east of the nearby Laptev Sea Coast settlement Tiksi and approximately 130 km south of

the Lena Delta (Fig. 1). North Siberia is very sparsely inhabited, save the few, remote, and mostly small settlements. Lake El'gene-Kyuele is located in the Arctic according to different definitions: e.g. climatically by being below the July isotherm of 10 °C or ecologically by being beyond the northern treeline (tundra vegetation) (UArctic Atlas, n.d.).

2.2 Environmental setting

2.2.1 Climate

Thermokarst processes are inherently linked to climate; thus, it is important to understand the regional climatic attributes. According to the Köppen climate classification, the Lena Delta region and its hinterland are located in the belt of tundra climate, as a part of the polar climates, which is characterized by a temperature between 0 and 10 °C in the warmest month of the year (FAO, 2012). The study area is also located at the edge to a continental boreal climate with extremely severe winters (Kottek et al., 2006).

Lake El'gene-Kyuele is located more than 500 km north of the Arctic circle. The sun does not rise from the middle of November until the end of January, while in summer midnight sun occurs from the middle of May until the end of July (NOAA, n.d.). Hence, two annual seasons prevail: winter and summer. The study area is furthermore characterized by its high continentality. The large distance to the Atlantic and the elevated terrain in Central Asia and Eastern Siberia prevent moderating oceanic air masses from reaching the region (Franz, 1973). In Siberia (except the far east), cyclonic activity generally declines in eastward direction, as do humidity and precipitation. In winter Siberia is affected by a large and consistent anticyclone that originally develops south of Lake Baikal and causes low humidity (Franz, 1973; Shahgedanova, 2003). Depressions formed by the Icelandic- or the Aleutian low reach the study area only occasionally (Mock et al., 1998; Shahgedanova, 2003). During summer, an area of low pressure forms over Siberia due to increasing insolation and rising warm air masses. With a decreasing air pressure gradient from the Atlantic eastward, maritime air masses can reach the study region more easily, causing increasing precipitation during the summer months (Franz, 1973). However, this effect is supposedly stronger in more continental southern parts of Siberia. The nearby Laptev Sea is covered by sea-ice from October until June (Shahgedanova, 2003). Therefore, its smoothing effect on severe winter temperatures is rather low. Nevertheless, winter temperatures are attenuated in coastal areas compared to farther southern regions with

increasing continentality. Similarly, open-water conditions on Arctic lakes are short, causing a strong attenuation of limnic bio-productivity.

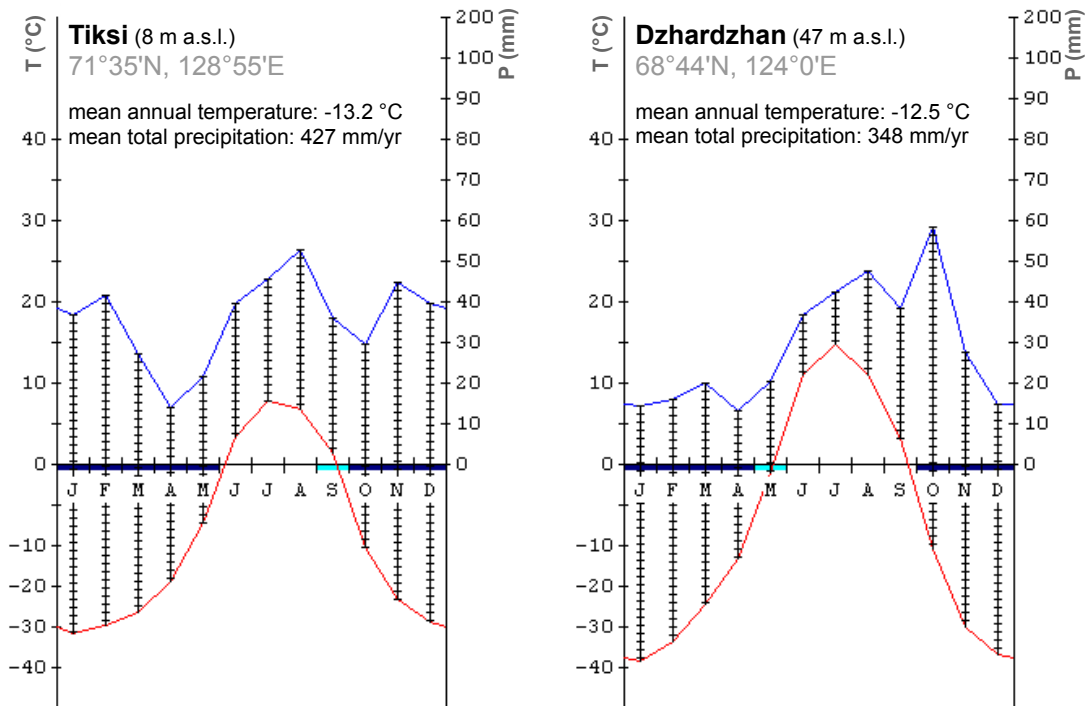


Fig. 2: Climographs of Tiksi and Dzhardzhan, Sakha Republic, Russia; diagrams derived from: <http://www.ucm.es/info/cif/> (accessed 20th August 2012), modified

Climate data is provided by the nearby weather station of the coastal settlement Tiksi (71°38'N, 128°52'E), and the more southern station of Dzhardzhan (68°45'N, 126°30'E) for the period from 1984 until 1994 (see Fig. 2, Rivas-Martínez, 1996). Long term climatic information is provided by the ROSHYDROMET (n.d.). The annual mean temperature of Tiksi is about -13.2 °C, whereas the average temperature varies from about 7.8 °C in July, to -31.9 °C in the coldest month of January. In general, the continentality increases in southward direction (Shahgedanova, 2003), causing a larger thermal variation in the southern station of Dzhardzhan. The annual temperature amplitude of the region is extreme, reaching up to 90 °C as its maximum (Shahgedanova, 2003). Negative temperatures predominate for about eight months of the year. The precipitation in the study region is low, averaging 319 mm annually. The annual monthly averages indicate a bimodal distribution with precipitation peaks during summer (June-September), and winter (December-February). Less precipitation is recorded from March until May, and from

October until November. In respect of the extremely low annual temperatures, the evapotranspiration is highly reduced, reaching an average of 273 mm/yr (Rivas-Martínez, 1996). Therefore, the regional climate is still humid despite the low annual precipitation. Snow possibly falls during a period of more than 260 days of the year and typically persists from the end of September until June (Shahgedanova, 2003). In spite of severe winter conditions, the snow cover at the Russian-German research station on the island of Samoylov, in the Lena Delta, is relatively thin, reaching thicknesses of less than half a meter in the last decade (Boike et al., 2008). However, strong winds may deflate snow at exposed sites and accumulate it in protected areas. In addition, wind data has been collected at the Samoylov station. According to Morgenstern (2005), wind patterns are seasonal: S-SW during winter, and N-NW during summer. The strongest winds in the Lena Delta are associated with winter storms, generating wind speeds up to 20 m/s (Morgenstern, 2005).

2.2.2 Regional geology and relief

Lake El'gene-Kyuele is located at the north-eastern margin of the Central Siberian Plateau that comprises a large region between the rivers Yenisei in the west, and Lena in the east. The basement of that complex originally formed the Siberian craton of Precambrian age, of which outcrops still appear e.g. as metamorphic rocks at the Anabar shield (Huh and Edmond, 1999). East of the Lena River, the Verkhoyansk mountains arise, reaching altitudes of about 2,000 m. The study area is located at the margin of the Chekanovsky Ridge that geologically consists of mesozoic sandstones (Franz, 1973; Markov, 1974) and is characterized by a hilly to smoothly mountainous relief with maximum elevations of about 500 m. The range extends in a NW-S-direction, marking the south-eastern boundary of the Lena Delta area (Fig. 1). To the north and west, the Arctic coastal plain is located adjacent to the Chekanovsky Ridge, whereas the Lena river valley cuts the south-eastern margin of the range. The Olenek Uplift, located west and south-west of the study area, contains Cambrian and Proterozoic formations (Knoll et al., 1995). According to the geological map of the USSR, the lake area and surroundings are underlain by Triassic and Jurassic bedrock (Markov, 1974). Furthermore, the study region is seismically active especially towards the Laptev Sea coastal area within the reaches of the submarine Gakkel Ridge (Drachev et al., 2003; Koronovsky, 2003). This forms the divergent tectonic plate boundary between the North American Plate and the Eurasian Plate, of which succeeding compressions may

produce earthquakes. Moreover, an active N-S oriented fault runs through the Lena Delta (Alekseev and Drouchits, 2004).

Quaternary sediments occur as fluvial deposits in the nearby river valleys (Franz, 1973), whereas Pleistocene loess-like accumulation plains a.k.a. Ice Complex formations (Fig. 9) cover large areas of the Arctic lowlands (Schirrmeister et al., 2011b).

2.2.3 Soils

Arctic Siberian soils are classified as cryosols according to the taxonomy of the World Reference Base for Soil Resources¹ (WRB) (FAO, 2006). Cryosols cover 13 % of the global land surface and are widely distributed in the Arctic, Subarctic, permafrost-affected Boreal, and also in parts of the Antarctic (Fig. 3a, USDA, 1999). They are formed in permafrost environments with an annual thawing of the uppermost horizon (active layer) during summer. Thus, cryosols only comprise an A and a C horizon of pedogenetically affected and non-affected material, respectively (Fig. 3c). The parent material does not necessarily affect cryosols, which may be glacial till, aeolian, alluvial, colluvial, and residual materials (FAO, 2006). In Cryosols, the permafrost table (a.k.a. gelic horizon) impedes drainage, causing water saturation, and thus anoxic and often redoximorphic conditions within the active layer/topsoil (Blume et al., 2009). Due to the generally low temperatures and large thermal variation, the mechanical effect of cryogenic weathering is immense (French, 2007). It occurs when ice forms in micro-cracks of the soil clasts (Fig. 3b). Repeated freeze–thaw cycles produce volume widening and consequent disintegration, resulting in silty particles between 10 and 50 μm in diameter (French, 2007; Schwamborn et al., 2006). In addition, chemical weathering also occurs in cryosols and can occur as carbonate dissolution or in-situ development of secondary clay minerals (Allen et al., 2001; Thorn et al., 2001). Additional important cryogenic soil features are cryoturbated (highly mixed) horizons, frost heave, thermal cracking, ice segregation, and a patterned ground microrelief (French, 2007). The activity of soil fauna is highly impeded, causing a low decomposition of organic matter and the formation of peat. In general, soils of the study region contain large carbon contents of 34-49.9 kg C/m² (Jones et al., 2010).

¹ a.k.a. gelisols according to the United States Department of Agriculture (USDA), or cryozems according to the Russian Federation (FAO, 2006)

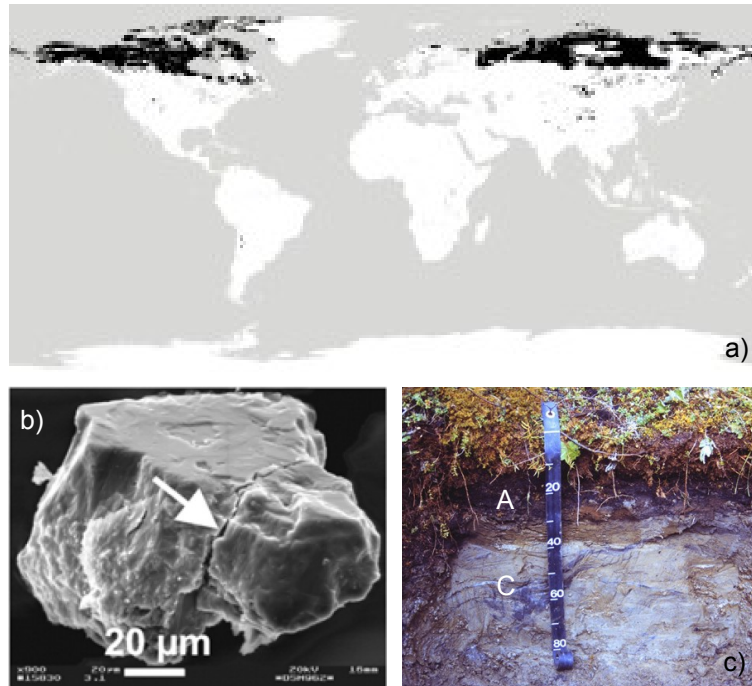


Fig. 3: a) Circum-Arctic distribution of cryosols according to the USDA (1999), b) microcracks in a grain (see arrow) due to cryogenic widening (Schwamborn et al., 2006), c) exemplary cryosol with an organic-rich cryoturbated active layer (A horizon) and permafrost table with bedrock material unaffected of pedogenesis (C horizon) (USDA, 1999)

Depending on local environmental factors, a distinct soil genesis occurs. According to the Soil Atlas of the Northern Circumpolar Region, the soil of the study area is described as a histic cryosol: a non-cryoturbated permafrost affected soil with a peaty topsoil (Jones et al., 2010). In rocky and mountainous areas of the study region, soil genesis is highly impeded (Zamotaev, 2003) due to the deficiency of fine grained parent material and organic matter, and increased geomorphological instability (e.g. by solifluction). Thus, turbic (cryoturbated) cryosols and poorly developed leptosols occur, often accompanied by outcropping rocks (Jones et al., 2010). Lastly, fluvisols predominate in the fluvial influenced regions such as river valleys and the Lena Delta, whereas west of the study area patches of acidic organic-carbon-rich podzols occur (Jones et al., 2010).

2.2.4 Vegetation

Arctic vegetation is forced to adapt to a short growing period and to harsh environmental conditions, i.e.: the severe climate, cryogenic geomorphology, and often an unfavourable water supply. Therefore, the Arctic is often characterized by a relatively low biodiversity

(Franz, 1973). The region Northern Siberia is almost unaffected by direct human activity or by recent fires (Sukhinin et al., 2004). Lake El'gene-Kyuele is located within the circumarctic tundra belt. This region is characterized by its extremely short annual plant growing period and a poor vertical structure. The reduced height of the vegetation provides a protection from the cold and harsh wind, taking advantage of the protective snow cover (Franz, 1973).

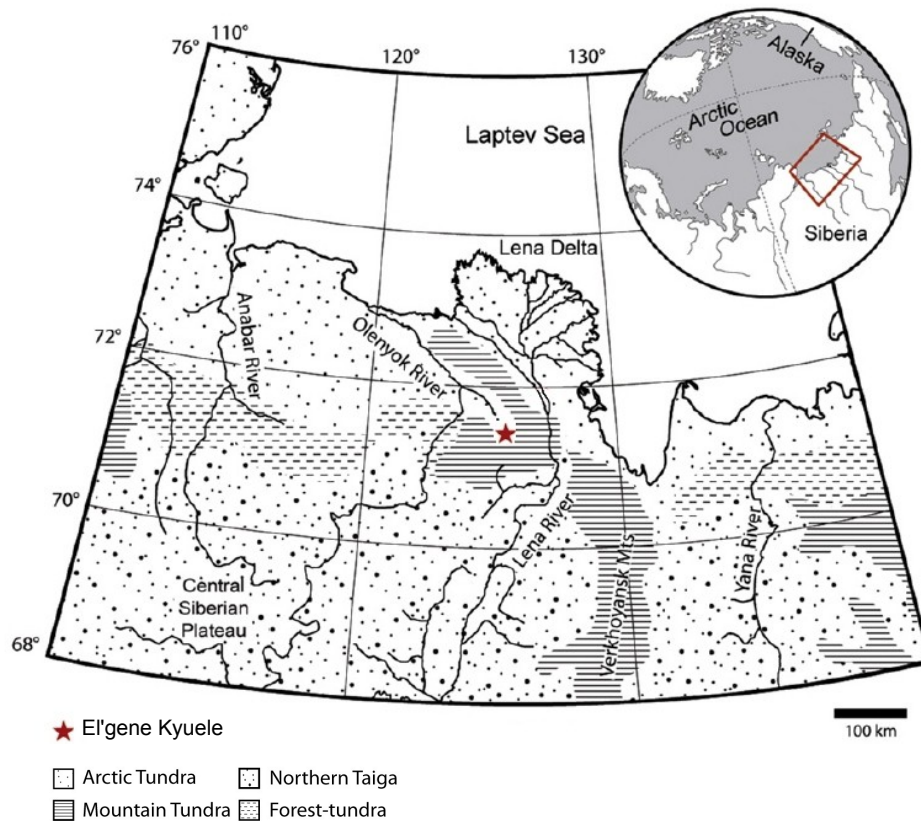


Fig. 4: Vegetation units of the study region according to Biskaborn et al. (2012a), modified

According to Wielgolaski and Goodall (1997), the tundra is generally characterized by a horizontally patterned vegetation structure, which is controlled by the following factors:

- permafrost and active cryogenic processes,
- high competition of different taxa at the same growth height due to impeded vertical layering, and
- biological adaptive peculiarities of the species to the extreme environment: (a) compact growth forming dense mats and cushions, and (b) slow growth.

The northern tree-line in Siberia is formed by larch, birch, spruce or pine trees (Binney et al., 2009). The study area is devoid of trees, although scarce *Larix gmelinii* trees occur 2 km to the north-northwest (Biskaborn et al., in press), and northern taiga environment (open *Larix* woodlands) appears approximately 50 km to the south nearby the river Eekit (Fig. 4, Tishkov, 2003). Shahgedanova and Kuznetsov (2003) categorized the study region as the transition from the southern tundra to the northern taiga subzones. However, the mountainous terrain provides somewhat harsher conditions for plants growth.

According to the Circumpolar Arctic Vegetation Map (CAVM), the study area is classified as a part of the erect dwarf-shrub tundra (category: *S1*) and low-shrub tundra (category: *S2*), which are characterized by a continuous plant cover (80-100 %) and basically consists of dwarf-shrubs (e.g. *Betula*, *Vaccinium*, *Salix*), mosses (e.g. *Hylocomium splendens*, *Anulacomnium turgidum*, *Dicranum*), and lichens (e.g. *Stereocaulon*, *Cladonia*, *Flavocetraria*) (CAVM Team, 2003). Due to the unfavourable climatic conditions of the Arctic, vertical plant growth is highly attenuated. Characteristically for tundra ecosystems, Poaceae and Cyperaceae appear abundantly in the study area (Biskaborn et al., in press). Furthermore, mainly *Betula nana*, *Alnus fruticosa*, and Ericaceae sp. appear as dwarf shrubby individuals. The vegetation composition of the study area is also azonal because it is affected by locally specific environmental characteristics, such as elevation, insolation, exposition, ground humidity, etc. Thus, in more elevated positions of the Chekanovski Ridge, the vegetation alternates to a graminoid, prostrate dwarf-shrub, forb tundra (category: *G2*) with a rather moderate plant cover of 40-80 % due to less favourable growing conditions (CAVM Team, 2003).

2.3 Periglacial environment

2.3.1 North Siberian permafrost

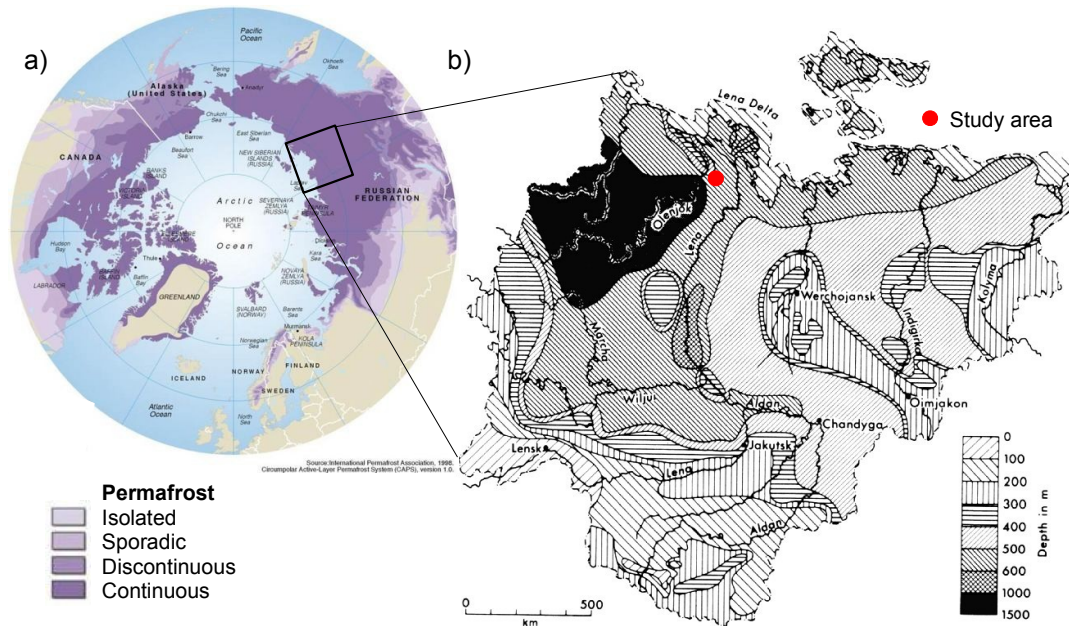


Fig. 5: a) Circumpolar distribution of permafrost in the northern hemisphere with Yakutia located within the black rectangle (UNEP/GRID-Arendal, 1998), b) permafrost depth in Yakutia/Russia (Czudek and Demek, 1973), modified

Permafrost is defined as subterranean ground (i.e. soil and/or rock) that remains at or below 0°C for at least two consecutive years (French, 2007). It underlies approximately 20 % of the world's land area and 23.9 % of the land area in the Northern Hemisphere (Zhang et al., 1999), with the largest extent in Siberia. With respect to water content, permafrost is categorized as dry in mountainous rocky areas and as ice-rich in northern Siberian lowlands (containing 50-80 % of water) (Weise, 1983). Regarding its spatial distribution, permafrost is subdivided into continuous (covering 90-100 % of the underground), discontinuous (50-90 %), sporadic (10-50 %) and isolated permafrost (0-10 %) (Fig. 5a). Beneath Lake El'gene-Kyuele, permafrost is continuous and reaches a thickness of about 500-600 m (Fig. 5b, Czudek and Demek, 1973). As its maximum, permafrost ground reaches a depth of more than 1 km in the Anabar region south-west of the study area. Apart from the climatic influences, the thickness and distribution of permafrost and of the active layer are also affected by local factors such as the vegetation, snow cover, ground humidity, etc.

The active layer is the subterranean layer above the permafrost table that thaws during summer and re-freezes in winter. In the study area, it extends to a depth of ~40 cm, as measured during fieldwork in August 2009 and September 2010 (Biskaborn et al., in press). Permanently unfrozen zones within and below the permafrost ground are denominated as taliks (French, 2007). They usually occur beneath water bodies such as rivers or lakes, which do not completely freeze in winter. Supra-permafrost taliks may occur between the permafrost table and the active layer, when the annual thawing of permafrost predominates the freezing (e.g. at relict permafrost) (French, 2007).

2.3.2 Ice Complex sediments

The above mentioned Ice Complex sediments, which form the large loess region of Western Beringia, are genetically different from the Pleistocene loess belt of the northern mid latitudes (Schirrmeister et al., 2011b). Recent studies have supported the concept of a nival lithogenesis of Ice Complex sediments during the Late Pleistocene (Kunitsky et al., 2002; Schirrmeister et al., 2011b). This concept is based on a perennial deposition of snow patches in topographically protected areas, which accumulate abundant plant detritus and fine-grained sediments of niveo-eolian origin (Kunitsky et al., 2002). These deposits were later transported downslope by melt-water run-off. Moreover, Schirrmeister et al. (2011b) argue that intense frost-weathering produced large amounts of silty to fine-sandy debris. Subsequently, different transport mechanisms distributed the fine-grained material over the Arctic lowlands and formed large accumulation plains (Schirrmeister et al., 2008, 2003). Except for the theory of nivation and frost-weathering, other hypotheses have been supported, as well, e.g. of eolian Ice Complex genesis (Brigham-Grette, 2001; Zimov et al., 2006).

Ice Complex sediments are reported to be commonly rich in organic carbon of 2-5 % (Zimov et al., 2006) and usually contain high ground-ice contents up to 65-90 vol-%, including the formation of large syngenetic ice wedges (Schirrmeister et al., 2011b). The corresponding outcroppings are often summarized by the term Yedoma, which nowadays occurs at riverbanks, the sea coast, and thermokarst slopes of Northern Siberia and Western Beringia (Fig. 9b, Zimov et al., 2006). These occur within the study area in particular in the surroundings of the Chekanovski ridge, which are covered by large Pleistocene accumulation plains of Ice Complex sediments (Kunitsky et al., 2002; Schirrmeister et al., 2003).

2.3.3 Thermokarst and lake formation

The following section provides only a general overview of thermokarst phenomena, while the thermokarst-related landscape dynamics of Lake El'gene-Kyuele will be discussed in detail in chapter 5. The term thermokarst is defined as the process and the characteristic landforms resulting from the thawing of ice-rich permafrost or massive ground-ice (Van Everdingen, 2005). Thermokarst lakes are formed by permafrost down-wearing: thermal disturbances induce descendent thawing of ice-rich permafrost ground and cause growth of active layer depth (Fig. 6a, Czudek and Demek, 1970). Consequently, these processes facilitate the formation of basin structures by terrain subsidence and the accumulation of melt-water (Fig. 6a). Accumulating water acts as a positive feedback to the process, i.e. further thawing, the formation of thermokarst lakes, and thus the growth of sub-lake talik (Washburn, 1979).

Until now, large areas of Pleistocene Ice Complex sediments have been affected by thermokarst and thermokarst-related processes; e.g. about 78 % of the surface of the nearby Lena-Anabar coastal lowland (Grosse et al., 2005). Lake formation is one of the most obvious landscape features in Arctic lowlands, facilitated by a flat terrain, humid and cold climatic conditions, and often a reduced subterranean drainage (Walker and Harris, 1976).

Thermokarst activity is connected with different geomorphological processes, depending on the topographic setting. While thermokarst lake formation prevails in a flat terrain, a more dissected relief commonly leads to permafrost back-wearing with the parallel retreat of steep walls and the formations of gullies (Czudek and Demek, 1970). A retrogressive slope failure, resulting from thawing ice-rich permafrost, is known as thaw slumping (Washburn, 1979). In addition, the so called thermal erosion has a combined effect of thawing ice and mechanical transport of sediments (Van Everdingen, 2005). Thermoerosional valleys occur frequently in the study area, as they carve deeply through the local Ice Complex accumulation plains. They are formed by the tributaries and outflows of the thermokarst lakes (Fig. 9a).

Thermokarst lakes are highly dynamic in the geomorphological sense (French, 2007). One main sedimentary process is erosion at the thermokarst slopes and the deposition of diamicton on the bottom of the lake basin (Murton, 2001; Romanovskii et al., 2000).

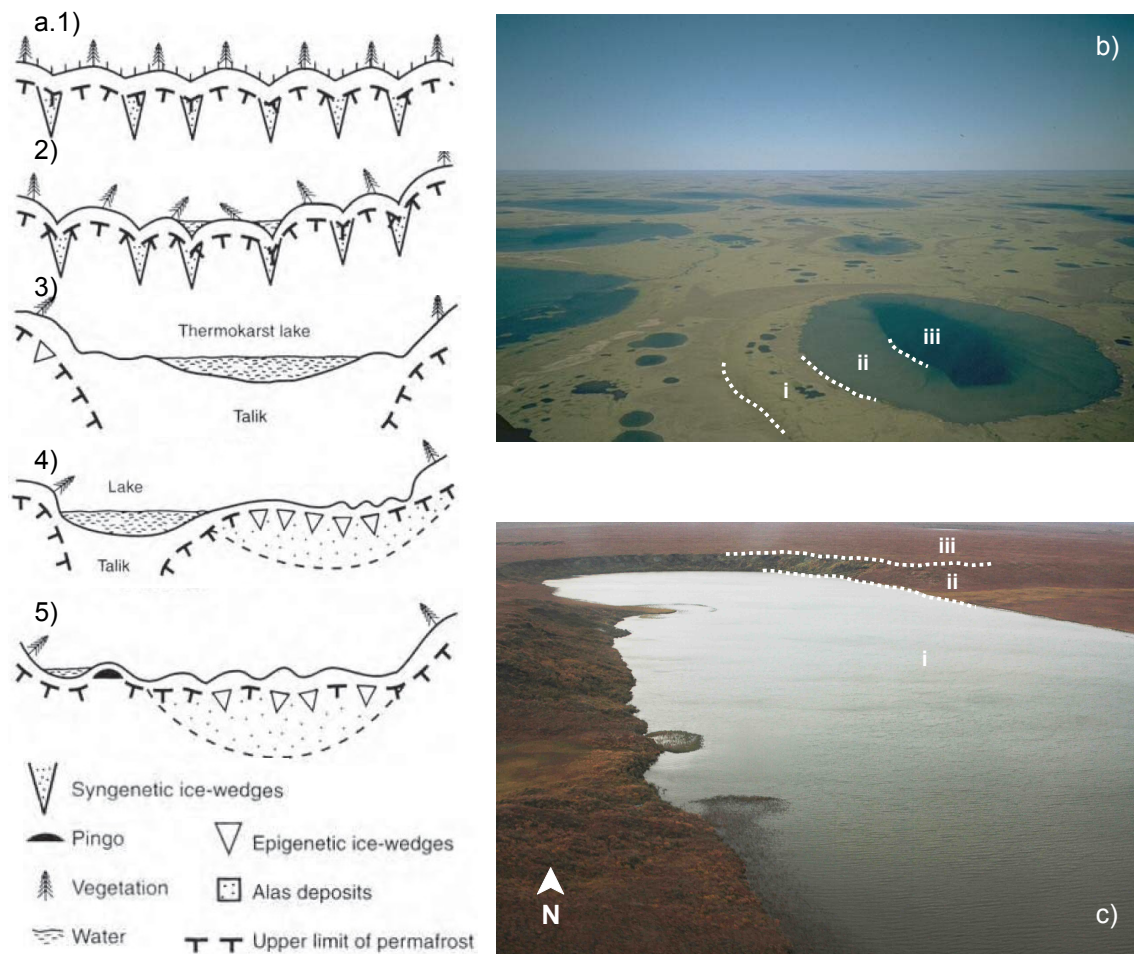


Fig. 6: a) Cyclic development of Yakutian alases: 1. Initial permafrost degradation in a lowland relief with the formation of thermokarst mounds by thawing ice-wedges, 2. Dujoda stage with the accumulation of melt-water, 3. Alas formation with lake and talik growth, 4. Lake drainage and migration, 5. Re-freezing of talik with the formation of epigenetic ice-wedges and pingos (Czudek and Demek, 1970; Soloviev, 1973, as reviewed by French, 2007), b) exemplary aerial photograph of thermokarst lakes in the Lena Delta, with the visual distinction of (i) the thermokarst basin, (ii) the shallow lake shelf and (iii) the central deep pool (Morgenstern, 2005; photo by G. Schwamborn; modified), c) aerial view of Lake El'gene-Kyuele, with the visual distinction of the (i) lake surface, (ii) the thermokarst depression and (iii) the surrounding ice-complex deposits (photo by B. Biskaborn, modified)

In the continental Siberian taiga environment, thermokarst and lake development differ from those of the Arctic coastal lowlands. A typical Yakutian thermokarst formation is known as alases, which is defined as a large depression that originates from the thawing of thick and exceedingly ice-rich permafrost (Van Everdingen, 2005). As indicated by Czudek and Demek (1970), most alases and thermokarst lakes do not reach a high age (Fig. 6a).

Because of slow and constant talik growth, old lakes tend to drain easily.

Thermokarst basins and lakes occur in distinct forms, while their margins are mostly smooth curved (Fig. 6b/c, Morgenstern et al., 2011). Depressions in the Lena Delta are situated less than 10 m below the surrounding uplands (Lantuit et al., 2007), whereas the corresponding lakes are mostly shallow (Hopkins, 1949). Regarding its vertical layering, the lakes often include a central deep pool, which is responsible for talik formation, and a shallow shelf area that completely freezes in winter, underlain by permafrost ground (Fig. 6b, Burn, 2005).

2.3.4 Ice-wedge polygons

The study region Northern Siberia is widely covered by ice-wedges (Weise, 1983). They develop by repeated thermal contraction and formation of cracks in ice-rich permafrost, into which melting snow penetrates during summer and then re-freezes (Mackay, 1974; Washburn, 1979). On the surface, ice-wedges develop a polygon structure. High-centred polygons develop by the thawing of the ice-wedges and occur in well-drained uplands north-west of Lake El'gene-Kyuele (Biskaborn et al., in press). Low-centred polygons develop where ramparts alongside the ice-wedges jut out, occurring in the poorly drained lowlands of the study area (Biskaborn et al., in press). In addition, this study revealed that ice-wedge polygons occur orthogonally shaped and parallel oriented to the longitudinal axis of the lake.

Ice-wedges are often interrelated to thermokarst processes, as their thawing provides melt-water accumulation and alas genesis (Czudek and Demek, 1970). Thermokarst-mounds (a.k.a baydzherakh) are hummocky landforms, which remain from high-centred ice-wedge polygons after the thawing of its surrounding ice-wedges (French, 2007). The thawed ice-wedges form troughs, which separate the grouped and similarly shaped thermokarst-mounds from each other. They occur at the northern shoreline of Lake El'gene-Kyuele and reach significant altitudes due to the lateral melt-water run-off at the inclined thermokarst slope (Fig. 9e).

2.4 The study site: Lake El'gene-Kyuele

Lake El'gene-Kyuele is situated at an altitude of approximately 150 m a.s.l. and directly south of the watershed of the rivers Lena and Olenyok (Fig. 7). It is oriented

approximately NW-SE. The shorelines of the oblong lake are relatively straight to the NE and somewhat arched to the SW. The lake is ca. 2.95 km long and < 1 km wide (0.34 km in the north and 0.6 km in the south). As a characteristic of most thermokarst lakes, El'gene-Kyuele is relatively shallow, reaching an approximate depth of 4-5 m in its centre and a maximum depth of 10.5 m at the northern edge (Fig. 8b). According to Biskaborn (2012b), thermokarst sediments on the lake bottom are > 4 m thick. Steep cliffs in Ice Complex sediments characterize the northern and north-western shoreline, whereas the terrain is flat to the south. The eastern shore is bordered by palaeo-lake sediments, which crop out up to several metres. These are dealt with in-depth in the description of the outcrop PG2038-1. A palaeo-shoreline is located at a certain distance east of the current shoreline (Biskaborn et al., in press).

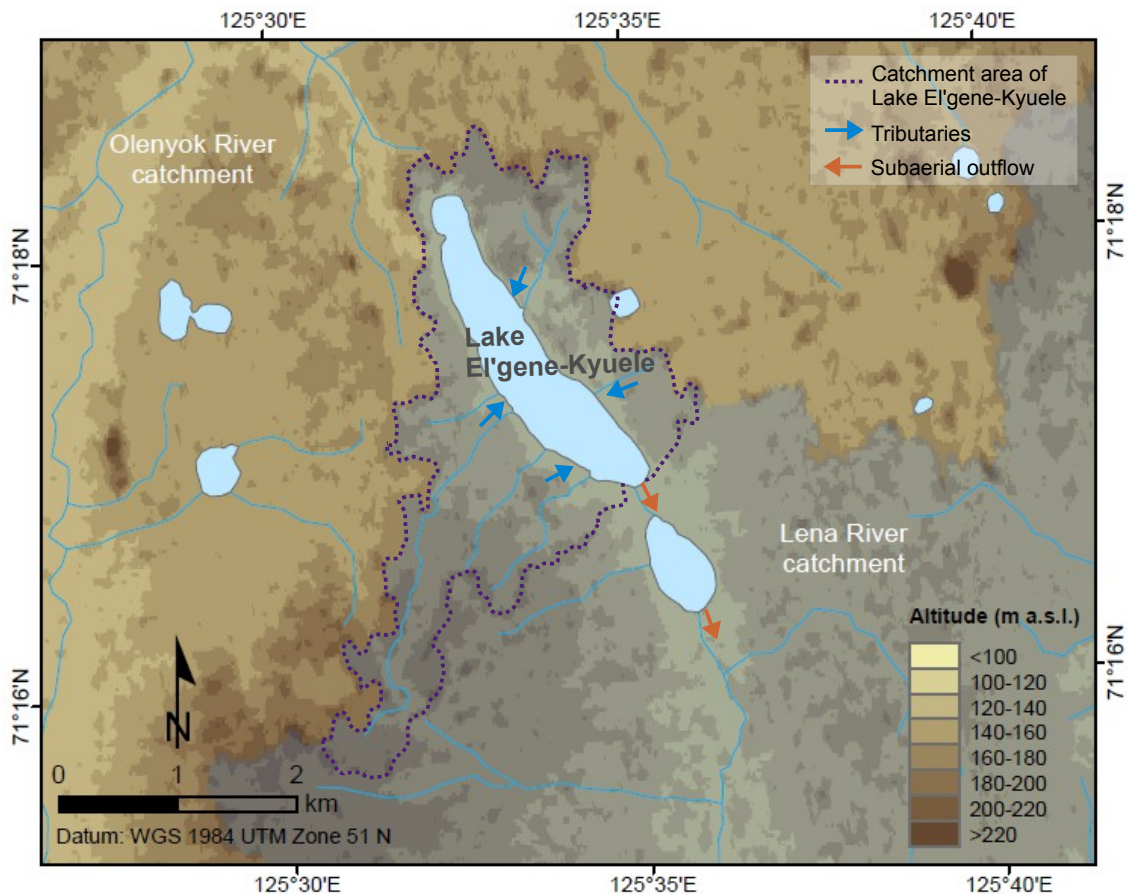


Fig. 7: Calculated watershed position of river catchments of the Lena (marked dark) and the Olenyok, including the calculated catchment area of Lake El'gene-Kyuele and its main subaerial outflow and tributaries; based on ASTER DEM data (available at: <http://earthexplorer.usgs.gov/>, accessed at 10th November 2012)

As a characteristic of thermokarst lakes, the catchment area of Lake El'gene-Kyuele has a rather small extension (Fig. 7). It comprises the thermokarst depression and a few minor tributaries, which mostly come from south-western direction. The watershed position of the lake catchment also reduces lateral water inflow. Moreover, the lake has one subaerial outlet, which runs off in south-eastern direction and thus is a tributary of the Lena river. The surface water of Lake El'gene-Kyuele is circumneutral by reaching a pH of 7 (Fig. 8a). Electrical conductivity is relatively low $\sim 67 \mu\text{S}/\text{cm}$, while the concentrations of the nutrients PO_4^{3-} and NO_3^- reach values below 0.10 and 0.15 mg/l, respectively. Combined with a high secchi-depth of 2.5 m, the latter values indicate a oligotrophic to mesotrophic state of the lake. All hydrochemical parameters were determined during summer conditions.

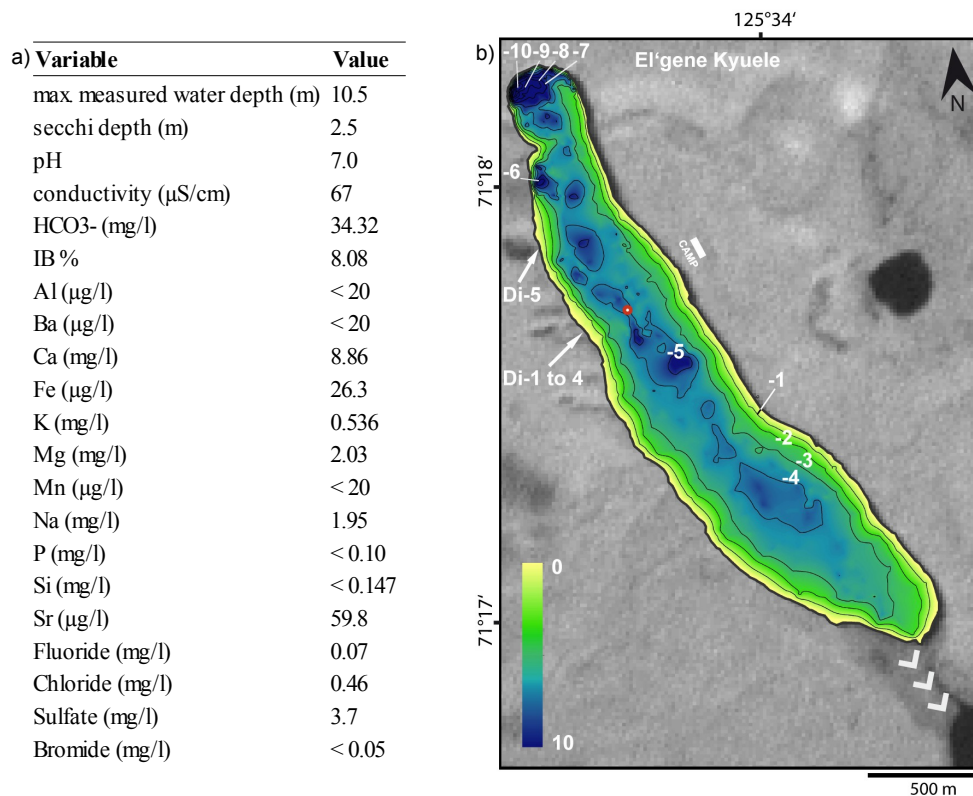


Fig. 8: a) Hydrochemical parameters of the surface waters of Lake El'gene-Kyuele (Biskaborn et al., in press), b) Interpolated bathymetric map of measured soundings of Lake El'gene-Kyuele, using a natural neighbour algorithm (Biskaborn et al., in press)



Fig. 9: Photographs of the study area: a) tributary of Lake El'gene-Kyuele flowing towards the western shoreline and creating a thermoerosional valley (photo by B. Diekmann), b) outcropping Ice Complex sediments/Yedoma (upper greyish sediments) at the Lena Delta (Morgenstern et al., 2011), c) retrogressive thaw slumps at the western slope of the thermokarst basin of Lake El'gene-Kyuele with sediment flow directed towards the lake (photo by B. Diekmann), d) ponding, as an initial thermokarst process, between high-centered ice-wedge polygons on Ice Complex sediments north of Lake El'gene-Kyuele (photo by B. Diekmann), e) Lake-view of El'gene-Kyuele with thermokarst mounds/baydzherakhs in the foreground (photo by B. Diekmann)

3 Methods and material

This chapter presents the multidisciplinary scientific approach, applied to accomplish the study objectives. The methodology is based on field work and on laboratory analyses, including statistical analyses and graphical visualization.

3.1 GIS analysis and mapping

Freely available data was used and processed using the ArcGIS 10.1 software for maps used in this study. The ASTER digital elevation model (DEM), provided by United States Geological Survey (USGS, 2012), was used in order to determine lake and river catchment areas in Fig. 7 by applying different hydrological raster algorithms (see appendix). The ASTER DEM provides a spatial resolution of 30 * 30 m, which may be insufficient for an exact depiction of small thermokarst catchments. However, the isohypses of the topographical map of Yakutia show a similar spatial distribution. Lakes, rivers, and creeks were manually digitized upon a GeoFUSE (2012) image. In Fig. 29, thermokarst basins were manually digitized along their upper margin slopes following Morgenstern et al. (2011). Thermokarst basins were visually clearly distinguishable from the surrounding Ice Complex uplands. The flow directions and Lena-Olenyok-watershed of Fig. 29 were derived from the watershed proceedings at Fig. 7. The bathymetric map (Fig. 8b) was created by Biskaborn et al. (in press) using a natural neighbour interpolation in ArcGIS. Lastly, this study utilizes a Landsat 7 ETM+ panchromatic image from the 5th August 2000 (Fig. 12, USGS, 2012) and a circumpolar DEM with a 100 * 100 m spatial resolution (Fig. 1, Santoro and Strozzi, 2012).

3.2 Field work

Lake El'gene-Kyuele was first investigated by the AWI during a helicopter expedition in summer of 2009 (Herzschuh et al., 2009). In September of the following year, the German-Russian expedition "Lena 2010" carried out more comprehensive sedimentological and geochemical studies (Biskaborn et al., in press). The modern geomorphological and hydrological state of the thermokarst basin of Lake El'gene-Kyuele was investigated by Biskaborn et al. (in press). Lake water was hydrochemically analysed for

pH, conductivity, oxygen values, anions, and cations. Furthermore, the lake bathymetry was measured by echo soundings at a high spatial resolution of 1,770 bathymetric data points. Into the lake bottom sediments, several sediment cores were drilled (Biskaborn et al., in press). The outcrop PG2038-1, which is situated immediately at the eastern lake shore, was excavated, photographed, and described by notable features. The individual samples, which include a depth of 5 cm of sediment material, were taken one below the other. At a total outcrop length of 350 cm, 70 samples were obtained. The entire sample material was packed into labelled plastic bags and sent to the AWI research unit Potsdam (Telegrafenberg A45, 14473 Potsdam, Germany).

3.3 Laboratory analyses

Most laboratory analyses and all sample preparation steps took place at the AWI in Potsdam. The sample material was stored in a dark cooling room at 4 °C. At PG2038-1 every second sample was selected for laboratory analysis in order to keep equidistance and representativeness. Hence, a total of 35 samples was examined. The lab analytical steps applied at PG2038-1, are depicted by the flow chart below (Fig. 10):

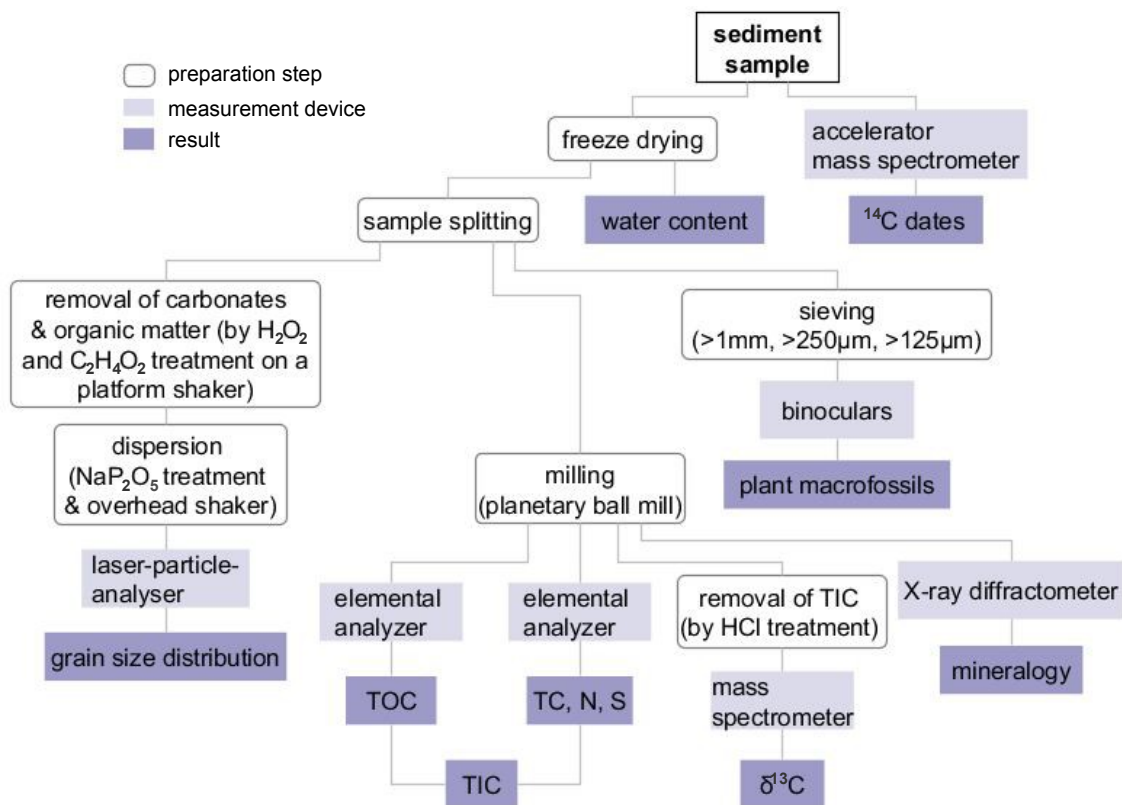


Fig. 10: Flow chart of the applied laboratory methods

3.3.1 Dating

Radiocarbon dating was carried out for age determination of selected fossil material. The method utilises the radioactive β^- decay of the unstable carbon isotope ^{14}C to ^{14}N in dead organisms (Bronk Ramsey, 2008). Radiocarbon, which contains a relatively short half-life (a.k.a. Cambridge half-life) of ca. 5,730 yr (Godwin, 1962), covers a maximum detection range of ca. 50,000 yr (Balter, 2006; Guilderson et al., 2005). In practice, neither the rate of $^{14}\text{CO}_2$ production in the upper earth atmosphere nor its distribution among the atmosphere, terrestrial biosphere, and oceans are permanently the same (e.g. Stuiver and Quay, 1981; Guilderson et al., 2005). Therefore, the radiocarbon age determination requires a conversion (calibration) of radiocarbon dates into calendar ages. The calibration can be based on data from marine carbonates such as corals (Reimer et al., 2011), dendrochronology (annual growth of tree rings), lake sediments, ice cores, etc. (Balter, 2006).

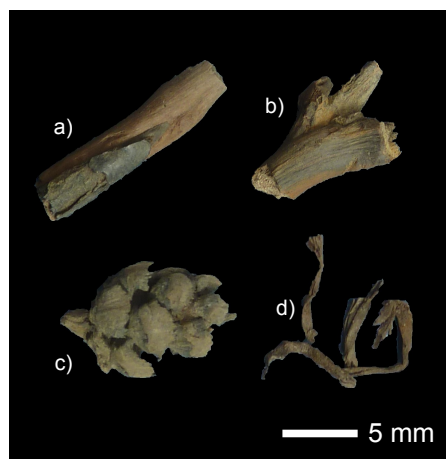


Fig. 11: Selected objects for radiocarbon dating: (a) wood remain (115-120 cm dbs), (b) wood remain (185-190 cm dbs), (c) *Larix gmelinii* cone (295-300 cm dbs), (d) peat remains (330 cm dbs)

The age determination of several objects of the outcrop PG2038-1 was carried out by AMS radiocarbon dating. As suitable samples for dating, mostly remains of wooden plants were selected as far as they could be found (Fig. 11). An amount of five different radiocarbon samples were selected at certain distances, whereas an equidistant dating could not be managed. Two wood remains at a depth of 115-120 cm and 185-190 cm were utilized. At the depth of 295-300 cm a well conserved cone of *Larix gmelinii* was found, of which three scales were utilized. In the bottom section, peat remains at a depth of 330 cm

were taken to date the basis of the outcrop. At the transition from unit V to unit VI bark remains at a depth of 25-30 cm were selected for dating. The objects were freeze-dried, freed carefully from impurities by a brush, and photographed with a Panasonic Lumix DCM-TZ8. For AMS radiocarbon dating, the samples were sent to the Poznan Radiocarbon Laboratory in Poland (ul. Rubież 46, 61-612 Poznan, Poland). There the samples were freed from carbonate and from the alkali-soluble organic fraction in order to measure the humin fraction. At the uppermost sample at 25-30 cm, the bulk organic fraction was measured additionally, which includes humins and humic acids. The determined ^{14}C AMS years were converted into calendar ages using the CalPal online calibration tool (available at: <http://www.calpal-online.de/>, Danzeglocke et al., 2012). CalPal uses the CalPal-2007-Hulu calibration curve, which is based on the U/Th-dated speleothem records of the Chinese Hulu Cave (Weninger and Jöris, 2008). The calibrated dates are expressed as years before present (yr BP = years before AD+1950). The so attained calendar dates are used exclusively throughout this study.

3.3.2 Sedimentology

3.3.2.1 Freeze-drying and water content

Wet samples were freeze-dried (using a ZIRBUS technology Sublimator 3-4-5), because the sublimation procedure is gentle toward the material. The water content percentage was assessed gravimetrically by applying the following equation:

$$\text{Water content (\%)} = ((W_{\text{wet sample}} - W_{\text{dry sample}}) / W_{\text{wet sample}}) * 100$$

The water content is expressed by the weight difference of the wet and the dry sample weights, divided by the wet sample weight, and multiplied by 100. Subsequently, the samples were manually homogenized and split into two equal parts for particle size analysis and for biogeochemical and mineralogical analyses (Fig. 10).

3.3.2.2 Particle size analysis

Particle size analysis is essential in sedimentological research, as it reveals important information about transport processes (the depositional environment), accumulation circumstances, etc. of clastic sediments. Particles are subdivided into the following classes, depending on their diameter:

Tab. 1: Distinction of different particle sizes (Last, 2002a)

Size	Clay	Silt			Sand			Gravel	...
		fine	middle	coarse	fine	middle	coarse		
metric (μm)	< 2	< 6.3	< 20	< 63	< 200	< 630	< 2000	> 2000	...
Φ -grade	9	7	6	4	2	1	-1	≤ -3	

In order to obtain completely dispersed particles and thus sample material in a measurable state, a time-consuming preparation is inevitable (Fig. 10). Especially the fine-grained fractions tend to adhere to organic matter and carbonates (Blume et al., 2009), leading to a significant quantitative underestimation. Despite not having detected carbonates in preceding investigations of nearby archives (Biskaborn et al., in press), a quantity of 100 ml of 10% acetic acid ($\text{C}_2\text{H}_4\text{O}_2$) was added to the sample material for 24 hours in order to prevent the possibility of any existing inorganic carbon. In order to destroy the organic compounds, the particles underwent a hydrogen peroxide (H_2O_2) treatment (10 ml of 35% H_2O_2 solution) on a platform shaker for 3 times a week and a maximum duration of 5 weeks. From time to time a drop of concentrated ammonia (NH_3) was added to neutralize the acidic property of H_2O_2 , because optimal oxidation kinetics could be achieved within a neutral pH-value. By subsequent washing, centrifuging (using a ThermoScientific Heraeus Cryofuge 8500i and a Heraeus Multifuge 3s) and the succeeding decantation, the particles got separated from the containing liquid chemicals. By the addition of ammonia solution and tetrasodium pyrophosphate ($\text{Na}_4\text{P}_2\text{O}_7 \cdot 10 \text{H}_2\text{O} + \text{NH}_3$) as well as an overnight placement on an overhead shaker, an efficient dispersion and homogenization of the sample material was achieved. For the measurement, the sample was split into 8 equal sub-samples, of which at least 2 and partly up to 5 sub-samples were measured by laser diffraction, depending on their (non-)homogeneity. Lastly, the average values were calculated out of the different sub-samples. Particle sizes coarser than 1,000 μm could not be detected by laser diffractometry and had to be sieved and weighed manually.

The particle size distribution was determined using a Beckmann Coulter LS 200 laser particle analyzer. Particle size measurement is based on the intensity of the radially symmetrical laser diffraction as it passes through the liquid sample mixture (Beuselinck et al., 1998). Thus, smaller particles tend to produce a greater laser diffraction than coarse particles. The diffracted beams can get recorded by photomultipliers and converted into a quantitative grain size distribution by applying the theory of Fraunhofer diffraction (Beuselinck et al., 1998; Lee Black et al., 1996).

3.3.2.3 Mineralogy

Minerals, the inorganic fraction of sediments or rocks, often dominate the sediments of soils, lakes, and their surroundings. The mineralogical composition may serve as a useful palaeoenvironmental proxy, by providing information about the sediment provenance and transport mechanisms (Last, 2002b).

For the determination of the mineral contents, the samples were prepared by freeze-drying and grinding, as explained below in section 3.3.3.1. Reference standards were not necessary for the sample material, because quartz minerals commonly show an obvious peak for calibration. The mineralogical composition of the sediment material was detected by X-ray diffractometry (XRD) at the head location of the AWI in Bremerhaven, using a Panalytic Empyrean X-ray diffractometer. XRD applies the property that the wavelength of X-radiation (from 10 to 0.01 nm) has a similar dimension like the spacings of planes (rows of atoms) in minerals, which provides the diffraction (scattering) of the beam as multiple reflections. The reflection directions depend on the mineral-specific distance between the atoms and the peak intensities depend on the constructive (or deconstructive) interference of the radiation according to the Bragg's law (Last, 2002b). The mineral peak area intensities were determined graphically and calculated with the Apple MacIntosh based software *Macdiff* (Petschick, 2012). The mineral determination is semi-quantitative by the ratio calculation of individual peak intensities against each other or against the sum of total peak area intensities (mineral intensity vs. TI) following Vogt (2009).

3.3.3 Biogeochemistry

3.3.3.1 Elemental analysis

The sediment organic matter provides useful information about the original organic material, i.e. type, amount, state of conservation or decomposition, depositional environment, etc. (Meyers and Teranes, 2002). A basic parameter in sedimentological research is the content of total organic carbon (TOC), by determining the quantity of organic matter in sediments. The calculation of the TOC/N-ratio allows far-reaching palaeo-ecological implications by the distinction of aquatic and terrestrial sources of organic matter (Meyers, 1994). In addition, the TOC/N ratio of terrigenous sediments is used as an indicator for succeeding humification and mineralization, because microbial activity mostly fixes nitrogen, whereas carbon gets oxidized (Bengtsson et al., 2003;

Janssen, 1996). Lastly, the C/N ratio is a useful value in pedology, because it mirrors the availability of nitrogen, an essential element for plant growth, and thus reflects the fertility of soil (Blume et al., 2009).

For biogeochemical measurements the samples were first ground (Fig. 10) and thus homogenized by a planetary ball mill (FRITSCH pulverisette) with agate containers and balls. For organic rich samples such as peat, special sintered corundum containers and balls were used. For measurement of carbon, nitrogen, and sulphur (CNS), the sample material was weighed between 8-8.5 mg and folded into special zinc boxes together with a spatula tip of tungsten(VI)oxide (WO_3) as a catalyst. The measurement of all three elements was carried out simultaneously by an elemental analyzer (Elementar Vario EL), which incinerates the samples at approximately 1,000 °C in an oxygen enriched atmosphere of helium as a carrier gas (Handbook elementar vario el III, 2001; Verardo et al., 1990). The products of the oxidation were reduced to N_2 , CO_2 and SO_2 by a copper reduction reactor, separated by gas chromatography and measured quantitatively by thermal conductivity detection (Handbook elementar vario el III, 2001). In the first place, three blank measurements were carried out for elemental background determination. Different standards with known elemental composition were used for the calibration of the device. In between and after the measurement certain control standards were utilized to check the measurement accuracy. Each sample was measured twice, of which the average values were calculated. One sample (295-300 cm dbs) had to be measured a second time, due to diverging results above average.

The total organic carbon (TOC) values were measured thereafter by a Vario MAX C analyzer with similar measurement principles. However, nitrogen is used as a carrier gas and the samples are burnt at a lower temperature, in order to detect only CO_2 from organic sources (Handbook elementar vario max C, 2012). For calibration two different standards were used for samples with few and high carbon contents. Similar to the CNS determination, each TOC measurement was carried out twice and control standards were applied in between and after the measurements. The total inorganic carbon (TIC) was calculated by subtraction of the organic carbon from total carbon:

$$\text{TIC} = \text{TC} - \text{TOC}$$

The percentages of carbonate can be calculated out of the TIC values, by multiplication by the factor 8.33. The factor is based on the division of the relative molecular mass of CaCO_3 ($M_r = {}^{40}\text{Ca} + {}^{12}\text{C} + 16(^{\ast 3})\text{O}_3 = 100$) by the relative molecular mass of carbon (12): $100 / 12 = 8.3\bar{3}$

$$\text{Carbonates} = \text{TIC} * 8.33$$

Resulting from the succeeded CNS and TOC measurements, the TOC/N ratios were determined by their elemental weight percentages. According to Meyers and Teranes (2002), the results were multiplied by the atomic weights of N (14) and C (12) in order to obtain the atomic mass ratios ($\text{TOC}/\text{N}_{\text{atomic}}$):

$$\text{TOC}/\text{N}_{\text{atomic}} = \text{TOC}/\text{N} * 1.167$$

3.3.3.2 Stable carbon isotopes

Next to the unstable isotope ${}^{14}\text{C}$, carbon has two stable isotopes: ${}^{12}\text{C}$ and ${}^{13}\text{C}$. The $\delta^{13}\text{C}$ value represents the sample's ${}^{13}\text{C}/{}^{12}\text{C}$ -ratio in relation to the internationally accepted Pee Dee Belemnite standard (PDB), which is based on Cretaceous marine fossils from the Pee Dee formation in South Carolina/United States of America and contains an anomalously high ${}^{13}\text{C}/{}^{12}\text{C}$ ratio of 0.0112372 (Craig, 1957). $\delta^{13}\text{C}$ is a useful parameter for the characterization of sediment organic matter by facilitating the distinction of palaeoenvironmental conditions. Alongside with other implications, the stable carbon isotope ratio can be used in aquatic environments to distinguish bioproductivity rates within the water body and thus provides information about the past trophic situation of the lake (Meyers and Teranes, 2002). Furthermore, $\delta^{13}\text{C}$ values can be applied for determination of the original plant source. Thus, C3 and C4 plants apply different metabolic pathways of carbon fixation during photosynthesis, leading to significantly higher ${}^{13}\text{C}/{}^{12}\text{C}$ -ratios in C4 plants than in C3 plants, which mostly discriminate the heavier ${}^{13}\text{C}$.

For the analysis of stable carbon isotopes of organic matter, the freeze-dried and ground sample material had to be freed from inorganic carbon. Therefore, an amount of ca. 2 g of sample material was treated with 1.3 mol hydrochloric acid (HCl) for 3 hours at 97.7 °C on a heating platform. For a re-separation of the acid, the samples were washed with purified

water and vacuum filtrated. Subsequently, the sample material was placed into a drying cabinet for desiccation at a temperature of 50 °C and carefully homogenized by mortar and pestle. For measurement, the prepared samples were folded into tin capsules at a quantity, which was defined by the following equation:

$$\text{Sample (mg)} = 45/\text{TOC}$$

The measurement of the stable isotope composition of organic carbon was carried out at the stable isotopes laboratory of the AWI in Potsdam by applying a combination of an elemental analyzer (Flash EA 1112 Series, Thermo Finnigan), a CONFLO III gas mixing device, and a Thermo Finnigan MAT Delta-S mass spectrometer. The sample material was combusted to CO₂ by catalytic tube combustion in an oxygen enriched atmosphere, which then was led into the mass spectrometer. During mass spectrometry, the gas gets ionized, accelerated by an electric field, and separated by their mass-to-charge ratio by an electromagnetic field (Craig, 1957). The detected ions were converted into a quantitative ¹³C/¹²C ratio. In addition, a CO₂ standard gas of known isotopic composition is measured and set into relation to the sample gas for determination of the isotopic ratio. Control standards were measured after every seventh measurement. The δ¹³C values are expressed relative to the Pee Dee Belemnite standard (PDB) in parts per mil notation (‰) by applying the following equation:

$$\delta^{13}\text{C} = \left(\frac{^{13}\text{C}/^{12}\text{C}_{\text{sample}}}{^{13}\text{C}/^{12}\text{C}_{\text{PDB}}} - 1 \right) * 1000 \text{ ‰}$$

3.3.4 Plant macrofossil analysis

Macrofossils are defined as identifiable plant remains, which can be seen without magnification (Birks and Birks, 1980). Nevertheless, a stereo microscope is mostly needed for the exact identification. As a bioindicator, plant macrofossils are a useful proxy for reconstruction the past vegetation composition and its palaeoecological implications.

For plant macrofossil analysis, a quantity of 50 ml of material was taken from each sample of PG2038-1. They were washed through sieves of 125 µm, 250 µm and 1 mm mesh sizes. The identifiable plant material from the 250 µm and 1 mm meshes was picked using a Zeiss Stemi SV 11 and a Zeiss Stemi 2000-C stereo microscope. Only a few sub-samples of the 125 µm fraction were observed, due to the absence of any identifiable plant remains.

Samples with mainly fine sediment particles, of which compaction impeded a proper sieving, were treated with the dispersion agent tetrasodium pyrophosphate and placed overnight on a platform shaker. As identifiable plant remains, seeds, fruits, buds, needles, and leaves were picked. Besides plant macrofossils, also further fossils such as insect remains *Daphnia* eggs, and sclerotia of the ectomycorrhizal fungus *Cenococcum geophilum* were considered because they provide palaeoecological information. The identification of mosses, wood remains, and insects is beyond the scope of this study, which is why merely their existence was recorded. The picked samples were drought in a drying cabinet at a maximum of 50 °C. The identification of the selected macrofossils was carried out using different seed identification manuals (Anderberg, 1994; Beijerinck, 1947; Berggren, 1981), helpful photographs of precedent literature (Kienast et al., 2011, 2008, 2005, 2001; van Geel et al., 2008; Wetterich et al., 2008; Zazula et al., 2007), the reference plant collections at the AWI in Potsdam, and the consultation with Juliane Wolter. In addition, this study benefited from the helpful advices of Dr. Frank Kienast and the reference collection at the Senckenberg Research Station of Quaternary Palaeontology in Weimar. For taxonomic determination, I followed the Integrated Taxonomic Identification System (ITIS, 2013) and Czerepanov (2007). Not all species could exactly be identified, while occasionally resembling species (e.g. *Betula* cf. *pendula*) or the genera (e.g. *Carex* sp.) were determined. Identifiable plant material is differently preserved, and thus does not represent the quantity and distribution of the real existing taxa. That's why the reconstruction of past vegetation composition is rather qualitative. According to Dierßen (1996), the plants were categorized into different communities, in order to reveal palaeoenvironmental information.

4 Results

4.1 Lithostratigraphy and geochronology

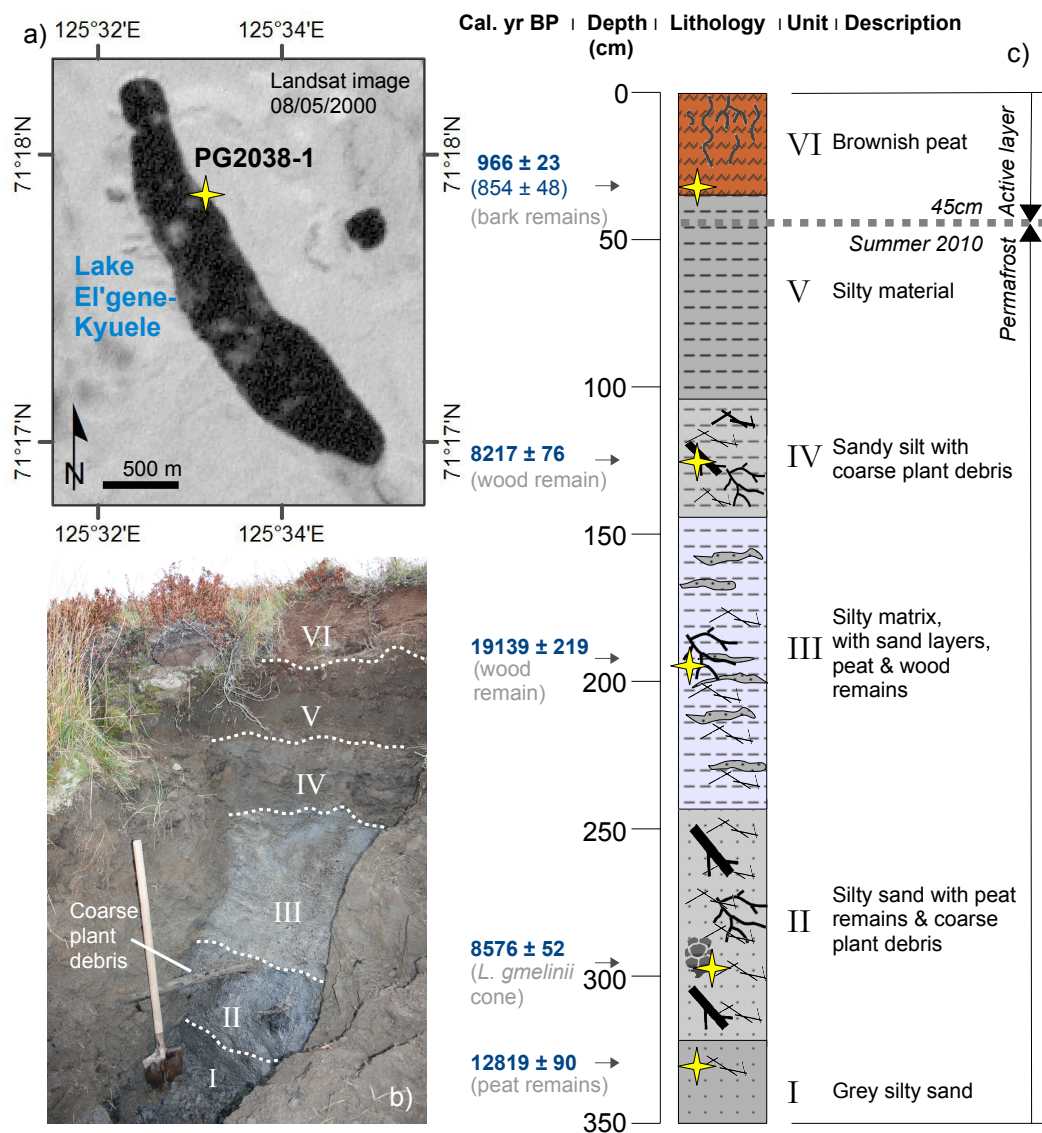


Fig. 12: Depiction of the outcrop PG2038-1: a) Location at the eastern shore of Lake El'gene-Kyuele (base map: Landsat 7 ETM+, panchromatic image, 08/05/2000, derived from: <http://earthexplorer.usgs.gov/>); b) photography of PG2038-1 during fieldwork in 2010, including 6 macroscopically distinguished units, note the coarse plant debris in unit II (photo by B. Diekmann, modified), c) schematic lithostratigraphy of the outcrop units of PG2038-1, including calibrated results of radiocarbon dating, the active layer depth, and the observed macroscopic characteristics of each outcrop unit

In accordance with macroscopically observed criteria during fieldwork and the results of later presented laboratory analyses, a division of the profile PG2038-1 into 6 different units was undertaken as depicted in Fig. 12b/c. In general, the outcrop contains abundant greyish, silty sand in the lower section between 100 and 350 cm dbs, whereas sandy layers are positioned within a silty matrix in unit III between 140-240 cm dbs. The upper outcrop section between 0 and 100 cm dbs is composed of fine-grained, silty material. Coarse organic debris occurs at different quantities depending on its depth, while wood remains were observed from unit II to unit IV. Macroscopic plant material was generally accompanied by abundant peat remains. The uppermost 30 cm of the outcrop are marked by recent to subrecent plant debris. In summer of 2010, the local active layer reached a depth of 45 cm, which forms the vertical restriction of modern soil formation.

Tab. 2: Results of the ^{14}C AMS dating, including the radiocarbon ages before and after the calibration and the type of dated organic matter

Dbs (cm)	Lab ID (in Poznan)	Dated material	Uncal. AMS ages (yr BP)	Cal. yr BP	Sample type
25-30	Poz-50561	bark remains	930 \pm 35	854 \pm 48	bulk organic fraction
	Poz-50563		1,050 \pm 30	966 \pm 23	
115-120	Poz-49475	wood remain	7,380 \pm 50	8,217 \pm 76	humins fraction
185-190	Poz-49476	wood remain	15,990 \pm 70	19,139 \pm 219	
295-300	Poz-49477	cone scales of <i>Larix gmelinii</i>	7,800 \pm 50	8,576 \pm 52	
330	Poz-49478	peat remains	10,840 \pm 70	12,819 \pm 90	

The calibrated ages differ significantly from the measured ^{14}C AMS years (Tab. 2). The peaty sample Poz-49478 at the bottom section of PG2038-1 (330 cm dbs; unit I) has an age of 12,819 \pm 90 cal. yr BP. Furthermore, the samples Poz-49475 and Poz-49477 of the central units II (115-120 cm dbs) and IV (295-300 cm dbs) with abundant wood remains were dated at about 8,217 \pm 76 and 8,576 \pm 52 cal. yr BP, respectively. The maximum detected age within the outcrop is about 19,139 \pm 219 cal. yr BP at a depth of 185-190 cm (Poz-49476, unit III), which is thus forming a significant age inversion. The ages of the bark remains at a depth of 25-30 cm at the transition from the silty unit V to the peaty uppermost unit VI are about 966 \pm 23 cal. yr BP based on the humins fraction (Poz-50563) and about 854 \pm 48 cal. yr BP based on the bulk organic fraction (Poz-50561).

4.2 Sedimentology and mineralogy

The sedimentological results partly support the distinction of horizons during fieldwork, e.g. considering the water contents of the sample material (Fig. 13). They range from 16.39 to 51.79 wt-%. The highest water percentages occur in unit VI and the lowest in unit III.

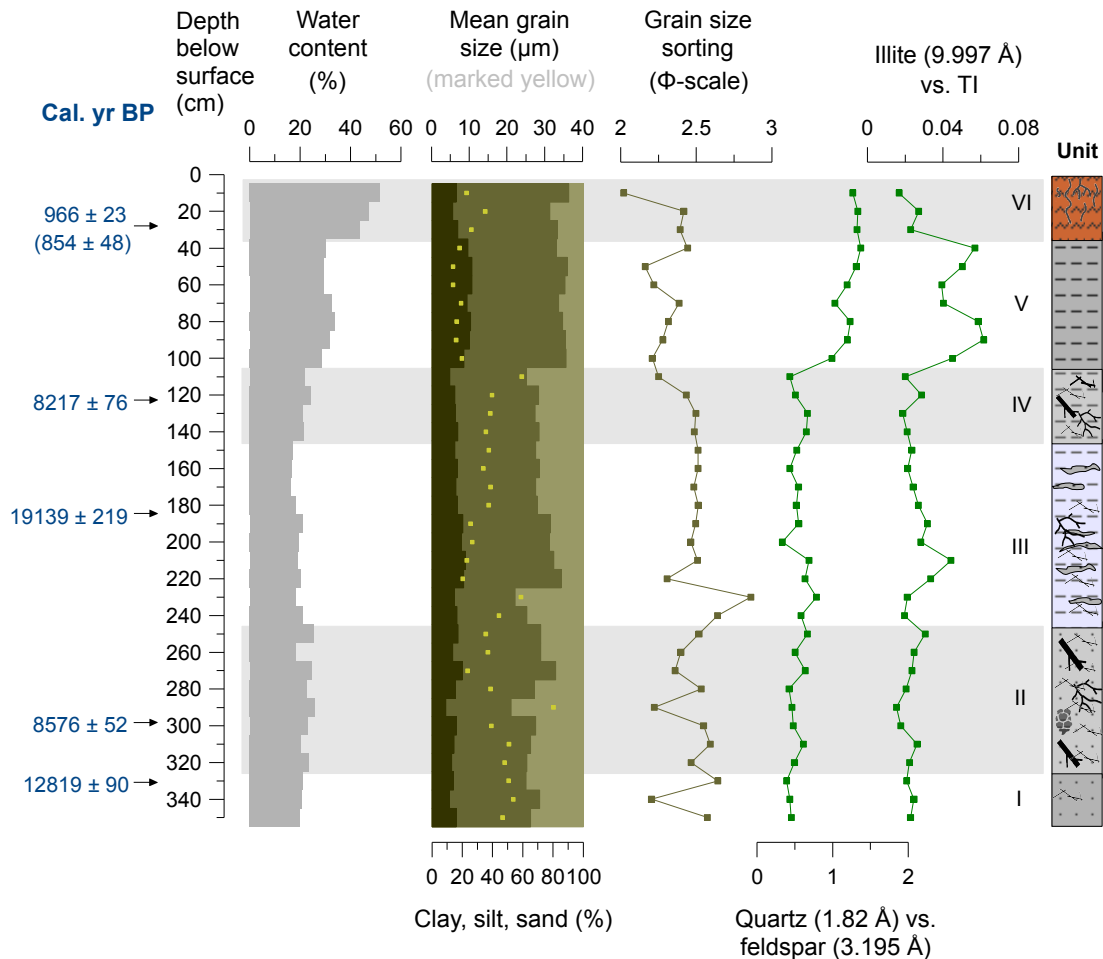


Fig. 13: Results of water content, grain size, and mineralogical laboratory analyses, plotted in relation to the depth below the surface (dbs) and outcrop sections

Because mineral detection is semi-quantitative, the absolute mineral contents are hardly comparable to each other. The minerals quartz and anorthite, which is an end-member of plagioclase feldspar, dominate the anorganic fraction of the outcrop by reaching the highest peak intensities during XRD measurement. Both minerals show fluctuations at the transition from unit II to unit III. Anorthite reaches its highest values from unit I to unit IV, whereas a sharp decline occurs in the units V and VI. Correspondingly, quartz peaks

increase significantly in the units V and VI. The less abundant clay mineral illite has a minor peak in unit III at 205-210 cm dbs and two more pronounced peaks in unit II at about 35-40 and 85-90 cm dbs. Carbonate minerals in the form of calcite or aragonite peaks were not detected during XRD analysis.

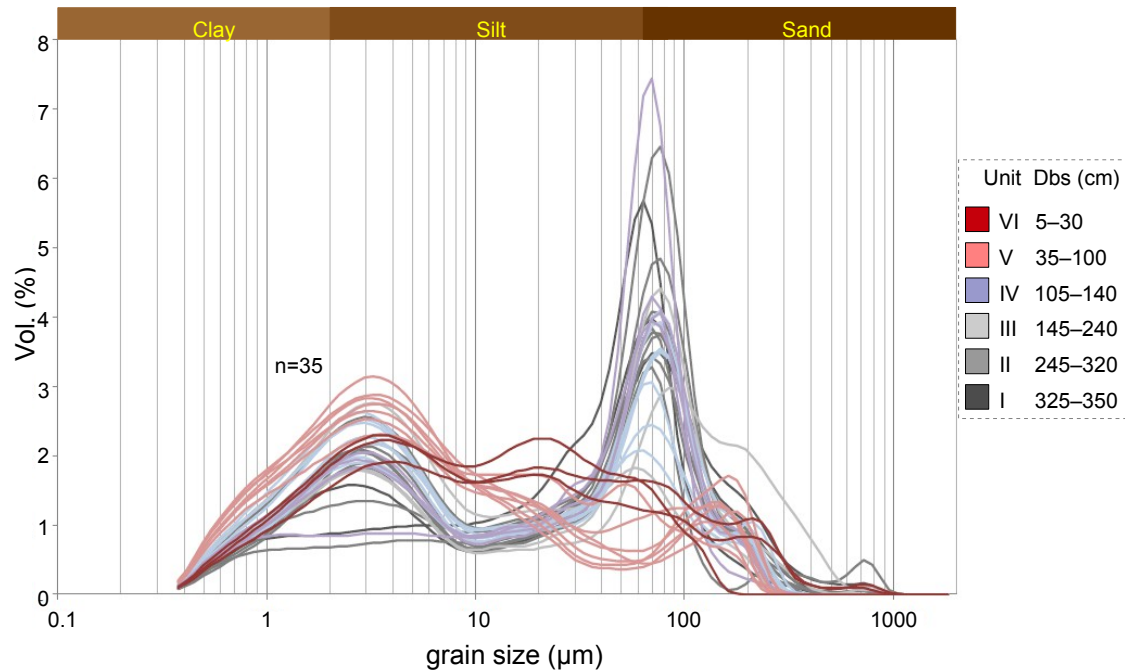


Fig. 14: Grain size distribution of PG2038-1, detected by laser diffractometry

During grain size analysis, the measurement of relatively wide sections of sample material, containing a depth of 5 cm, cannot provide a high stratigraphic resolution. Thus, fine intersections such as the sandy layers in unit III could not be emphasized and were only regarded during fieldwork. As depicted by the box plot in Fig. 15a, the units II and III are characterized by the largest variation of mean grain sizes, whereas the units I and V are more homogeneous. However, regarding the inclusive standard deviation, which defines the grain size sorting, of about 2.02-2.86 (Fig. 13), all outcrop units of the archive PG2038-1 contain a relative wide range of grain sizes from fine sandy to coarse clayey material (Fig. 14) and are thus characterized as “very poorly sorted” (Folk, 1966). The quantities of clay range from 8.99 to 26.46 vol-%, of silt from 40.25 to 74.46 vol-%, and of sand from 9.53 to 47.62 vol-%. The mean grain size ranges from 5.7 μm (at 45-50 cm dbs) to 32.3 μm (at 285-290 cm dbs), while it generally shows an increasing trend with depth. Four types/sections of grain size distribution could be distinguished:

- i. The samples at a depth of 100-350 cm mainly show a bimodal distribution with local peaks at about 2-4 μm (fine silt) and 60-80 μm (fine sand).
- ii. In between the first grain-size section, several spikes occur with an increased mean grain size and a highly pronounced peak of the fine sand fraction (e.g. 105-110 cm, 225-230 cm and 285-290 cm dbs).
- iii. The uppermost samples between 0-30 cm dbs are dominated by a large silt fraction.
- iv. At a depth of 30-100 cm, large silt contents are accompanied by increasing clay quantities.

According to Shepard (1954, as reviewed by Last, 2002a), the corresponding grain size distributions are classified as (i) sandy silt, (ii) silty sand, (iii) silt to sandy silt and (iv) clayey silt (Fig. 15b). The grain size skewness of the samples is parallel to the mean grain size: thus according to (Last, 2002a), the lowest mean grain sizes in unit V are strongly coarse-skewed, whereas coarser grain sizes (e.g. in the units I, II, and IV) are fine- to strongly fine-skewed (see appendix).

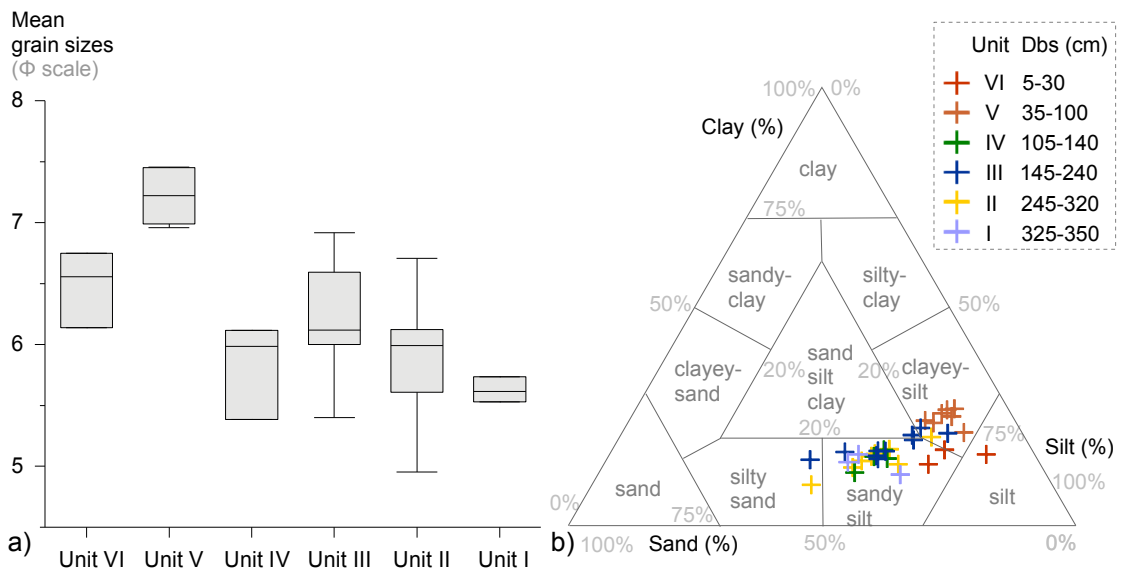


Fig. 15: a) Box plot of the mean grain sizes of PG2038-1, indicating homogeneously finer material in unit V, homogeneously coarser material in unit I, and a wide range of fine and coarse material in the units II and III, b) lithological classes according to Shepard (1954, as reviewed by Last, 2002a)

4.3 Biogeochemistry

The analysis of CNS, TOC, and $\delta^{13}\text{C}$ revealed significant variations between the outcrop sections (Fig. 16). The elemental analysis yielded a wide range of total carbon contents (TC) between 0.92 to 29.83 wt-% and total nitrogen contents between 0.07 and 1.43 wt-%. The largest part of the TC corresponds to the TOC, which is why both values are very close. TOC contents range between 0.7 and 28.75 wt-% with mostly low values from unit I to unit V (0.7-3.27 wt-%). The lowest values occur in the units I and III, whereas significantly higher values were measured in the peaty uppermost unit VI (20.16-28.75 wt-%). The TIC contents are rather low, ranging from 0.12 to 1.08 wt-%. The CaCO_3 contents were calculated at a range from 1.01 to 9.01 wt-%. A CaCO_3 peak occurs in unit III at 215-220 cm dbb at about 4.26 wt-%. The highest values up to 9.01 wt-% occur in the units V and VI where they are gradually increasing in ascending direction. The remaining CaCO_3 values are homogeneously low. However, the possible existence or absence of inorganic carbon and calcium carbonate will explicitly be discussed in chapter 5.

The $\text{TOC}/\text{N}_{\text{atomic}}$ values range from 11 to 23.98. Local peaks occur in unit II (14.67-18.97), unit IV (13.04-15.44), and in unit VI (21.88-23.98) where the highest values were measured. Relatively low values were obtained in unit III (11-14.32) and unit V (11.02-11.93). The values in the units II and IV show some obvious inner fluctuations.

The determination of the $\delta^{13}\text{C}$ values comprised a range from -24.72 to -31.4 ‰ vs. PDB. The lowest values occur in unit V where $\delta^{13}\text{C}$ values gradually decrease until -31.4 ‰ vs. PDB (at 55-60cm dbb) and subsequently increase again. The highest values occur in unit III by ranging between -26.35 and -24.72 ‰ vs. PDB (the latter value at 205-210 cm dbb). The samples of the remaining units yield a relatively homogeneous range of $\delta^{13}\text{C}$ values (unit I: -26.39 to -27 ‰ vs. PDB; unit II: -26.29 to -27.8 ‰ vs. PDB; unit IV: -26.66 to -27.27 ‰ vs. PDB; unit VI: -28 to -28.4 ‰ vs. PDB). In the whole outcrop no significant spikes were measured, whereas in unit II slight fluctuations occur. In general, the obtained results from $\delta^{13}\text{C}$ analysis correspond with the $\text{TOC}/\text{N}_{\text{atomic}}$ values and moreover confirm the above proposed vertical distinction of layers/units.

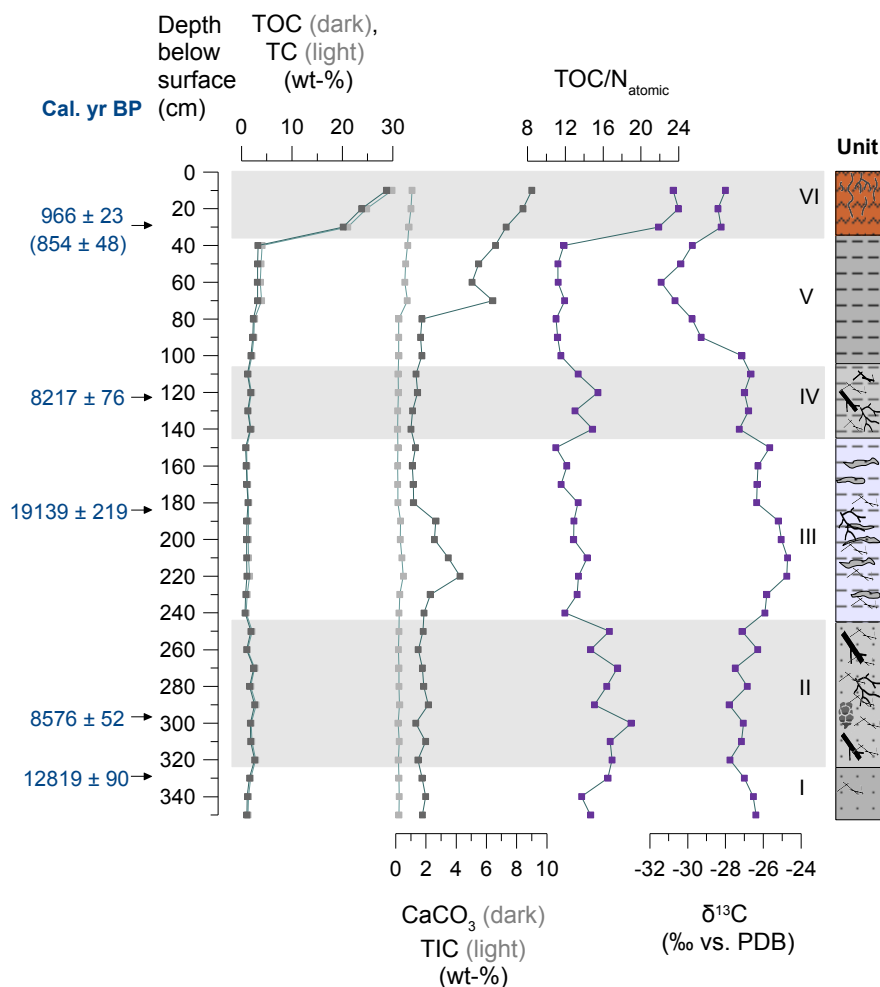


Fig. 16: Results of the biogeochemical laboratory analyses, plotted in relation to the depth below the surface and outcrop sections

4.4 Plant macrofossils

Detected subfossil plant remains in PG2038-1 were fruits, seeds, oospores, wood, charcoal, leaves, needles, buds, and roots. The material is differently preserved and often remained only as fragments. In addition to plant macrofossils, also moss remains, insect remains, *Daphnia* eggs, and sclerotia of the fungus *Cenococcum geophilum* were found. An overview of all obtained fossil material is demonstrated in Tab. 3.

A total number of 210 found plant macrofossils of 26 different species were detected, occurring in all outcrop units (Tab. 4). Abundant material was found in the units I, II, and IV, including leaves, needles, and *Daphnia* ephippia. Compared to that, conspicuously few findings were made in the units III, V and VI. Moss and wood remains were observed in all

units of PG2038-1. Insect remains were found frequently and *Cenococcum geophilum* occurred abundantly throughout the whole outcrop except in unit V, which was devoid of both. Plant roots occurred basically in the uppermost units V and VI, charcoal pieces were observed in the units I and II, and fossil rodent excrements were found in unit II. The determined plant taxa are demonstrated in Tab. 4 and in Fig. 17, Fig. 18, and Fig. 19.

Tab. 3: Semiquantitative overview of the fossil material: explanation:

+++ abundant (>10 counts), ++ frequent (6-10 counts), + occasional (3-5 counts), - rare (<3 counts)

Sample	Plant macro-fossils ²	Wood remains	Moss remains	Leafs	Needles	Roots	Insect remains	<i>Daphnia ephippia</i>	<i>Cenococcum geophilum</i>
5-10		+++		++		+++	++		++
15-20	+	++		+		+++	++		++
25-30		+	++			+++	++		+
35-40			+			+			
45-50			++			+	-		
55-60	++	++	++			++			
65-70	-	+	+++			+++			
75-80			+			++			
85-90		+	-			+			
95-100	-		-						++
105-110	+++	++	+++	++	+		+	+	+++
115-120	+	+	+++	+			++	+	++
125-130		+	+++				+		+
135-140	-	++	+++				+		+
145-150			+				+		++
155-160		+	+			+	+		+++
165-170	-	+					++		+++
175-180	+	++	+				++		+++
185-190		+++							+++
195-200	+	++		+			++		+++
205-210	-	+							++
215-220		++							+++
225-230	-	+			-		-	-	+
235-240	++	++	+		+	+	+	++	+
245-250	+++	+++	+	++	++		++	++	++
255-260	+	+++	++	+	+		+		+++
265-270	+	+++	+		+		+	+	++
275-280	+	+++	+	++	+		+	+	+++
285-290	++	+++	+	+	++		++		+++
295-300	+++	+++	+		+++		+	+	+++
305-310	++	+++	++	++	+++		++	+	+++
515-320	++	+++	+		+++			++	+++
325-330	++	++	++		++		++	++	++
335-340	++	++	+	+	+		++	+	+
345-350	-	+	+		-		++	-	+

² Including identifiable seeds and fruits; excluding the further mentioned macrofossils

Tab. 4: Overview of plant macrofossils and corresponding syntaxa/plant communities

Syntaxa (according to Dierßen, 1996)	Taxa	Type	Finds ³	Unit
Steppe & dry Arctic upland vegetation Koelerio-Corynepherea Klika ap. Klika & Nowák 1941 & Carici rupestris–Kobresietea Ohba 1974	<i>cf. Dryas octopetala</i> L.	leaf fragment	2	II
	<i>Potentilla</i> sp. L.	nutlet	1	III
	<i>Potentilla arenosa</i> , (Turcz.) Juz.	nutlet	2	I, III
	<i>Potentilla cf. nivea</i> L.	nutlet	2	III
	<i>Potentilla cf. hyparctica</i> Malte	nutlet	4	II & III
	<i>Potentilla cf. stipularis</i> L.	nutlet	5	II & III
Arctic pioneer vegetation Thlaspithea rotundifolia Br.–Bl. 1948	<i>Cerastium cf. arvense</i> L.	seed	2	I & III
	<i>Papaver</i> sect. <i>Scapiflora</i> Reichenb.	seed	1	II
Taiga vegetation Vaccinio-Piceetea Br.–Bl. 1939	<i>Betula cf. pendula</i> Roth	leaf fragment, nutlet	6	I & II
	<i>Larix gmelinii</i> (Rupr.) Rupr	cone, seed, fascicle, needle	43	I-IV
Shrub tundra Betulo–Adenostyletea, Br.–Bl. et R. Tx. 1943	<i>Alnus viridis</i> ssp. <i>fruticosa</i> (Rupr.) Nyman	nutlet, catkin scale	6	II & IV
	<i>cf. Arctous rubra</i> (Rehder & Wilson) Nakai	Fruit stone	1	II
	<i>Betula nana</i> L.	leaf fragment, nutlet	3	IV
	Betulaceae sp.	nutlet	10	I-IV
	<i>Vaccinium vitis-idaea</i> L.	berry, leaf	4	II
Wetland vegetation Scheuchzerio-Caricetea nigrae (Nordh. 1936) R. Tx. 1937 & Oxycocco-Sphagnetetea Br.–Bl. & R. Tx. 1943	<i>Carex</i> sect. <i>Phacocystis</i> Dumort.	nutlet	18	I-IV
	<i>Epilobium palustre</i> L.	seed	1	II
	<i>Eriophorum brachyantherum</i> Trautv. & C.A. Mey.	archene	7	I-III
	<i>Eriophorum</i> sp. L.	archene	1	III
	<i>cf. Trichophorum uniflorum</i> (Trautv.) Malyshev & Lukitsch.	seed	1	II
Aquatic sublittoral and littoral vegetation Charatea fragilis Fukarek ex Krausch 1964 & Potamogetonetea pectinati R. Tx. & Prsg. 1942	Characeae sp.	oospore	8	V
	<i>Hippuris vulgaris</i> L.	nutlet	2	IV
	<i>Potamogeton cf. filiformis</i> Pers.	fruit stone	1	III
	<i>Potamogeton cf. vaginatus</i> Turcz.	fruit stone	1	V
without identification	<i>Carex</i> sp. L.	nutlet	3	II, III & VI
	<i>cf. Salix</i> sp. L.	bud	6	III & IV

³ The occurrence of *Larix gmelinii* needles in one sample is counted as 1

The most abundant taxon of PG2038-1 is *Larix gmelinii*, summarizing 43 found plant remains. They occurred as seeds, fascicles (short shoots), needles, and a female cone between the units I and IV. In unit II, leaves and a fossil berry of *Vaccinium* cf. *vitis-idaea*, leaf fragments of cf. *Dryas octopetala*, and fruit remains with a fruit stone of cf. *Arctostaphylos rubra* were found. Different buds of cf. *Salix* sp. occurred in the units III and IV. Cyperaceae is represented by *Carex* sect. *Phacocystis* (unit I-IV), cf. *Trichophorum uniflorum* (unit II), and *Eriophorum brachyantherum* (units I-III). A number of nutlets of partly hardly distinguishable *Potentilla* species was found in the units I, II, and III. The proposed species are *Potentilla* cf. *stipularis*, *P.* cf. *hyperbatica*, and *P.* cf. *arenosa*. Two *Potentilla nivea* nutlets were found in unit III. In the units III and IV, seeds of *Cerastium* cf. *arvense* were found. As species of the family *Betulaceae*, finds were made of *Alnus viridis* ssp. *fruticosa* in the units II and IV, *Betula nana* in unit IV, and *Betula* cf. *pendula* in the units I and II. *B.* cf. *pendula* was preferred before *B. pubescens*, which preferably inhabits more western and less continental regions of Russia (Krasnoborov and Malyshev, 2003). The preserved plant material includes leaf fragments, nutlets, and catkin scales. From unit I to unit IV, a number of *Betulaceae* nutlet fragments was found, of which the exact species could not certainly be determined. In unit II, seeds of *Epilobium palustre* and *Papaver* sect. *Scapiflora* were found. Nutlets of *Hippuris vulgaris* occurred in unit IV, a *Potamogeton* cf. *vaginatus* fruit stone occurred in unit V, and a *Potamogeton* cf. *filiformis* fruit stone occurred in unit III. Lastly, the unit V also contained a number of oospores of Characeae algae.

Consequently, plant communities (syntaxa) were defined because they are ecologically correlated to certain locations and are thus suitable for the determination of palaeoenvironmental conditions. The different plant taxa were categorized into six different syntaxa (Tab. 4), following preceding classifications (Dierßen, 1996; Kienast et al., 2011). The determined plant macrofossils represent the occurrence of Steppe & dry Arctic upland vegetation (Koelerio-Corynephoretea Klika ap. Klika & Nowák 1941 & Carici rupestris–Kobresietea Ohba 1974) in the units I-III, Arctic pioneer vegetation (Thlaspithea rotundifolii Br.-Bl. 1948) in units I to III, Taiga vegetation (Vaccinio-Piceetea Br.-Bl. 1939) in the units I-IV, shrub tundra vegetation (Betulo–Adenostyletea, Br.-Bl. et R. Tx. 1943) in the units I to IV, wetland vegetation (Scheuchzerio-Caricetea nigrae (Nordh. 1936) R. Tx. 1937 & Oxycocco-Sphagnetetea Br.-Bl. & R. Tx. 1943) in the units I-IV, and aquatic sublittoral and littoral vegetation (Charatea fragilis Fukarek ex Krausch 1964 & Potamogetonetea pectinati R. Tx. & Prsg. 1942) from unit III to V. Genera without an

exact species determination such as cf. *Salix* sp. and *Carex* sp. remained without identification of plant communities, whereas other species like *Potentilla* sp., may be ascribed to more than one plant community.

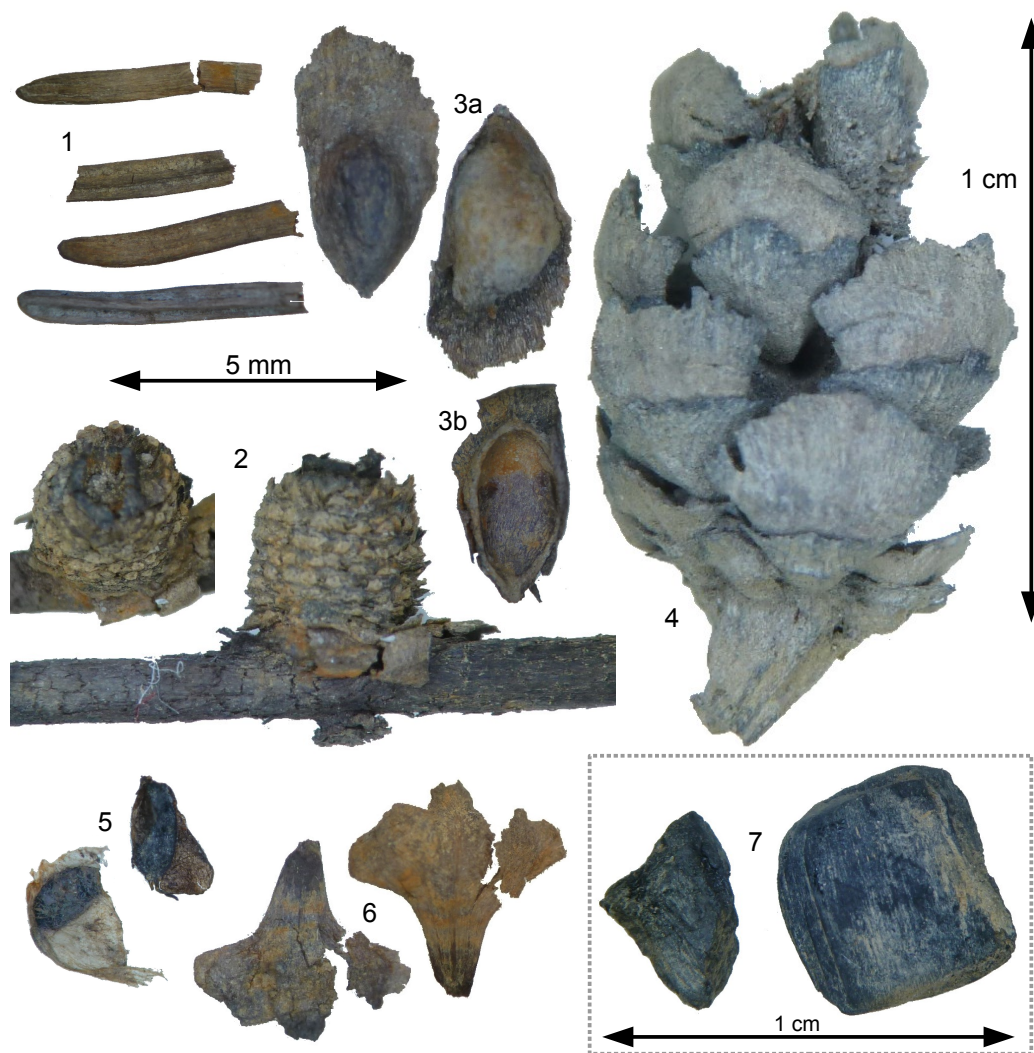


Fig. 17: Macrofossils indicative for taiga ecosystem (the outcrop units of PG2038-1 are put in braces), *Larix gmelinii* remains: 1 – needles (III), 2 – twig with a fascicle (short shoot), top and side view (II), 3a – seed, both sides (III), 3b – hollow seed fragment (II), 4 – mature female cone (II); Birch tree (*Betula* cf. *pendula*) remains: 5 – two different nutlets (II), 6 – catkin scale, both sides; 7 – charcoal remains (I)

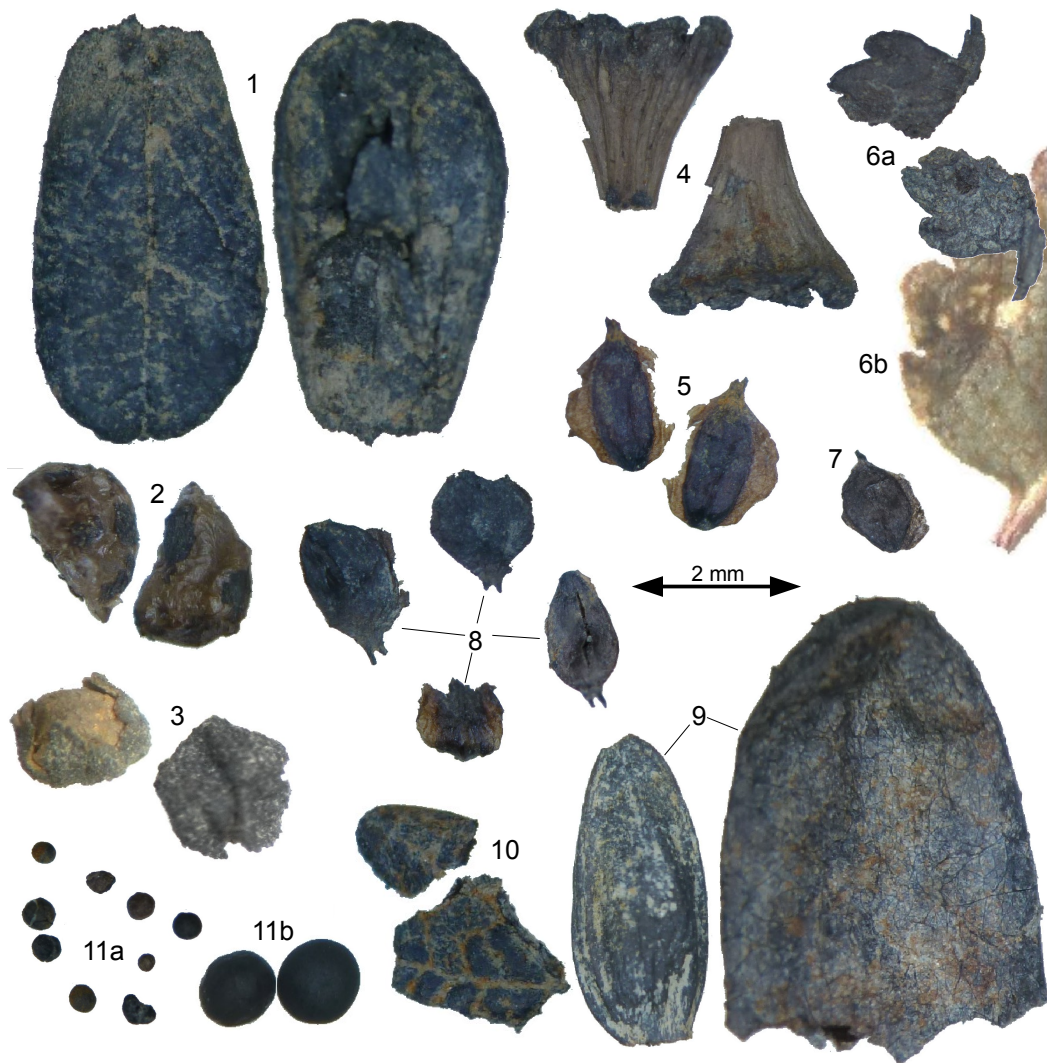


Fig. 18: Macrofossils indicative for Arctic and Subarctic wooden shrubs: 1 – *Vaccinium vitis-idaea*, leaf, both sides (II), 2 – cf. *V. vitis-idaea*, berry, two sides (III), 3 – cf. *Arctous rubra*, fruit-stone with remains of epicarp, two sides, (II), 4 – *Alnus viridis* ssp. *fruticosa*, catkin scale, both sides (IV), 5 – *A. fruticosa*, nutlet, both sides (II), 6a – *Betula nana*, fossil leaf fragment, both sides (IV), 6b – *B. nana*, modern leaf (Kienast et al., 2008), 7 – *Betula* cf. *nana*, nutlet fragment (IV), 8 – *Betulaceae*, four different nutlet fragments (II), 9 – cf. *Salix* sp., two different buds (III & IV), 10 – cf. *Dryas octopetala*, fossil leaf fragments (II), 11a – *Cenococcum geophilum*, fossil sclerotia (II), 11b – *C. geophilum*, modern sclerotia (VI)

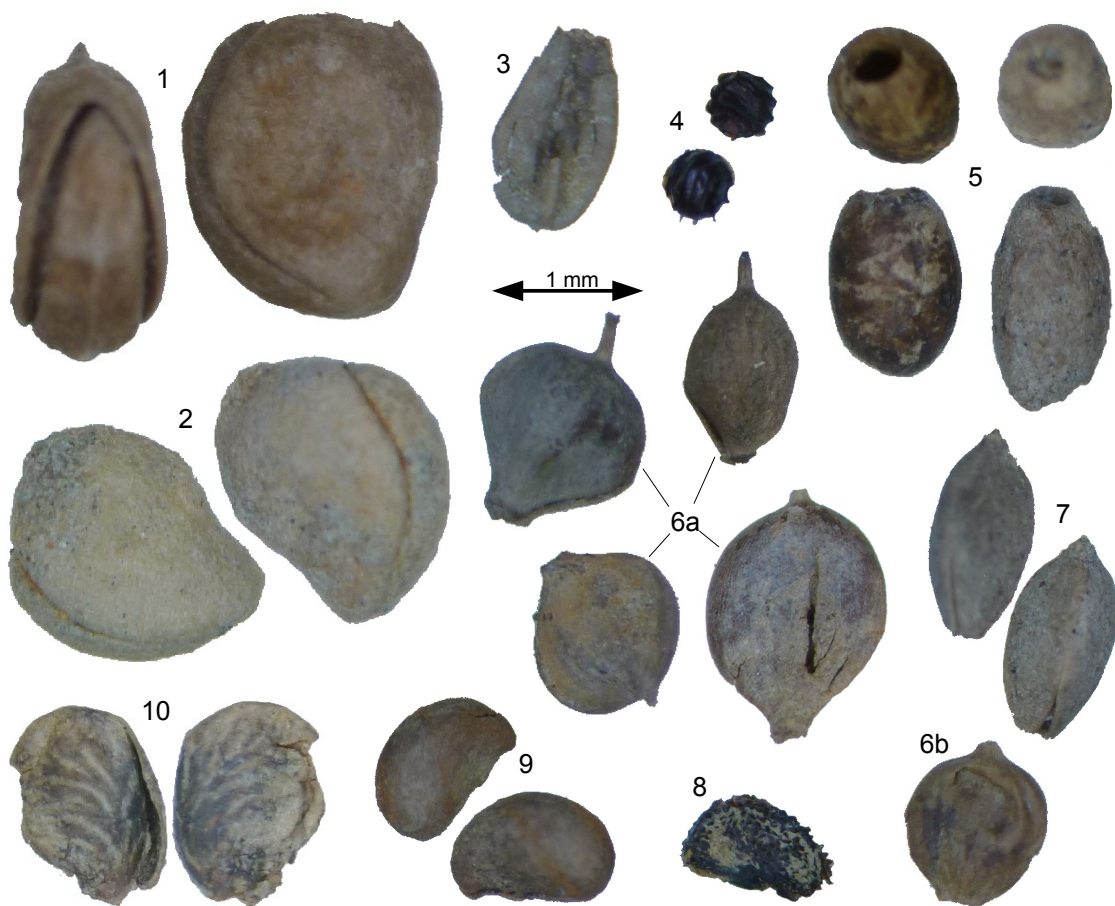


Fig. 19: 1-7 plants indicative for moist or lacustrine environments: 1 – *Potamogeton* cf. *vaginatus*, fruitstone, two sides of a fruit stone with a closed lid (V), 2 – *Potamogeton* cf. *filiformis*, fruitstone (slightly shorter than *P. vaginatus*) (III), 3 – *Eriophorum brachyantherum*, archene (I), 4 – *Characeae*, two different oospores (V), 5 – *Hippuris vulgaris*, two different nutlets, side & top view (unit IV), 6a – *Carex* sect. *Phacocystis*, four different nutlets, 6b – nutlet with preserved perigynium (I-III), 7 – cf. *Trichoporum uniflorum*, two sides of a nutlet (II); 8-10 plants adapted to low moisture: 8 – *Cerastium* cf. *arvense*, seed (III), 9 – *Potentilla* cf. *hypartica*, both sides of a nutlet (II), 10 – *Potentilla* cf. *nivea*, both sides of a nutlet fragment (III)



Fig. 20: Animal macrofossils: 1 – *Daphnia* sp., three different ephippia (II), 2 – different insect remains, central: fossil *Curculionidae* head with snout (II)

5 Interpretation and discussion

5.1 Proxy interpretation and reconstruction of the past sedimentary processes

In this chapter, the origin, transport, accumulation, and reworking of clastic and biogenic sediment compounds of the outcrop PG2038-1 are interpreted and discussed. In general, high fluctuations of all proxies indicate different sedimentary milieus. The results of this study emphasize a complex geomorphological shoreline and basin evolution of Lake El'gene-Kyuele.

5.1.1 Allogenic clastic sediments

The largest portion of the analysed clastic sediments is allogenic, as thermokarst lakes are generally known for their high geomorphological dynamics. An end-member algorithm for definition of different sediment sources, developed by Dietze et al. (2012), was applied by Biskaborn et al. (in press) for Lake El'gene-Kyuele. That study proposed different clastic sediment sources in the lake catchment, which likewise occur in this study and are interpreted as: (i) fine sand with washed-out fine particles at the lake shoreline, and (ii) clayey to silty particles as a part of the background basin sedimentation.

A large sediment compound in this study is the fine-sand fraction (ca. 50-100 μm) of the lower outcrop units I, II, and partly III and IV of PG2038-1, which mostly contains quartz and plagioclase feldspar minerals. These deposits are interpreted as relocated and reworked terrigenous sediments, which possibly originate from thaw slumps at the thermokarst slopes. Modern retrogressive thaw slumps occur at the northern and north-western shoreline of Lake El'gene-Kyuele and end up in small alluvial fans (Biskaborn et al., in press). As observed in the Canadian Arctic, common sediment transport mechanisms are different alluvial processes and large debris flows of highly mixed diamicton, which continue basinward as subaquatic flows (Murton, 2001). In addition, in a subaquatic milieu, the fine-sandy sediments are possibly supplied by wave abrasion and bank collapse at the shoreline. French (2007) demonstrated the generally large impact of wave abrasion on thermokarst lake shores by estimating lateral bank erosion rates of 15-25 cm/yr. As the fine sand occurs abundantly in various archives of the study area, it possibly originates from sedimentary rock of the geologic formations of mesozoic age situated below and

near the lake, such as the Chekanovsky Ridge, and was provided by the polygenetic Ice Complex formation (Schirrmeister et al., 2011). For exact information about the provenance of the fine sand, mineralogical investigations of the surrounding bed rocks are required.

As a second large group, fine-silty to coarse-clayey deposits (ca. 1-5 μm) are abundant in PG2038-1 (e.g. in unit V). This sediment fraction is interpreted as washed-out shoreline sediments, which were easily carried away as suspension load (Biskaborn et al., in press). In addition, fine-silty deposits in Northern Siberia were partly regarded as loess of aeolian origin (e.g. Brigham-Grette, 2001; Zimov et al., 2006). However, this loess theory is rejected for Northern Yakutia due to the absence of glaciations throughout the Late Quaternary (Schirrmeister et al., 2011). The combination of fine-grained deposits with elevated illite peaks indicate a lacustrine detrital input in unit V and in parts of the units III and IV. This material tends to stay in the suspension load and settles during calm weather conditions and beneath the winter ice cover (Murton, 2001). The lacustrine sedimentation of fine particles prevails in the central and more profound lake basin, augmented by negligible currents and impeded wave stress (Hjulstrom, 1939). The absence of coarse grain sizes in unit V indicates little contribution of terrigenous sediment input due to an increased distance from the shoreline.

However, as observed especially in the units III and IV of PG2038-1, heterogeneous sediment facies occur as sand layers in a silty matrix and indicate alternating depositional environments. According to Murton (2001), incoming terrigenous deposits tend to form sheets or lenses within the thermokarst lake. This effect prevails in shallow margin areas of the lake that coarser sediments can reach more easily. Biskaborn et al. (in press) has argued that alternating phases of geomorphological activity and stability in the thermokarst basin led to mass movement events of terrigenous sediments towards the lake basin in repeated change with lacustrine detrital input. Phases of geomorphological stability are closely connected with shoreline-parallel, outcropping ice-wedges. In addition, geomorphological activity is indicated by the disturbed radiocarbon ages of the units III ($19,139 \pm 219$ cal. yr BP) and IV ($8,217 \pm 76$ cal. yr BP), indicating the input of older sediments from an up-slope site.

5.1.2 Authigenic clastic sediments

Authigenic material is regarded as settled, loose sediments, which undergo a postburial

alteration (Last, 2002b). The depositional archive of PG2038-1 does not contain macroscopic cryogenic features, such as cryoturbation, patterned ground, or frost sorting. Predominating fine-grained, allogenic deposits in the topmost unit VI have undergone a subrecent alteration by active pedogenesis above the permafrost table. One of the main mechanical effects has been cryogenic weathering. At water-saturated conditions, intense freeze-thaw cycles physically destroyed quartz grains, which end up as particles of the silt fraction between 10-50 μm (Schwamborn et al., 2012). However, the frequent deviation from this range in other units and other archives of Lake El'gene-Kyuele indicate that frost weathering has only had low importance on most sediments of the study site. As a possible reason, the intensity of cryogenic weathering was reduced for much of the Holocene by either being under constant permafrost conditions or by being under unfrozen conditions within the sub-lake talik. However, the topmost unit VI has been longer within the active layer where large thermal variations produced cryogenic detritus.

In addition, as demonstrated by studies in the northern Swedish Arctic, chemical weathering and the formation of secondary minerals can be significant in cold environments (Allen et al., 2001; Thorn et al., 2001). Feldspar minerals are more vulnerable than quartz grains to leaching by an acidic soil solution (hydrolysis), which implicates the quartz/feldspar ratio as an indicator for the state of chemical weathering (Nesbitt et al., 1997). Hence, the ratio tends to increase with advancing soil genesis. Correspondingly, the mineral illite is a secondary mineral, which develops by the chemical weathering of feldspar (Blume et al., 2009). This is possibly the origin of illite-enriched, fine-silty detritus, which were later washed-out and accumulated by lacustrine sedimentation especially in the unit V with the highest quartz/feldspar ratios of the outcrop PG2038-1.

5.1.3 Biogenic input

Sediments of Lake El'gene-Kyuele are devoid of biogenic input of carbonates or silicates due to the absence of diatoms and ostracods. However, the biogeochemical proxies of this study support the sedimentological reconstruction and revealed different palaeoenvironmental information.

The outcrop PG2038-1 is characterized by large amounts of well-preserved organic matter, which is reflected by high TOC concentrations in units I, II, and in the uppermost unit VI. As a typical consequence of the cold climate, all outcrop units are poorly affected by

microbial decomposition. In unit I and possibly at the bottom of unit II, organic plant matter possibly originates from the accumulation of terrestrial peat during the pre-thermokarst phase. In unit VI, high TOC contents are contributed by recent terrestrial plant remains and by the impeded input of clastic sediments. A further source of sediment organic matter in PG2038-1 are old, carbon-rich Ice Complex sediments, which were easily reworked by thermokarst processes. This is indicated by the radiocarbon age of wood remains in unit III ($19,139 \pm 219$ cal. yr BP) reaching back to the Late Pleistocene. However, younger ages of the further radiocarbon samples implicate the dominating Holocene origin of plant remains.

The varying TOC/N ratios of the outcrop PG2038-1 emphasize the changing depositional environments at the study site and additionally facilitate the reconstruction of the primary source of the dead plant remains. The highest values up to 20 in the units II, IV, and VI go alongside with coarse, macroscopically detected plant debris and are generally indicative for an increased input of vascular plants that contain abundant cellulose (Fig. 21, Meyers and Lallier-Verges, 1999; Meyers, 1994). They are mostly of terrigenous origin, such as grasses or trees. However, selective degradation of land plants favours the decomposition of carbon before nitrogen and partly produced a posterior shift to lower TOC/N values (Meyers and Teranes, 2002).

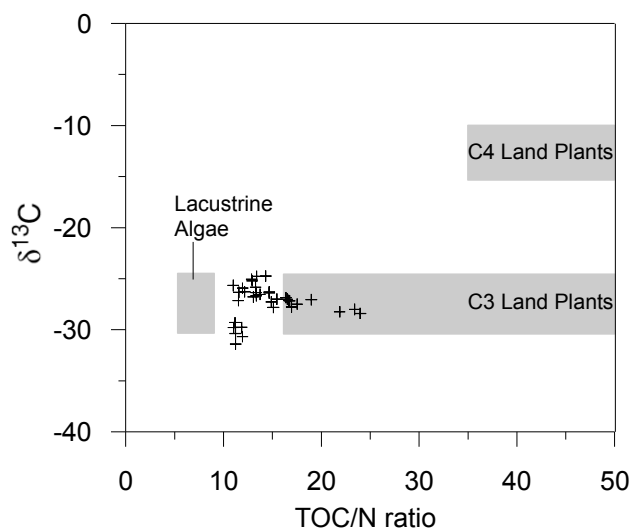


Fig. 21: Correlation of the TOC/N_{atomic} values with the $\delta^{13}C$ values of PG2038-1; comparison to the expected values according to (Meyers and Lallier-Verges, 1999)

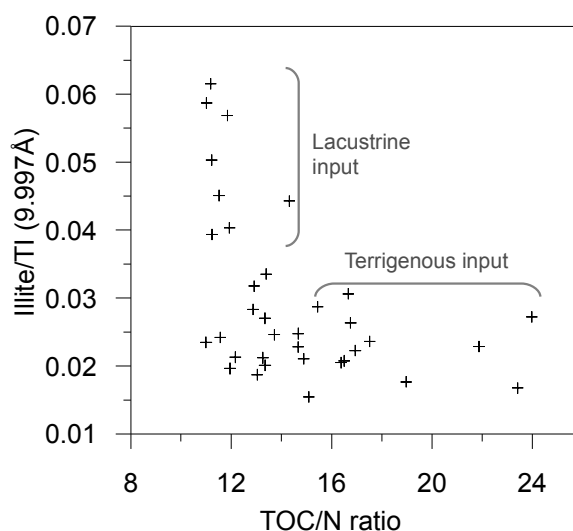


Fig. 22: Distinction of lacustrine and terrigenous sediment input at PG2038-1 using the TOC/N ratio and the semi-quantitative illite content

In general, all sediments of the outcrop PG2038-1 with high TOC/N values correlate well with the terrigenous input of clastic sediments, whereas low TOC/N ratios correlate with lacustrine detritus (Fig. 22). Minor fluctuations of the terrigenous TOC/N ratios and $\delta^{13}\text{C}$ values in the units II and IV are indicative for the input of varying plant sources in different sediment layers and for differential decomposition of the plant remains.

Lacustrine organic matter was revealed in unit V and partly in unit III by very low TOC/N ratios, indicating sources of non-vascular, protein-rich plants like lake algae (Meyers and Teranes, 2002; Meyers, 2003). However, the obtained TOC/N ratios about 10-12 are somewhat higher than predicted at about <10 (Fig. 21). This is caused by the nitrogen deficiency, which commonly affects lake plants in oligotrophic (nutrient poor) Arctic lakes (Olsen et al., 2013). In addition, TOC/N ratios of lake algae can increase during sinking and early sedimentation as nitrogen-rich proteins are selectively degraded (Meyers and Teranes, 2002). The TOC/N ratios in the central section of unit III ranging from 12 to 14 are also indicative for a combined contribution of algae and vascular plants, which occurs at the margin of the lake basin.

The $\delta^{13}\text{C}$ values of all outcrop units are indicative for C3 plants, which highly discriminate against ^{13}C (e.g. O'Leary, 1988). In the terrigenous units I, II, IV, and VI, the values range about -26 to -28 ‰ vs. PDB. $\delta^{13}\text{C}$ values of sediments mostly show a similar amount or

slight enrichment of ^{13}C compared to the original vegetation (Dzurec et al., 1985), whereas a minor post-sedimentary fractionation possibly depends on a differential microbial decomposition between lignin and cellulose of dead organic matter (Melillo et al., 1989). C3 plants are represented by the great majority (ca. 95 %) of plants on earth, e.g. by wooden plants or by phytoplankton in lacustrine environments (Osborne and Beerling, 2006). The second large group of C4 plants is mostly connected to regions with high insolation and elevated daytime temperatures (e.g. tropic Poaceae and Cyperaceae) (Ehleringer et al., 1997), which makes the occurrence in the study area rather unlikely. The $^{13}\text{C}/^{12}\text{C}$ -ratio of plants also depends on the constantly fluctuating $^{13}\text{CO}_2$ content in the atmosphere, which can be caused by varying methane emissions (Krull and Retallack, 2000), changes in atmospheric CO_2 concentration (Hollander and McKenzie, 1991), the combustion of fossil fuel (Peterson and Fry, 1987), etc.

Different results of the stable carbon isotope analysis were achieved in the outcrop units of lacustrine sedimentation with dominating algal organic matter. Unit III is characterized by the highest, or rather the least negative, $\delta^{13}\text{C}$ values about > -25 ‰ vs. PDB that are caused by high bioproductivity rates in the lake water. Thus, when accelerated algae growth causes a depletion of $^{12}\text{CO}_2$ in the lake water during C3 photosynthesis, consequently the following plants are forced to use increased amounts of $^{13}\text{CO}_2$ to build up organic biomass (Brenner et al., 1999; Olsen et al., 2013; Wolfe et al., 1999). In addition, algae possibly used HCO_3^- with an increased $\delta^{13}\text{C}$ value as the primary source of carbon when the amount of available CO_2 decreased during phases of high photosynthetic activity (Meyers and Teranes, 2002). Hence, in unit III a phase of more favourable circumstances for plant growth occurred. Possible reasons are warmer climatic conditions or a better availability of nutrients.

In contrast to unit III, the $\delta^{13}\text{C}$ values of unit V are extremely low by reaching down to -32 ‰ vs. PDB. Possibly, a reduced plant bioproductivity caused high amounts of $^{12}\text{CO}_2$ in the lake water and thus very low $\delta^{13}\text{C}$ values in the sedimentary record. After this large decrease, $\delta^{13}\text{C}$ values and bioproductivity were slowly increasing again.

Tab. 5: Overview of sedimentological implications of the outcrop units of PG2038-1 revealed by geochronological, sedimentological, and biogeochemical investigations; the deduced thermokarst stages are discussed in Chpt. 5.3

Unit	I	II	III	IV	V	VI
Thermokarst stage (see Chpt. 5.3)	a	a-b	b	b	c	d
Cal ¹⁴C AMS yr BP (dbs)⁴	12,819 ± 90 (330 cm)	8,576 ± 52 (295-300 cm)	19,139 ± 219 (185-190 cm)	8,217 ± 76 (123 cm)		854 ± 48 / 966 ± 23 (25-30 cm)
Clastic sediments	Terrigenous fine sand & fine silt	Relocated terrigenous fine sand & fine silt	Interchanging lacustrine fine silty, partly illite-enriched detritus & relocated terrigenous sand	Relocated terrigenous fine sand & lacustrine fine silty detritus	Lacustrine fine silty, illite-enriched detritus	Fine silty detritus & middle-coarse silt by frost weathering
Organic matter source	Terrigenous peat	Terrigenous peat	Lake algae with high bioproductivity & terrigenous plant remains	Mainly terrigenous plant remains	Lake algae with very low bioproductivity	Terrigenous peat
Depositional environment	Subaerial	Subaerial to semi-terrestrial	Shallow lacustrine	Lacustrine	Deep lacustrine	Subaerial in-situ

5.1.4 The question of carbonate existence

It still remains unresolved whether or not inorganic carbon exists in the sediments of Lake El'gene-Kyuele. The calculated CaCO₃ values of the profile sections III, V, and VI are prominent. However, a complete absence of carbonates occurs in samples of low measured TIC values because minor measurement differences of the CNS and TOC elemental analysers are considered: The measured control standards of the TC measurement deviated about -0.5 % and of the TOC measurement about 0.62 % from their default values, and the relative standard deviation of the control standards at the TC and TOC measurements are about 0.966 % and 0.079 %, respectively.

HCl tests as an evidence for the existence of TIC showed little reaction of some samples.

⁴ This does not represent the accumulation age of the outcrop unit but the age of the measured radiocarbon samples

However, apart from carbonates, other chemical compounds, such as pyrite, react with HCl, as well. The absence of the minerals calcite and aragonite in the El'gene-Kyuele catchment during XRD measurement and also during preceding investigations (Biskaborn et al., in press) indicate the absence of CaCO₃ in the local sediments.

5.1.5 Application of the radiocarbon ages

The radiocarbon ages were applied for a chronological orientation and for a correlation with the Late Quaternary sedimentary history. Reservoir effects are probably insignificant in the lake catchment, because the absence of active volcanism and old carbonates indicates that ¹⁴C only originates from atmospheric carbon. A post-sedimentary cryogenic mixing of the radiocarbon samples is also unlikely, because they did not stay within the active layer during most time. However, especially the radiocarbon ages emphasize the high geomorphological activity of an Arctic thermokarst landscape. The outcrop PG2038-1 has an average sedimentation rate of 0.26 mm/yr from the lowermost, presumably in-situ radiocarbon sample at 330 cm dbs to the top.

Because of the doubtful age-depth-distribution of PG2038-1 especially of the samples in unit III (8,217 ± 76 cal. yr BP) and in unit IV (19,139 ± 219 cal. yr BP), the radiocarbon dates are regarded critically. They represent the age of older reworked deposits but not the age of deposition at the study site. This is especially indicated by the conspicuous age inversion and by the correlation of samples to fluctuating sediment facies. For instance, the radiocarbon sample in unit III was found in combination with fine-sandy layers that have a different origin than the silty matrix. The material represents old organic matter of reworked Ice Complex deposits but does not represent the prevailing accumulation of lacustrine detritus during that time. Because of absent plant remains, the lacustrine phases of the units III and V could not directly be dated.

The two lowermost radiocarbon samples can possibly, but not certainly, reflect an in-situ sedimentation because the *Larix* cone at 295-300 cm dbs (8,576 ± 52 cal. yr BP) appeared nearby a fossil larch trunk and in chronological continuation of the peat at 330cm dbs (12,819 ± 90 cal. yr BP).

Bark remains of the uppermost radiocarbon samples at 25-30 cm dbs were dated in order to achieve a temporal approximation of the end of the lacustrine stage at PG2038-1. It represents the transition from mostly minerogenic lacustrine detritus, to subrecent

terrestrial peat deposits in the upper unit VI that do not have lacustrine features in its clastic sediments, biogenic proxies, and macrofossil assemblage. The first subsample of the bulk organic fraction has a radiocarbon age of 854 ± 48 cal. yr BP, whereas the second subsample of the humin fraction reached 966 ± 23 cal. yr BP. The bulk organic fraction is also affected by younger humic acids as a part of the humified soil organic matter (Blume et al., 2009). Thus, the broadly resembling ages make the sedimentation date of the bark remains somewhat more reliable because few impurities of a younger or older age have been mixed-in later by pedogenesis.

5.2 Vegetation reconstruction and palaeoenvironmental implications

Plant macrofossil analysis has different advantages compared to palynological studies: Species can often be determined at the precise taxonomic level (Birks and Birks, 1980) and the occurrence of plant macrofossils is more restricted to their origin than pollen, facilitating the spatial reconstruction of the past vegetation and of local environmental conditions (e.g. Kienast et al., 2011, 2008, 2005). However, in loose sediments at Lake El'gene-Kyuele, different transport mechanisms have caused a relocation of plant parts. Birks (1991) demonstrated how terrestrial plant remains in Arctic lake environments are transported by wind during winter and by melt-water and stream-water during summer (Fig. 23). Because of large debris flows, fragile plant macrofossils, such as fossil leaves, were often destroyed, whereas robust nutlets persisted. Therefore, the spatial composition of the palaeovegetation neither at the position of PG2038-1 nor at any other certain location cannot exactly be reconstructed. However, the macrofossil assemblage provides the reconstruction where and under what circumstances the samples originate by applying the principle of uniformitarianism.

The plant macrofossil analysis has revealed a different palaeovegetation compared to today (Binney et al., 2009; CAVM Team, 2003), indicating different palaeoenvironmental and palaeoclimatic conditions. For reconstruction of the past vegetation and implications on local thermokarst processes, the determined plants were grouped according to their ecological requirements following Kienast et al. (2008, 2005, 2001). The plant communities cannot be strictly separated, because they merge at their transitions and may appear as combinations (Kienast et al., 2008). In addition, the nearby occurrence of taxa with different environmental requirements indicate a little spatial differentiation of plant communities.

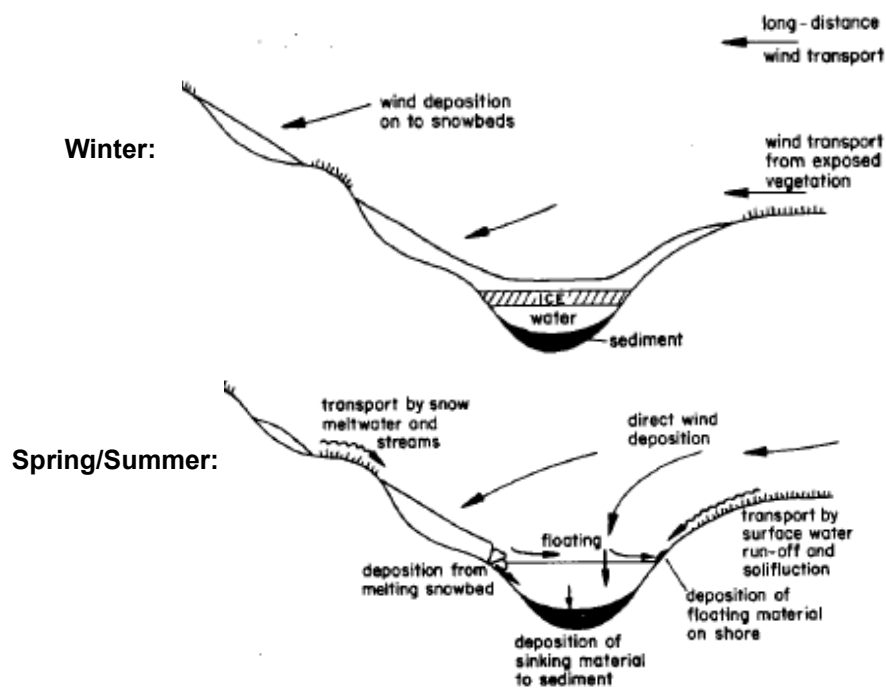


Fig. 23: Relocation procedures of plant remains into lakes in Arctic environments north of the tree-line during winter by wind transport and during summer by water run-off (Birks, 1991)

Shrub tundra

Tundra shrubs have possibly formed a large portion of the vegetation cover throughout the entire thermokarst evolution of Lake El'gene-Kyuele, which is indicated by the abundant occurrence of Betulaceae plant macrofossils in the sedimentary archive of PG2038-1. In general, the plant community of shrub tundra (Betulo–Adenostyletea, Br.–Bl. et R. Tx. 1943) is wide-spread and exists in circum-Arctic environments (CAVM Team, 2003). In the study area, it has been represented by the Betulaceae species *Betula nana* and *Alnus fruticosa* (synonym: *Duschekia fruticosa*), and by the Ericaceae species *Arctous rubra* and *Vaccinium vitis-idaea*.

In the surroundings of Lake El'gene-Kyuele, different morphological occurrences of shrub tundra were observed. Erect dwarf-shrub tundra (category *S1*) occurs in elevated and exposed areas (climatic subzone: *D*) of Pleistocene accumulation plains (Fig. 27, CAVM Team, 2003) that are characterized by more unfavourable circumstances for vertical plant growth. In topographically protected areas on the thermokarst slopes, taller individuals of low-shrub tundra occur (Fig. 25b, category: *S2*, subzone *E*) due to milder conditions by the

attenuation of fierce winds and the prevention of waterlogging at well-drained inclinations. During winter, snowdrifts pile up at lee positions and form a protective cover for plants against wind abrasion and severe frost. Taller shrubs indicate the proximity of the study area to the northern tree-line (Shahgedanova and Kuznetsov, 2003). However, such a morphological distinction of the shrubs is not possible for the fossil record by observation of the macrofossil assemblage.

Forest tundra and the northern treeline

The forest tundra, or northern taiga (Vaccinio-Piceetea Br.–Bl. 1939), is associated with the presence of trees, which occurred in the study area during the Holocene Thermal Maximum (HTM) as a part of the Early Holocene. In the outcrop PG2038-1, larch remains were dated back to ~8,500 cal. yr BP, whereas Biskaborn (2012, personal communication) found evidence for larch trees around Lake El'gene-Kyuele between >10,000 and ca. 6,500 cal. yr BP. In addition, *Larix* remains were also recorded in unit I of PG2038-1 as remains of the Late Pleistocene. The more northerly presence of larch trees during the Late Pleistocene and the Early Holocene compared to today is also reported by Binney et al. (2009). Within the outcrop PG2038-1, larch remains occur alongside abundant shrub remains of Betulaceae and Ericaceae, indicating open taiga woodlands with tundra elements.

The northernmost occurrence of larch and birch trees in Siberia is associated to the northern tree-line (Fig. 24, Binney et al., 2009; Shahgedanova and Kuznetsov, 2003). The macrofossil finds of this study are in accordance with the reported northern migration of trees during the HTM (Binney et al., 2009; MacDonald et al., 2000). Binney et al. (2009) reported about the common occurrence of birch trees during the early Holocene along the northern coastline. The northern tree-line in Siberia is not a consistent line but stretches along a broad terrain up to several hundreds of kilometres and forms a gradual transition from tundra to taiga (Franz, 1973). The presence of azonal forests is reported to occur north of the tree-line as isolated patches, e.g. alongside rivers 2 km north-east of Lake El'gene-Kyuele (Biskaborn et al., in press).

The remains of tree taxa were accompanied by charcoal remains, indicating the occurrence of fires during the early Holocene. Increased fires were also reported for the same period at central Yakutian study sites (Biskaborn et al., 2012a; Katamura et al., 2009; Werner et al., 2010). However, compared to these studies, fires at Lake El'gene-Kyuele occurred in a far

more northerly region. Past fires in the Arctic were also implicated by Murton (2001) regarding his charcoal finds in thermokarst structures of the Canadian Tuktoyaktuk Coastlands. Katamura et al. (2009) connected increased fires with the formation of thermokarst lakes in central Yakutia about 11,000-9,000 cal yr BP. That correlation does also occur in this study. In addition, Early Holocene fires largely affected older peat and wood remains of Late Pleistocene origin as well, possibly generating a hiatus in the Pre-Holocene plant macrofossil archive.

Lastly, Kremenetski et al. (1998), MacDonald et al. (2000), and Wolfe et al. (1999) reported about the retreat of boreal forests and the wide establishment of tundra in Northern Siberia at about 4,000 cal. yr BP.

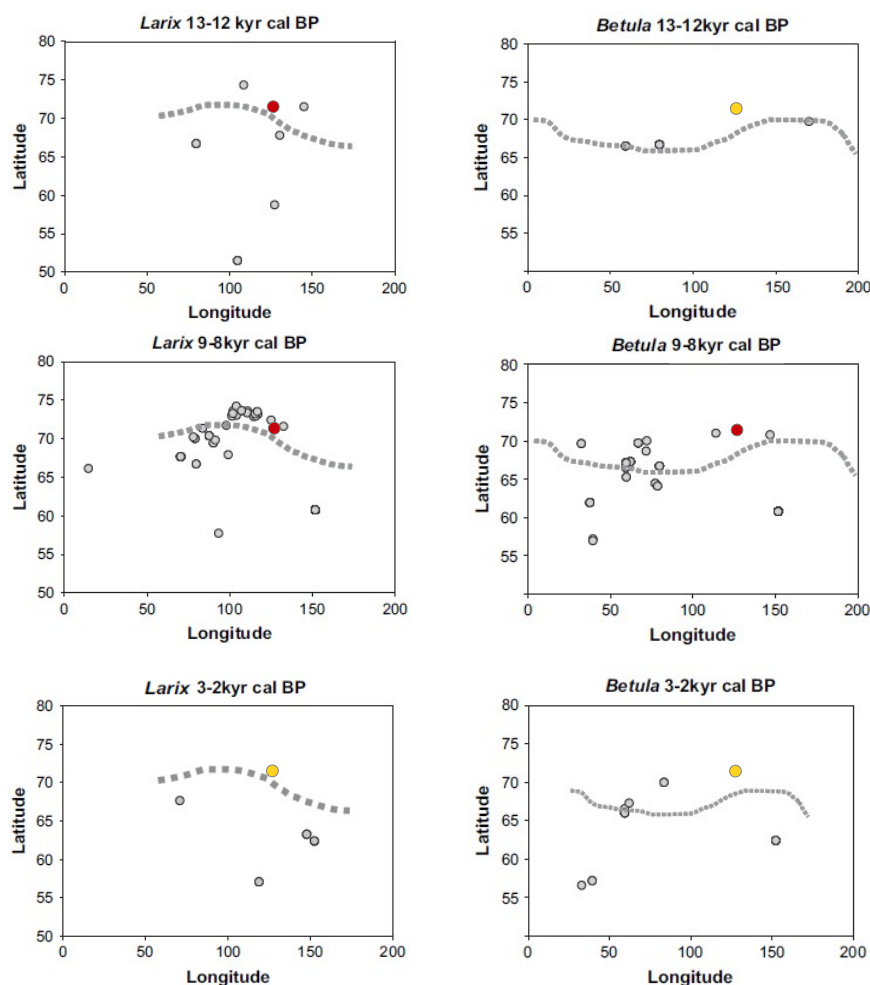


Fig. 24: Late Quaternary occurrence of *Larix* and *Betula* trees in northern Eurasia according to (Binney et al., 2009, modified); the dashed lines indicate the modern range limits of both taxa; the coloured points indicate the approximate location of Lake El'gene-Kyuele (71°17'N, 125°34'E); red points: macrofossil finds, yellow points: no macrofossil finds

Aquatic plants

Aquatic vegetation is represented by the communities *Potamogetonetea pectinati* R. Tx. & Prsg. 1942 and *Charatea fragilis* Fukarek ex Krausch 1964. The determined taxa are *Potamogeton* cf. *vaginatus*, *Potamogeton filiformis*, *Hippuris vulgaris*, and Characeae sp. Aquatic vegetation is associated with lacustrine sediments in the units III, IV, and V. All recorded plants are indicative for shallow lakes and ponds of boreal environments with circumneutral to slightly alkaline, and oligotrophic to mesotrophic freshwater (Dierßen, 1996). *H. vulgaris* likely occurs in brackish ponds and lakes with fluctuating water level, whereas *P. vaginatus* and *P. filiformis* are reported to be adapted on fluctuating salt contents caused by aridity (Kienast et al., 2008, 2005). The community *Charatea fragilis* commonly builds up turfs on the lake floor of the littoral and sublittoral zone (Dierßen, 1996). As far as sufficient sun light penetrates the water. Characeae occur deeper than the above mentioned plants, which is thus indicating the possibly deepest lacustrine stage of the archive PG2038-1 in unit V.

Wetland vegetation

The study of multispectral satellite data shows that soils within a transect from the thermokarst basin margin towards the lake are characterized by increasing organic matter content, and decreasing drainage and active layer depth (Ulrich et al., 2009). Consequently, possible concentric variations of the vegetation cover occur within the thermokarst basin. Plants of the wetland community *Scheuchzerio-Caricitea nigrae* (Nordh. 1936) R. Tx. 1937, which possibly occurred in a close circle around the lake, were recorded alongside the above mentioned *Larix* remains of Early Holocene origin. In the archive PG2038-1, the plant community is represented by the occurrence of *Eriophorum brachyantherum*, different *Carex* sect. *Phacocystis*, *Epilobium palustre*, and *Trichophorum uniflorum*. Nowadays *E. brachyantherum* and *Carex* sp. are common on moist locations in the surroundings of Lake El'gene-Kyuele (Fig. 25d). According to Kienast et al. (2008), *E. brachyantherum* is indicative for the proximity to the tree-line. Wetland plants are reported to be accompanied by abundant moss remains that generally grow densely beneath a relatively homogeneous plant cover (Fig. 25c, Matveyeva, 1994). The underlying soil substrate of this wetland community commonly includes oligotrophic to mesotrophic sediments, a thick peat layer, and high water contents (Dierßen, 1996; Matveyeva, 1994). Therefore, the plant remains

possibly originate from near-shore environments or from polygon mires with a shallow active layer.

Vegetation adapted to low moisture

Interestingly, the relocated terrigenous sediments of the units II and III contain different macrofossils that belong to plants adapted to low or fluctuating ground moisture. Steppe vegetation (Koelerio-Corynephoretea Klika ap. Klika & Nowák 1941) is represented by *Potentilla* cf. *stipularis*, *P.* cf. *arenosa*, *P.* cf. *hyarctica*, and cf. *Dryas octopetala*, which also occurs as a part of dwarf shrub tundra. These species are associated to dry sandy and often disturbed substrates with few soil organic matter (Dierßen, 1996). *Potentilla* cf. *nivea* is associated to diverse Arctic upland vegetation (Carici rupestris–Kobresietea Ohba 1974), indicating exposed locations with harsh climatic conditions and dry to moderately wet ground (Dierßen, 1996; Kienast et al., 2008; Matveyeva, 1994). The species *Cerastium* cf. *arvense* and *Papaver* sect. *Scapiflora* in the units I to III are associated to Arctic pioneer vegetation (*Thlaspithea rotundifolia* Br.-Bl. 1948), which occurs on terrain with coarse debris and increasing ground disturbances (Dierßen, 1996). Macrofossils of Poaceae grasses were not recorded in the fossil archive, possibly due to a worse state of preservation compared to other plant families.

In general, the occurrence of plants adapted to low moisture does not fit into the prevailing moist or aquatic, lacustrine environment of the units II and III. More likely is the possible input into the thermokarst basin by relocation from up-slope sites as demonstrated by Birks (1991). The environmental requirements of the plants indicate an origin from the exposed uplands. However, also older reworked Ice Complex deposits are a possible origin of meadow and steppe communities, because they were wide-spread in northern Siberia during the late Pleistocene (Andreev et al., 2011; Kienast et al., 2001). The so called tundra steppe was widely composed of Poaceae, Cyperaceae, *Artemisia*, Brassicaceae, and Caryophyllaceae that were associated to a climate of increased aridity and a higher continentality than today, caused by the far regression of the Arctic Sea (Andreev et al., 2011).

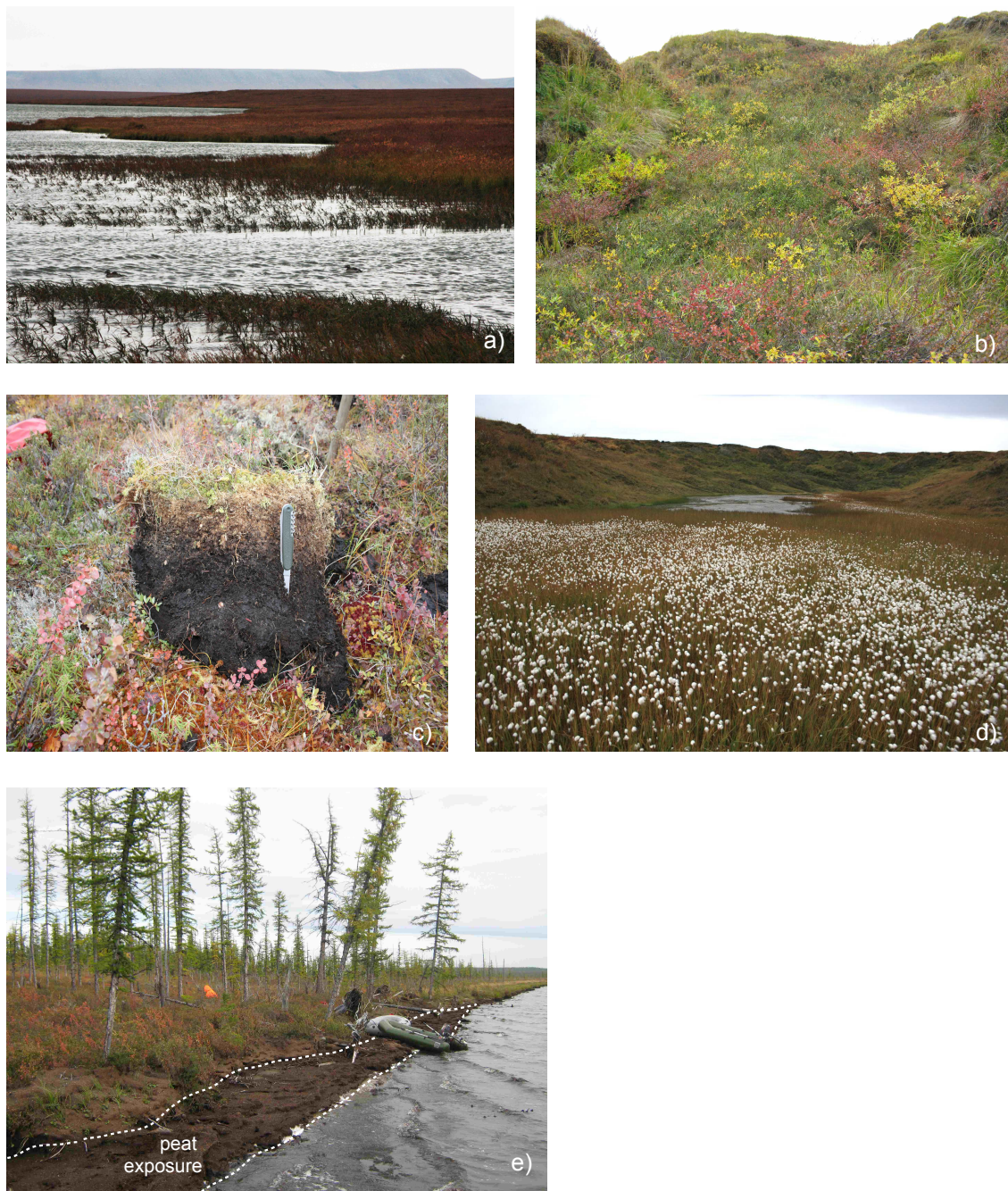
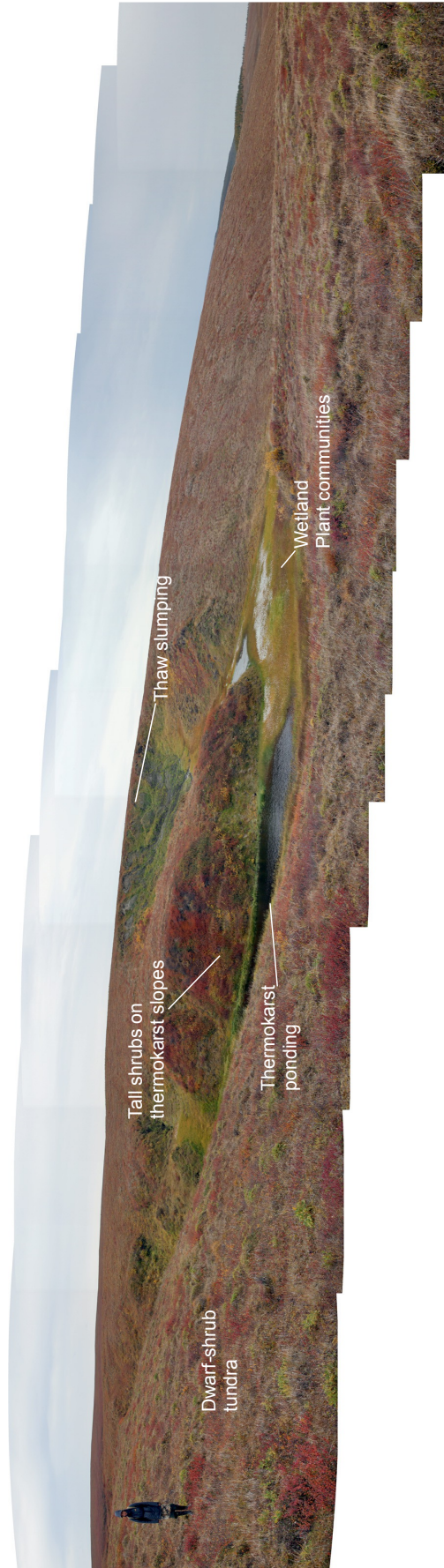


Fig. 25: Plant communities at Lake Elgene-Kyuele: a) littoral aquatic vegetation at the shoreline (photo by B.Biskaborn), b) taller low-shrub tundra at the thermokarst slope (photo by G.Müller), c) dense moss turfs above poorly decomposed peat of wetland communities close to the northern taiga Lake Kyutyunda (69°37,89' N, 123°39,42' E); similar material is reconstructed in the fossil record of El'gene-Kyuele (photo by G.Müller), d) wetland communities with abundant *Eriophorum brachyantherum* at a moist meadow (photo by B.Diekmann), e) Exemplary depiction of Lake Kyutyunda showing the shoreline in a northern taiga environment of Yakutia as it possibly occurred at Lake El'gene-Kyuele during the early Holocene; note the exposure of peat to wave abrasion as an example of the uncomplicated contribution of terrestrial plant remains into a lacustrine milieu (photo by G. Müller, modified)

Fig. 26:



Panoramic view of the Ice Complex accumulation plain north of Lake El'gene-Kyuele, which is dissected by different thermokarst structures including: ponding, thermoerosive valleys, and permafrost back-wearing with thaw-slumps at steep slopes; observable plant communities are dwarf-shrub tundra on the exposed uplands, taller tundra shrubs at the thermokarst slopes, and green wetland vegetation in the thermokarst basins and valley floors (photography by B.Diekmann, modified)

5.3 Late Quaternary thermokarst basin evolution and relative lake level variability

Thermokarst related evolution of sedimentary basins can generally be defined as a pre-depositional basin genesis as described by Einsele (2000), where sediment dynamics occur as a consequence of topographic changes. Relief subsidence causes sediment accumulation, whereas uplift is accompanied by erosion and sediment run-off. The sedimentological findings of this study indicate that the relative lake level has changed significantly at the eastern shore during the Late Quaternary. This chapter presents a reconstruction of the different stages of thermokarst evolution depending on the palaeoclimatic setting. The temporal variations of the depositional environments at the eastern slope of Lake El'gene-Kyuele in correlation to the topographic variations of the thermokarst basin are depicted in Fig. 27. I hereby propose the distinction of 4 stages of lake and basin evolution named by the letters from (a) to (d).

Late Pleistocene

During the Last Glacial Maximum, thermokarst processes were neither recorded in the study area nor in other study areas in the Siberian Arctic (e.g. Romanovskii et al., 2000). It is rather likely that pre-existing lakes of Eemian interglacial origin (Kienast et al., 2011) were destroyed by the wide-spread formation of Ice Complex accumulation plains.

The first stage (a) of Late Quaternary thermokarst evolution occurred during the ending Late Pleistocene a.k.a. Bølling-Allerød interstadial. This period was characterized by a climate amelioration in Yakutia (Müller et al., 2009) and in the Arctic (Andreev et al., 2009) with dry and continental conditions. For the Laptev Sea region, Andreev et al. (2011, 2009) and this study found evidence about even more favourable conditions for plant growth than today. The first large formation of thermokarst basins during the Bølling-Allerød interstadial was recorded in the Kolyma lowlands in NE Yakutia (Romanovskii et al.; 2000). However, the stage (a) of this study comprises a terrestrial to semi-terrestrial environment characterized by large accumulation of plant detritus (peat formation). For this phase, lacustrine characteristics have not been recorded at PG2038-1 but *Daphnia* eggs and plants adapted to wet ground (e.g. *Eriophorum brachyantherum*) indicate increasingly moist conditions. This is indicative for polygon ponds and mires that commonly form seasonally moist micro-habitats (Wolter, 2010). The lacustrine sediment archive PG2037 from the current central bottom of Lake El'gene-Kyuele includes similar peaty deposits at a core

depth of 390-450 cm db, at which radiocarbon ages also reach back to the Late Pleistocene (Biskaborn, 2012, personal communication). In addition, both archives contain highly minerogenic deposits beneath the peat layer, possibly representing the bedrock of Ice Complex sediments that subsided by talik formation. Thus, during the Late Pleistocene, probably large amounts of terrestrial phytomass was built-up, whereas thermokarst-related lake formation possibly proceeded later during the Holocene (Fig. 27).

However, regardless the above mentioned findings, it is still possible that thermokarst processes already occurred during the Late Pleistocene because this study can neither prove nor falsify that Lake El'gene-Kyuele already existed earlier at a smaller extent and/or another location. For the subsequent Younger Dryas cold period, Romanovskii et al. (2000) supposed the preservation of those lakes that already appeared during the Bølling-Allerød interstadial.

Early Holocene – Thermokarst initiation and lake growth

During the Holocene, the Arctic climate has undergone a sequence of minor climate fluctuations, which likely affected thermokarst processes in Northern Yakutia, i.e. the Holocene thermal maximum (HTM), the Neoglaciation, the Medieval Warm Period (MWP), and the Little Ice Age (LIA) (Miller et al., 2010a; White et al., 2010). The Early Holocene is certainly the period of the initiation of large thermokarst processes and the rapid expansion of Lake El'gene-Kyuele, including the stages (b.1) and (b.2) (Fig. 27). Because of high ice contents in Ice Complex sediments, the major terrain subsidence and shoreline retreat possibly occurred rapidly during a short period (Romanovskii et al., 2000). In the Laptev Sea region, the HTM already occurred during the Early Holocene: thus according to Andreev et al. (2004), the warmest mean temperatures during the Holocene, which were up to 2-3 °C warmer than today, occurred between ca. 10,300-9,200 cal. yr BP in the Lena Delta area, while increased temperatures lasted for the consequent six millennia. That period coincides with the results of this study and of the investigations by Biskaborn (2012b), of which radiocarbon dated finds of *Larix* macrofossils support warmer summer temperatures during the earliest Holocene. Correspondingly, Biskaborn et al. (2012a) demonstrated a delay of the onset of the HTM towards more southerly Yakutian regions, which possibly occurred in this study area, as well.

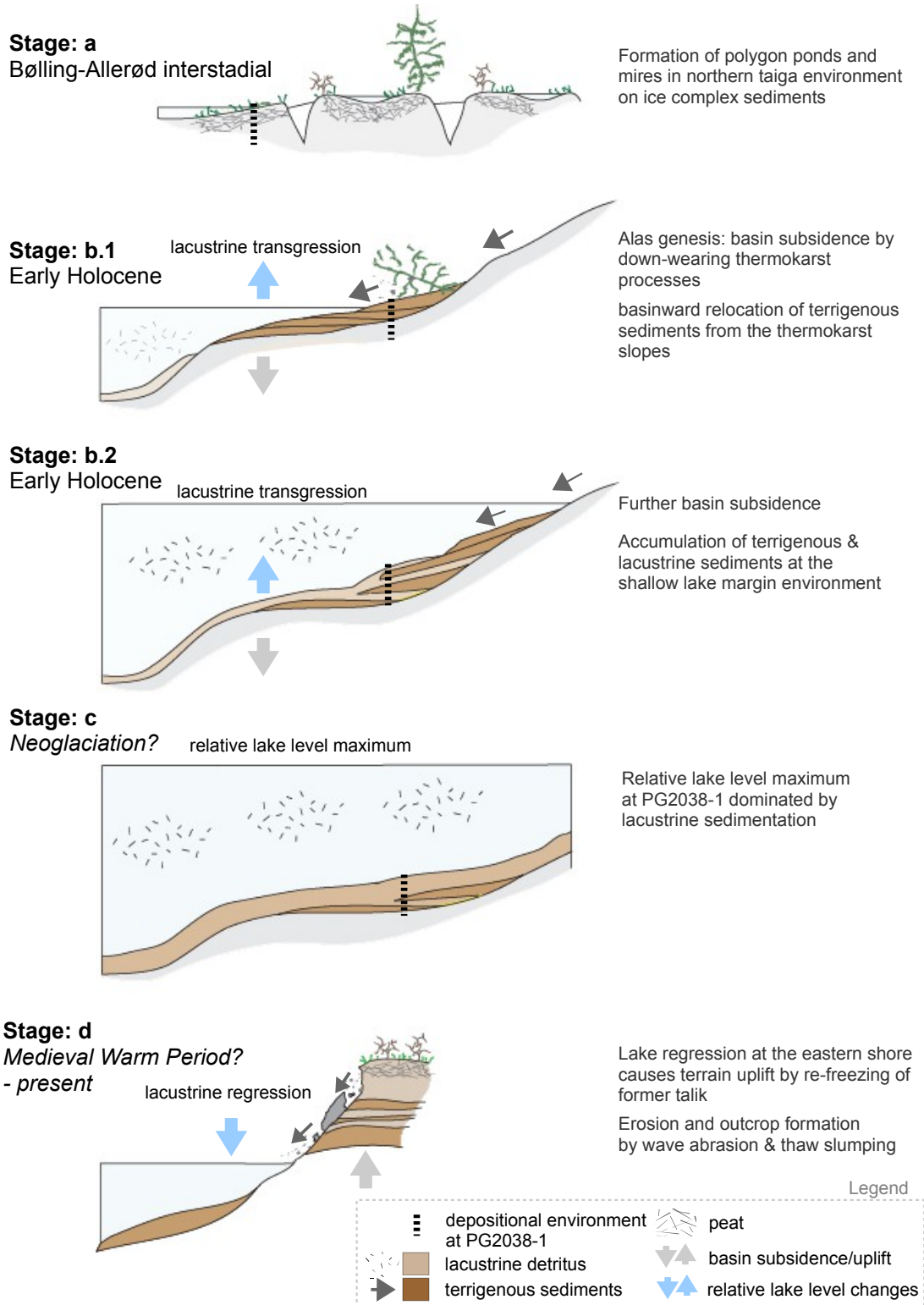


Fig. 27: Stages of Late Quaternary basin evolution, relative lake levels, and depositional environments at the eastern slope of Lake El'gene-Kyuele

The stage (b.1) is regarded as the initiation of thermokarst related processes in the study site. It is characterized by the increasing appearance of topographic changes and relief dissection, which is indicated by the high input of terrigenous clastic sediments and plant detritus. During this stage, thermokarst activity by down-wearing permafrost degradation caused terrain subsidence as described by Czudek and Demek (1970). The alas depression has consequently worked as a sink that increasingly favoured the accumulation of sediments and the concentration of melt-water. According to French (2007), the input of slope sediments is able to counteract and even reverse lake growth. However, during stage (b) lake transgression prevailed at Lake El'gene-Kyuele, causing the change from a terrestrial to a lacustrine environment. According to the concept of sequence stratigraphy, the different overlapping layers of incoming terrigenous sediments tend to stack up a retrograding stratification where water depth and distance to the shore increase (Van Wagoner et al., 1990). Terrigenous slope sediments, which are likely to create alluvial fans, mostly settled at the littoral zone and lake shelf.

During stage (b.2) the lake level was further rising, the distance to the shore increased, and the thermokarst basin subsided by talik formation. An increased water depth caused the beginning accumulation of lacustrine detritus. However, the archive PG2038-1 was still situated close to the margin of the lake basin where slope sediments could reach the study site. These circumstances led to relatively abrupt facies changes of alternating lacustrine detrital and terrigenous sediment layers as described by (Biskaborn et al., in press). Slope lateral input of terrigenous sediments has possibly also occurred as large catastrophic events because a thick package reached the basin bottom during a phase of an increased lake level, which is recorded e.g. in unit IV (105-145cm dbs) of the archive PG2038-1.

Lake level maximum

The stage (c) comprises a lacustrine stage with the relative maximum of the lake level at the outcrop site, which is witnessed by the accumulation of large and relatively homogeneous amounts of lacustrine detritus and the occurrence of Characeae oospores in unit V. The larger lake extension is implicated by the palaeo-shoreline and thermokarst basin margin several hundred metres east of the current eastern shoreline (Fig. 28). During the evolution of Lake El'gene-Kyuele, stage (c) has been the longest period by ranging about >7,000 yr, which is indicated by the radiocarbon ages and by the commonly slow sedimentation rate of lacustrine detritus in lakes of cold environments about <0.5 mm/yr (e.g. Biskaborn et

al., 2012a; Müller et al., 2009). Compared to this, earlier terrigenous sediment input occurred more rapidly as abrupt events.

The lake level maximum was further preserved by cooler climatic conditions and possibly stagnated during the Neoglaciation period, which slowly established about 4 kyr BP (Miller et al., 2010a). The more reduced annual thawing of the active layer precluded talik growth and lake drainage. In addition, a shallower active layer reduced permafrost degradation at the thermokarst slopes, and provided geomorphological stability that impeded thaw-slumps and debris flows towards the lake basin. Beneath the seasonally prolonged ice-cover, lacustrine detritus settled homogeneously. Lastly, a long seasonal ice-cover caused extremely low algae growth and low bioproductivity rates within the lake as indicated by the lowest recorded $\delta^{13}\text{C}$ values.

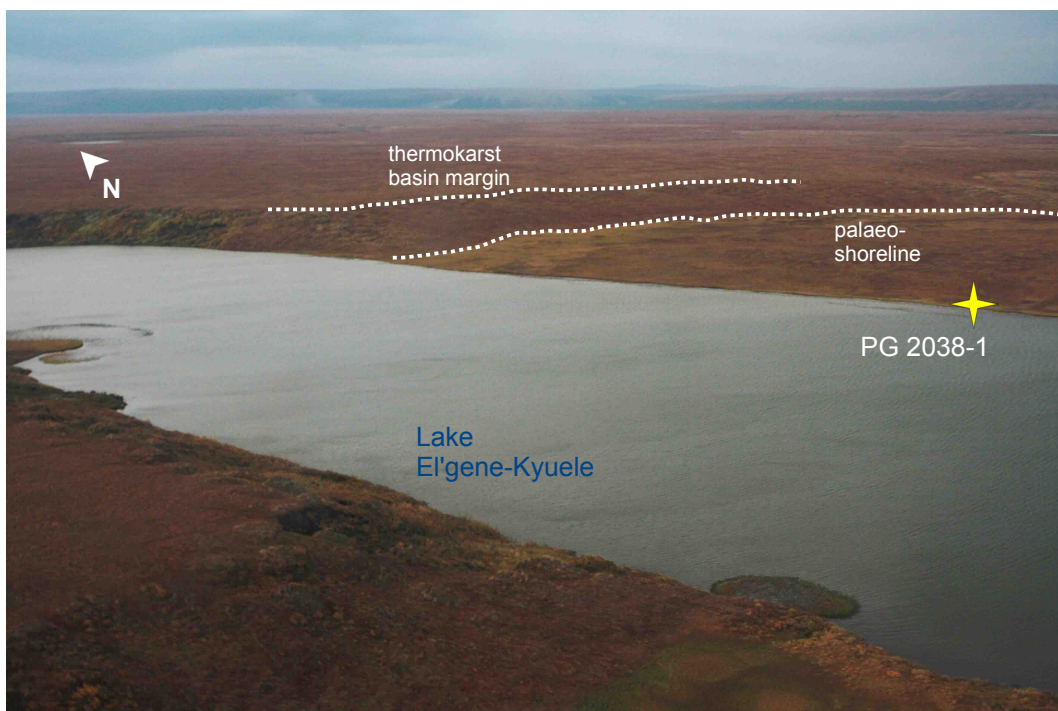


Fig. 28: Aerial view of the eastern margin of the El'gene-Kyuele thermokarst basin with the parallel palaeo-shoreline according to Biskaborn et al. (in press) and the approximate location of PG2038-1 as a part of the former lake bottom

Lacustrine regression

Lacustrine regression during stage (d) occurred approximately 1,000 yr BP according to the basal radiocarbon age of the uppermost peat about 966 ± 23 cal. yr BP. The retreat of the lake water facilitated the uplift of the thermokarst basin by re-freezing of former talik (Fig. 27). The shoreline thus prograded to the modern location of PG2038-1, facilitating the outcrop formation by wave abrasion and thaw slumping. Consequently after the lake regression, the uppermost outcrop section got exposed to subaerial conditions and has thus been affected by soil genesis and in-situ peat accumulation.

The lacustrine regression is likely triggered by drainage of Lake El'gene-Kyuele due to constant talik growth as described by (Czudek and Demek, 1970). Besides the modern southerly outflow, drainage possibly also occurred through a former additional outflow in E-NE-direction towards the Olenyok catchment. North-east of Lake El'gene-Kyuele, the lake catchment and the eastern palaeo-shoreline is directly connected with another large and widely drained thermokarst basin (Fig. 29).

Apart from drainage, the lake possibly also migrated in a westerly direction as it is carving into steep Ice Complex sediments to the north-west. The shoreline was characterised by differential silting in the east and lake transgression in the west. However, thermokarst- and lacustrine sediments of an Early Holocene age also occur in more western lake archives (Biskaborn et al., in press; Biskaborn, 2012b), implicating a westerly lake migration less pronounced than lake expansion and drainage.

However, it is not fully clear why exactly drainage occurred during that time. One possible explanation is a brief period of climate amelioration, i.e. the Medieval Warm Period (MWP), which caused talik growth and lake drainage. The investigation of chironomids and palynological data in the Lena Delta indicated somewhat warmer temperatures between ca. 2,300-1,400 cal. yr BP (Andreev et al., 2004). However, the MWP was mostly recorded in the Western Arctic but is not described as a global phenomenon (Hughes and Diaz, 1994; Miller et al., 2010a). In addition, a number of studies demonstrated how thermokarst processes and lake drainage are not necessarily controlled by climate variability (Biskaborn et al., in press; Burn and Smith, 1990; Katamura et al., 2009; Morgenstern et al., 2011). Thus, drainage is a common feature of large thermokarst lakes and strongly limits lake expansion (Czudek and Demek, 1970; Huissteden et al., 2011).

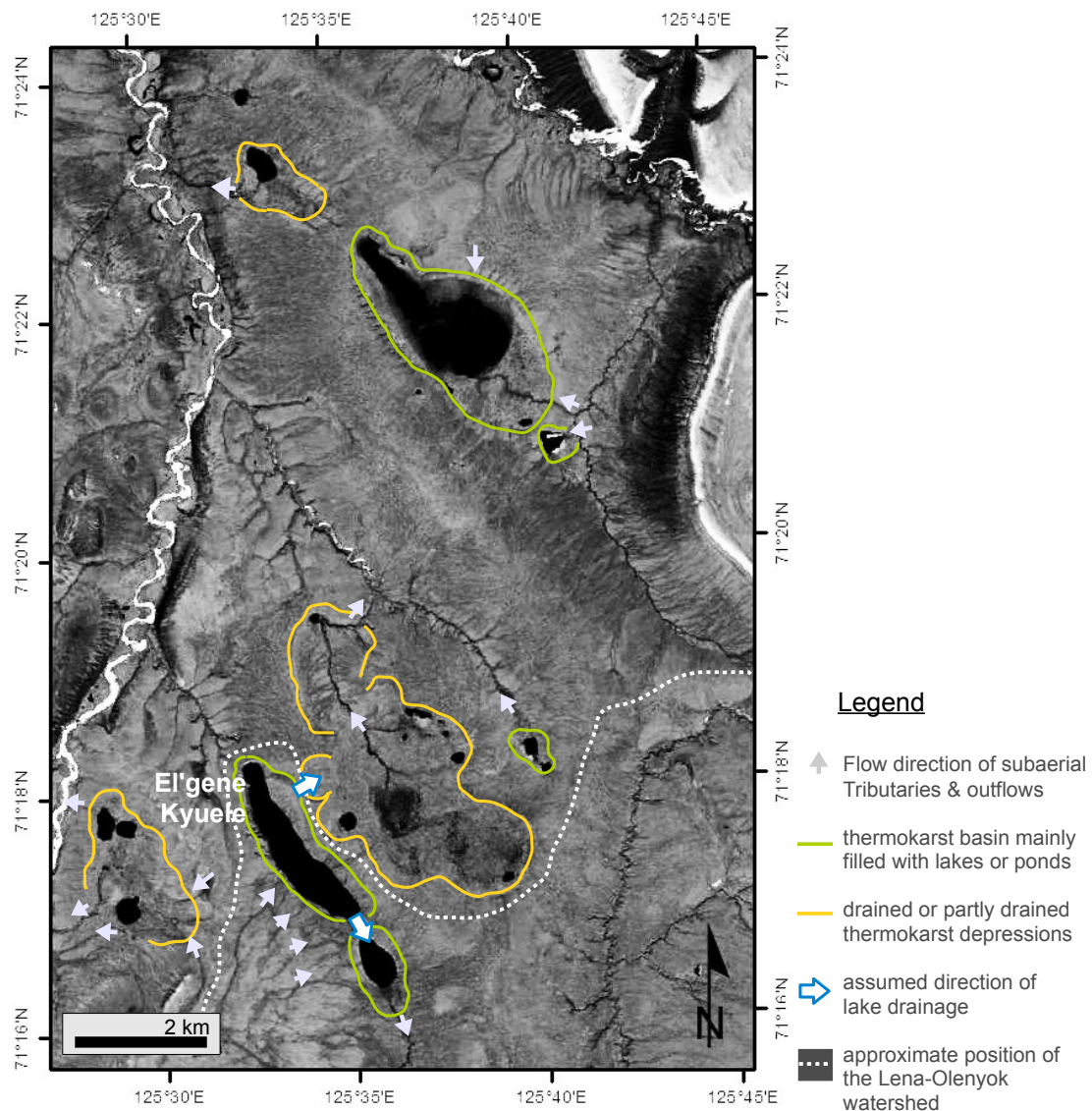


Fig. 29: Thermokarst basins at the Lena-Olenyok watershed manually digitized along their upper margins, including water-filled basins (green), drained/partially drained basins (yellow), and the approximate position of the Lena-Olenyok watershed (white dashed line); the broad blue-marked arrows indicate the assumed lake drainage directions; image available at: <http://geofuse.geoeye.com/landing/Default.aspx> (accessed 17th November 2012), modified.

Since the second half of the 20th century, the Arctic regions are confronted by a significant warming trend that is widely ascribed to the anthropogenic release of greenhouse gases (e.g. ACIA, 2005; IPCC, 2007). Correspondingly, thermokarst lakes are highly affected by this warming trend with regional peculiarities: Ponds in the high Arctic and thermokarst lakes in Siberian regions of discontinuous permafrost vanished drastically (Smith et al.,

2005; Smol and Douglas, 2007). Simultaneously, an increase of the total lake number and area is reported for northern Siberian areas of continuous permafrost (Smith et al., 2005). The spatial analysis of Landsat satellite images revealed that Lake El'gene-Kyuele had only insignificantly been affected by recent lake surface changes, whereas lakes in the Lena Delta have slightly grown (Pollozek, 2011). Throughout its evolution, the lake has probably never been completely drained because no sedimentological archive, neither at the lake bottom (Biskaborn, 2012b) nor at the current shore, does contain characteristic silting features, such as in-situ peat layers or cryomorphology. As interpreted by Biskaborn et al. (in press), the geological underground of the lake catchment has possibly impeded a complete drainage. However, besides drainage, also sediment input provides shrinkage of thermokarst lakes (French, 2007). Until today, thermokarst sediments have constantly filled the lake basin during the thaw seasons.

Since its formation, Lake El'gene-Kyuele has changed its shape in two different ways: horizontally by growth, drainage, and migration, and vertically by thermally induced subsidence and uplift. The evolution of thermokarst lakes reportedly undergoes cyclic processes that are completed by drainage tapping, silting, re-freezing of former talik, and subsequent uplifting of the basin with the possible formation of epigenetic ice-wedges and pingos (Czudek and Demek, 1970; French, 2007; Hopkins, 1949). Thaw-lake cycles reportedly occur in a relatively short period within a few millennia (French, 2007; Huissteden et al., 2011). At Lake El'gene-Kyuele, an incomplete cycle of lake expansion and partial drainage occurred during a time span of about 7,000 yr. Satellite images of the study area indicate different thermokarst basins that appear to be completely drained (Fig. 29), whereas other lakes such as El'gene-Kyuele are persisting. They are topographically favoured by the geological setting, by the existence of small tributaries, and by a reduced subaerial outflow.

6 Conclusions

Late Quaternary thermokarst processes and the palaeoenvironmental conditions at Lake El'gene-Kyuele were successfully reconstructed by sedimentological, biogeochemical, geochronological, and plant macrofossil analysis of sediments at the eastern shore. This is the main outcome of this study:

1. The thermokarst basin of Lake El'gene-Kyuele has been highly active in the geomorphological sense. Terrigenous input of diamicton is characterized by increased fine-sand contents, high TOC/N ratios, low illite-contents, and terrestrial plant macrofossils. It was provided by the thermokarst slopes and settled in the shallow lake margins. Lacustrine detrital input is characterized by increasing silt and clay contents, low TOC/N ratios, illite-enrichment, and aquatic plant macrofossils and settled in the deeper lake basin.
2. During the Pre-Holocene phase, the study area was characterized by the occurrence of bogs and mires, the presence of larch trees, and the accumulation of peat, while lacustrine features were not recorded.
3. During the Early Holocene/Holocene Thermal Maximum, the thermokarst Lake El'gene-Kyuele rapidly expanded and was characterized by a high limnic bioproductivity. The eastern slope was affected by lacustrine transgression and a relative lake level rise, inducing basin subsidence due to permafrost degradation, and the consequent input of thermokarst slope sediments and later lacustrine detritus. In addition, old, reworked sediments of the Pleistocene Ice Complex were recorded. The vegetation was composed of open taiga communities that included larches, tree birches, and tundra shrubs, implicating the northerly migration of the tree-line compared to today due to more favourable climate conditions. The occurrence of fires affected the vegetation and soil peat and likely triggered thermokarst processes.
4. The maximum lake level at the eastern slope occurred during the longest phase in the life of Lake El'gene-Kyuele, which stagnated throughout the Neoglacial cooling

period. It is indicated by Characeae oospores and by the homogeneous input of lacustrine detritus. The lowest limnic bioproductivity rates were recorded for this stage.

5. Partial drainage and a westerly lake migration occurred approximately 1,000 yr BP. Consequently, the eastern shore was affected by basin uplift and sediment erosion at exposed sites. Lake El'gene-Kyuele has never been completely drained.

References

- ACIA, 2005. Arctic Climate Impact Assessment - Scientific Report. Cambridge University Press.
- Alekseev, M.N., Drouchits, V.A., 2004. Quaternary fluvial sediments in the Russian Arctic and Subarctic: Late Cenozoic development of the Lena River system, northeastern Siberia. *Proceedings of the Geologists' Association* 115, 339–346.
- Allen, C., Darmody, R., Thorn, C., Dixon, J., Schlyter, P., 2001. Clay mineralogy, chemical weathering and landscape evolution in Arctic–Alpine Sweden. *Geoderma* 99, 277–294.
- Anderberg, A.L., 1994. Atlas of seeds and small fruits of Northwest-European plant species with morphological descriptions. Stockholm.: Part 4.
- Andreev, A., Tarasov, P., Schwamborn, G., Ilyashuk, B., Ilyashuk, E., Bobrov, A., Klimanov, V., Rachold, V., Hubberten, H.-W., 2004. Holocene paleoenvironmental records from Nikolay Lake, Lena River Delta, Arctic Russia. *Palaeogeography, Palaeoclimatology, Palaeoecology* 209, 197–217.
- Andreev, A.A., Grosse, G., Schirrmeister, L., Kuznetsova, T.V., Kuzmina, S.A., Bobrov, A.A., Tarasov, P.E., Novenko, E.Y., Meyer, H., Derevyagin, A.Y., others, 2009. Weichselian and Holocene paleoenvironmental history of the Bol'shoy Lyakhovsky Island, New Siberian Archipelago, Arctic Siberia. *Boreas* 38, 72–110.
- Andreev, A.A., Schirrmeister, L., Tarasov, P.E., Ganopolski, A., Brovkin, V., Siegert, C., Wetterich, S., Hubberten, H.W., 2011. Vegetation and climate history in the Laptev Sea region (Arctic Siberia) during Late Quaternary inferred from pollen records. *Quaternary Science Reviews* 30, 2182–2199.
- Balter, M., 2006. Radiocarbon Dating's Final Frontier. *Science* 313, 1560–1563.
- Beijerinck, W., 1947. *Zadenatlas der Nederlandsche flora, ten behoeve van de botanie, palaeontologie, bodemcouteur en warenkennis, omvattende, naast de inheemsche flora, onze belangrijkste cultuurgewassen en verschillende adventiefsoorten*. H. Veenman, Wageningen.
- Bengtsson, G., Bengtson, P., Månsson, K.F., 2003. Gross nitrogen mineralization-, immobilization-, and nitrification rates as a function of soil C/N ratio and microbial activity. *Soil Biology and Biochemistry* 35, 143–154.
- Berggren, G., 1981. *Atlas of Seeds and Small Fruits of Northwest-European Plant Species: Cyperaceae*. Statens naturvetenskapliga forskningsråd (distr.).
- Beuselinck, L., Govers, G., Poesen, J., Degraer, G., Froyen, L., 1998. Grain-size analysis by laser diffractometry: comparison with the sieve-pipette method. *CATENA* 32, 193–208.
- Binney, H.A., Willis, K.J., Edwards, M.E., Bhagwat, S.A., Anderson, P.M., Andreev, A.A., Blaauw, M., Damblon, F., Haesaerts, P., Kienast, F., others, 2009. The distribution of late-Quaternary woody taxa in northern Eurasia: evidence from a new macrofossil database. *Quaternary Science Reviews* 28, 2445–2464.
- Birks, H.H., 1991. Holocene vegetational history and climatic change in west Spitsbergen-plant macrofossils from Skardtjørna, an Arctic lake. *The Holocene* 1, 209–218.
- Birks, H.J.B., Birks, H.H., 1980. *Quaternary palaeoecology*. University Park Press.
- Biskaborn, B., Herzschuh, U., Bolshiyarov, D.Y., Dietze, E., Schwamborn, G., Diekmann, B., in press. Physico-chemical processes and cyclic depositional events in thermokarst lakes of the NE Siberian tundra. *Permafrost and Periglacial Processes*.

- Biskaborn, B.K., 2012b. Holocene Environmental Variability inferred from Lake Diatoms and Sediment Geochemistry in northeastern Siberia, Russia (Ph.D. thesis).
- Biskaborn, B.K., Herzschuh, U., Bolshiyarov, D., Savelieva, L., Diekmann, B., 2012a. Environmental variability in northeastern Siberia during the last ~ 13,300 yr inferred from lake diatoms and sediment–geochemical parameters. *Palaeogeography, Palaeoclimatology, Palaeoecology* 329–330, 22–36.
- Blume, H.-P., Brümmer, G.W., Horn, R., Kandeler, E., Kögel-Knabner, I., Kretzschmar, R., Stahr, K., Wilke, B.-M., Scheffer, Schachtschabel, P., Welp, G., Thiele-Bruhn, S., 2009. Scheffer/Schachtschabel: Lehrbuch der Bodenkunde, 16. Aufl. ed. Spektrum Akademischer Verlag.
- Boike, J., Wille, C., Abnizova, A., 2008. Climatology and summer energy and water balance of polygonal tundra in the Lena River Delta, Siberia. *Journal of Geophysical Research* 113, G03025.
- Brenner, M., Whitmore, T.J., Curtis, J.H., Hodell, D.A., Schelske, C.L., 1999. Stable isotope ($\delta^{13}\text{C}$ and $\delta^{15}\text{N}$) signatures of sedimented organic matter as indicators of historic lake trophic state. *Journal of Paleolimnology* 22, 205–221.
- Brigham-Grette, J., 2001a. New perspectives on Beringian Quaternary paleogeography, stratigraphy, and glacial history. *Quaternary Science Reviews* 20, 15–24.
- Brigham-Grette, J., 2001b. New perspectives on Beringian Quaternary paleogeography, stratigraphy, and glacial history. *Quaternary Science Reviews* 20, 15–24.
- Bronk Ramsey, C., 2008. Radiocarbon dating: Revolutions in Understanding*. *Archaeometry* 50, 249–275.
- Burn, C.R., 2005. Lake-bottom thermal regimes, western Arctic coast, Canada. *Permafrost and Periglacial Processes* 16, 355–367.
- Burn, C.R., Smith, M.W., 1990. Development of thermokarst lakes during the holocene at sites near Mayo, Yukon territory. *Permafrost and Periglacial Processes* 1, 161–175.
- CAVM Team, 2003. Circumpolar Arctic Vegetation Map, (1:7,500,000 scale), Conservation of Arctic Flora and Fauna (CAFF) Map No. 1. U.S. Fish and Wildlife Service, Anchorage, Alaska. URL <http://www.arcticatlas.org/maps/themes/cp/> (accessed 8.22.12).
- Craig, H., 1957. Isotopic standards for carbon and oxygen and correction factors for mass-spectrometric analysis of carbon dioxide. *Geochimica et Cosmochimica Acta* 12, 133–149.
- Czerepanov, S.K., 2007. *Vascular Plants of Russia and Adjacent States (the Former USSR)*. Cambridge University Press.
- Czudek, T., Demek, J., 1970. Thermokarst in Siberia and its influence on the development of lowland relief. *Quaternary Research* 1, 103–120.
- Czudek, T., Demek, J., 1973. Die Reliefentwicklung während der Dauerfrostbodendegradation. *Academia*.
- Danzeglocke, U., Jöris, O., Werninger, B., 2012. CalPal 2007 - Radiocarbon Calibration Online. URL <http://www.calpal-online.de/> (accessed 9.21.12).
- Davies, J.L., 1969. *Landforms of cold climates, An introduction to systematic geomorphology*; 3. M.I.T. Press, Cambridge, Mass.
- Dierßen, K., 1996. *Vegetation Nordeuropas*. Ulmer Stuttgart.
- Dietze, E., Hartmann, K., Diekmann, B., Ijmker, J., Lehmkuhl, F., Opitz, S., Stauch, G., Wünnemann, B., Borchers, A., 2012. An end-member algorithm for deciphering modern detrital processes from lake sediments of Lake Donggi Cona, NE Tibetan Plateau, China. *Sedimentary Geology* 243–244, 169–180.
- Drachev, S.S., Kaul, N., Beliaev, V.N., 2003. Eurasia spreading basin to Laptev Shelf

- transition: structural pattern and heat flow. *Geophysical Journal International* 152, 688–698.
- Dzurec, R.S., Boutton, T.W., Caldwell, M.M., Smith, B.N., 1985. Carbon isotope ratios of soil organic matter and their use in assessing community composition changes in Curlew Valley, Utah. *Oecologia* 66, 17–24.
- Ehleringer, J.R., Cerling, T.E., Helliker, B.R., 1997. C4 photosynthesis, atmospheric CO₂, and climate. *Oecologia* 112, 285–299.
- Einsele, G., 2000. *Sedimentary basins: evolution, facies, and sediment budget*. Springer.
- FAO, 2006. World reference base for soil resources 2006 - A framework for international classification, correlation and communication. URL <ftp://ftp.fao.org/docrep/fao/009/a0510e/a0510e00.pdf>
- FAO, n.d. Brief Guide to Koeppen Climate Classification System. Food and Agriculture Organization of the United Nations (FAO). URL <http://www.fao.org/sd/EIdirect/climate/EIsp0066.htm> (accessed 7.15.12).
- Folk, R.L., 1966. A Review of Grain-Size Parameters. *Sedimentology* 6, 73–93.
- Franz, H.-J., 1973. *Physische Geographie der Sowjetunion*. Hermann Haack.
- French, H., 2007. *The Periglacial Environment*, 3rd ed. Wiley.
- GeoFUSE, 2012. GeoFUSE Search & Discovery Platform. URL <http://geofuse.geoeye.com/landing/Default.aspx> (accessed 11.21.12).
- Godwin, H., 1962. Half-life of Radiocarbon. *Nature* 195, 984–984.
- Grosse, G., Schirrmeister, L., Kunitsky, V.V., Hubberten, H.W., 2005. The use of CORONA images in remote sensing of periglacial geomorphology: an illustration from the NE Siberian coast. *Permafrost and Periglacial Processes* 16, 163–172.
- Grosse, G., Schirrmeister, L., Malthus, T.J., 2006. Application of Landsat-7 satellite data and a DEM for the quantification of thermokarst-affected terrain types in the periglacial Lena-Anabar coastal lowland. *Polar Research* 25, 51–67.
- Grosse, G., Schirrmeister, L., Siegert, C., Kunitsky, V.V., Slagoda, E.A., Andreev, A.A., Dereviagn, A.Y., 2007. Geological and geomorphological evolution of a sedimentary periglacial landscape in northeast Siberia during the Late Quaternary. *Geomorphology* 86, 25–51.
- Guilderson, T.P., Reimer, P.J., Brown, T.A., 2005. The Boon and Bane of Radiocarbon Dating. *Science* 307, 362–364.
- Handbook elementar vario el III, 2001. *Elementar Analysensysteme GmbH*. Hanau.
- Handbook elementar vario max C, 2012. *Elementar Analysensysteme GmbH*. Hanau.
- Herzschuh, U., Bolshiyarov, D., Pstryakova, L., Boersma, M., Abramova, K., Zubrzycki, S., Biskaborn, B.K., Klemm, J., Vakhrameeva, P., 2009. Ecological state of permafrost lakes and their catchment along a North-South transect in north-central Yakutia: past and present., in: Boike Et Al., 2009. Russian-German Cooperation SYSTEM LAPTEV SEA: The Expedition Lena 2009. Reports on Polar and Marine Research, 600, 22-24.
- Hjulstrom, F., 1939. Transportation of Detritus by Moving Water. *Recent Marine Sediments* 142.
- Holland, M.M., Bitz, C.M., 2003. Polar amplification of climate change in coupled models. *Climate Dynamics* 21, 221–232.
- Hollander, D.J., McKenzie, J.A., 1991. CO₂ control on carbon-isotope fractionation during aqueous photosynthesis: A paleo-pCO₂ barometer. *Geology* 19, 929–932.
- Hopkins, D.M., 1949. Thaw lakes and thaw sinks in the Imuruk Lake area, Seward Peninsula, Alaska. *The Journal of Geology* 119–131.
- Hughes, M.K., Diaz, H.F., 1994. Was there a “medieval warm period”, and if so, where and

- when? *Climatic Change* 26, 109–142.
- Huh, Y., Edmond, J.M., 1999. The fluvial geochemistry of the rivers of Eastern Siberia: III. Tributaries of the Lena and Anabar draining the basement terrain of the Siberian Craton and the Trans-Baikal Highlands. *Geochimica et cosmochimica acta* 63, 967–987.
- Huissteden, J. van, Berrittella, C., Parmentier, F.J.W., Mi, Y., Maximov, T.C., Dolman, A.J., 2011. Methane emissions from permafrost thaw lakes limited by lake drainage. *Nature Climate Change* 1, 119–123.
- IPCC, 2007. Summary for Policymakers. Contribution of Working Groups I, II and III to the Fourth Assessment Report of the Intergovernmental Panel on Climate Change.
- ITIS, 2013. Integrated Taxonomic Information System. URL <http://www.itis.gov/> (accessed 1.31.13).
- Janssen, B.H., 1996. Nitrogen mineralization in relation to C:N ratio and decomposability of organic materials. *Plant and Soil* 181, 39–45.
- Jones, A., Stolbovay, V., Tarnocai, C., Broll, G., Spaargaren, O., Montanarella, L., others, 2010. Soil atlas of the Northern Circumpolar Region. European Commission.
- Katamura, F., Fukuda, M., Bosikov, N.P., Desyatkin, R.V., 2009. Charcoal records from thermokarst deposits in central Yakutia, eastern Siberia: Implications for forest fire history and thermokarst development. *Quaternary Research* 71, 36–40.
- Kaufman, D.S., 2009. An overview of late Holocene climate and environmental change inferred from Arctic lake sediment. *Journal of Paleolimnology* 41, 1–6.
- Kienast, F., Schirrmeyer, L., Siebert, C., Tarasov, P., 2005. Palaeobotanical evidence for warm summers in the East Siberian Arctic during the last cold stage. *Quaternary Research* 63, 283–300.
- Kienast, F., Siebert, C., Dereviagin, A., Mai, D.H., 2001. Climatic implications of Late Quaternary plant macrofossil assemblages from the Taymyr Peninsula, Siberia. *Global and Planetary Change* 31, 265–281.
- Kienast, F., Tarasov, P., Schirrmeyer, L., Grosse, G., Andreev, A.A., 2008. Continental climate in the East Siberian Arctic during the last interglacial: Implications from palaeobotanical records. *Global and Planetary Change* 60, 535–562.
- Kienast, F., Wetterich, S., Kuzmina, S., Schirrmeyer, L., Andreev, A.A., Tarasov, P., Nazarova, L., Kossler, A., Frolova, L., Kunitsky, V.V., 2011. Paleontological records indicate the occurrence of open woodlands in a dry inland climate at the present-day Arctic coast in western Beringia during the Last Interglacial. *Quaternary Science Reviews* 30, 2134–2159.
- Knoll, A.H., Grotzinger, J.P., Kaufman, A.J., Kolosov, P., 1995. Integrated approaches to terminal Proterozoic stratigraphy: an example from the Olenek Uplift, northeastern Siberia. *Precambrian Research* 73, 251–270.
- Koronovsky, N., 2003. Tectonics and Geology, in: Shahgedanova, M. (Ed.), *The Physical Geography of Northern Eurasia*. Oxford University Press, USA, pp. 1–35.
- Kottek, M., Grieser, J., Beck, C., Rudolf, B., Rubel, F., 2006. World map of the Köppen-Geiger climate classification updated. *Meteorologische Zeitschrift* 15, 259–263.
- Krasnoborov, I.M., Malyshev, L.I., 2003. *Flora of Siberia*. Volume 5: Salicaceae-Amaranthaceae. Science Publishers, Inc.
- Kremenetski, C.V., Sulerzhitsky, L.D., Hantemirov, R., 1998. Holocene history of the northern range limits of some trees and shrubs in Russia. *Arctic and Alpine Research* 317–333.
- Krull, E.S., Retallack, G.J., 2000. $\delta^{13}\text{C}$ depth profiles from paleosols across the Permian-Triassic boundary: Evidence for methane release. *Geological Society of America*

- Bulletin 112, 1459–1472.
- Kunitsky, V., Schirrmeister, L., Grosse, G., Kienast, F., 2002. Snow patches in nival landscapes and their role for the Ice Complex formation in the Laptev Sea coastal lowlands. *Polarforschung* 70, 53–67.
- Lantuit, H., Grigoriev, M.N., Grosse, G., Ulrich, M., 2007. Studies of oriented lakes and thermokarst depressions, in: L. Schirrmeister, D. Wagner, M. N. Grigoriev & D.Yu. Bolshiyonov (Eds.), *Russian–German Cooperation SYSTEM LAPTEV SEA — The Expedition Lena— 2005, Reports on Polar and Marine Research*, Vol. 550.
- Last, W.M., 2002a. Textural Analysis of Lake Sediments, in: Last, W.M., Smol, J.P. (Eds.), *Tracking Environmental Change Using Lake Sediments, Developments in Paleoenvironmental Research*. Springer Netherlands, pp. 41–81.
- Last, W.M., 2002b. Mineralogical Analysis of Lake Sediments, in: Last, W.M., Smol, J.P. (Eds.), *Tracking Environmental Change Using Lake Sediments, Developments in Paleoenvironmental Research*. Springer Netherlands, pp. 143–187.
- Lee Black, D., McQuay, M.Q., Bonin, M.P., 1996. Laser-based techniques for particle-size measurement: A review of sizing methods and their industrial applications. *Progress in Energy and Combustion Science* 22, 267–306.
- MacDonald, G.M., Velichko, A.A., Kremenetski, C.V., Borisova, O.K., Goleva, A.A., Andreev, A.A., Cwynar, L.C., Riding, R.T., Forman, S.L., Edwards, T.W.D., others, 2000. Holocene treeline history and climate change across northern Eurasia. *Quaternary Research* 53, 302–311.
- Mackay, J.R., 1974. Ice-Wedge Cracks, Garry Island, Northwest Territories. *Canadian Journal of Earth Sciences* 11, 1366–1383.
- Markov, F.G., 1974. Geological map of the USSR (new series). R-(50) -52 (Tixi). Map of pre-Quaternary formations (in Russian).
- Matveyeva, N.V., 1994. Floristic classification and ecology of tundra vegetation of the Taymyr Peninsula, northern Siberia. *Journal of Vegetation Science* 5, 813–828.
- Melillo, J.M., Aber, J.D., Linkins, A.E., Ricca, A., Fry, B., Nadelhoffer, K.J., 1989. Carbon and nitrogen dynamics along the decay continuum: plant litter to soil organic matter. *Plant and soil* 115, 189–198.
- Meyers, P.A., 1994. Preservation of elemental and isotopic source identification of sedimentary organic matter. *Chemical Geology* 114, 289–302.
- Meyers, P.A., 2003. Applications of organic geochemistry to paleolimnological reconstructions: a summary of examples from the Laurentian Great Lakes. *Organic geochemistry* 34, 261–289.
- Meyers, P.A., Lallier-Verges, E., 1999. Lacustrine sedimentary organic matter records of Late Quaternary paleoclimates. *Journal of Paleolimnology* 21, 345–372.
- Meyers, P.A., Teranes, J.L., 2002. Sediment Organic Matter, in: Last, W.M., Smol, J.P. (Eds.), *Tracking Environmental Change Using Lake Sediments, Developments in Paleoenvironmental Research*. Springer Netherlands, pp. 239–269.
- Miller, G.H., Brigham-Grette, J., Alley, R.B., Anderson, L., Bauch, H.A., Douglas, M.S.V., Edwards, M.E., Elias, S.A., Finney, B.P., Fitzpatrick, J.J., Funder, S.V., Herbert, T.D., Hinzman, L.D., Kaufman, D.S., MacDonald, G.M., Polyak, L., Robock, A., Serreze, M.C., Smol, J.P., Spielhagen, R., White, J.W.C., Wolfe, A.P., Wolff, E.W., 2010a. Temperature and precipitation history of the Arctic. *Quaternary Science Reviews* 29, 1679–1715.
- Mock, C.J., Bartlein, P.J., Anderson, P.M., 1998. Atmospheric circulation patterns and spatial climatic variations in Beringia. *International Journal of Climatology* 18, 1085–1104.

- Morgenstern, A., 2005. GIS-basierte Analyse der Morphometrie und räumlichen Verteilung von Seen im Lena-Delta, NO-Sibirien, Universität Potsdam (in German).
- Morgenstern, A., 2012. Thermokarst and thermal erosion: Degradation of Siberian ice-rich permafrost. Ph.D. thesis.
- Morgenstern, A., Grosse, G., Günther, F., Fedorova, I., Schirrmeister, L., 2011. Spatial analyses of thermokarst lakes and basins in Yedoma landscapes of the Lena Delta. *The Cryosphere* 5, 849–867.
- Morgenstern, A., Grosse, G., Schirrmeister, L., 2008. Genetic, morphological, and statistical characterization of lakes in the permafrost-dominated Lena Delta.
- Müller, S., Tarasov, P.E., Andreev, A., Diekmann, B., 2009. Late Glacial to Holocene environments in the present-day coldest region of the Northern Hemisphere inferred from a pollen record of Lake Billyakh, Verkhoyansk Mts., NE Siberia. *Climate of the Past* 5 73–84.
- Murton, J.B., 2001. Thermokarst sediments and sedimentary structures, Tuktoyaktuk Coastlands, western Arctic Canada. *Global and Planetary Change* 28, 175–192.
- Nesbitt, H.W., Fedo, C.M., Young, G.M., 1997. Quartz and feldspar stability, steady and non-steady-state weathering, and petrogenesis of siliciclastic sands and muds. *The Journal of Geology* 105, 173–192.
- NOAA, n.d. NOAA Solar Calculators. URL <http://www.esrl.noaa.gov/gmd/grad/solcalc/> (accessed 7.15.12).
- O’Leary, M.H., 1988. Carbon isotopes in photosynthesis. *Bioscience* 38, 328–336.
- Olsen, J., Anderson, N.J., Leng, M.J., 2013. Limnological controls on stable isotope records of late-Holocene palaeoenvironment change in SW Greenland: a paired lake study. *Quaternary Science Reviews*.
- Osborne, C.P., Beerling, D.J., 2006. Nature’s green revolution: the remarkable evolutionary rise of C4 plants. *Philosophical Transactions of the Royal Society of London, Series B, Biological Sciences* 361, 173–194.
- Peterson, B.J., Fry, B., 1987. Stable isotopes in ecosystem studies. *Annual review of ecology and systematics* 18, 293–320.
- Petschick, R., 2012. MacDiff - The user-friendly X-ray powder diffractometry analysis tool for Macintosh computers.. URL <http://www.geol-pal.uni-frankfurt.de/Staff/Homepages/Petschick/classicsoftware.html#MacDiff> (accessed 10.28.12).
- Pollozek, L., 2011. Temporal variability of permafrost formations in Northern Siberia based on Landsat data, Freie Universität Berlin (in German) (Bachelor’s thesis).
- Reimer, P.J., Baillie, M.G.L., Bard, E., Bayliss, A., Beck, J.W., Blackwell, P.G., Ramsey, C.B., Buck, C.E., Burr, G.S., Edwards, R.L., Friedrich, M., Grootes, P.M., Guilderson, T.P., Hajdas, I., Heaton, T.J., Hogg, A.G., Hughen, K.A., Kaiser, K.F., Kromer, B., McCormac, F.G., Manning, S.W., Reimer, R.W., Richards, D.A., Southon, J.R., Talamo, S., Turney, C.S.M., Plicht, J. van der, Weyhenmeyer, C.E., 2011. IntCal09 and Marine09 Radiocarbon Age Calibration Curves, 0-50,000 Years cal BP. *Radiocarbon* 51, 1111–1150.
- Rivas-Martínez, S., 1996. Climate diagrams, worldwide bioclimatic classification system. Phytosociological Research Center, Spain. Online database. URL <http://www.ucm.es/info/cif/> (accessed 9.28.12).
- Romanovskii, N.N., Hubberten, H.-W., Gavrillov, A.V., Tumskoy, V.E., Tipenko, G.S., Grigoriev, M.N., Siegert, C., 2000. Thermokarst and land–ocean interactions, Laptev sea region, Russia. *Permafrost and Periglacial Processes* 11, 137–152.
- ROSHYDROMET, n.d. World Weather Information Service - Tiksi. Russian Federal

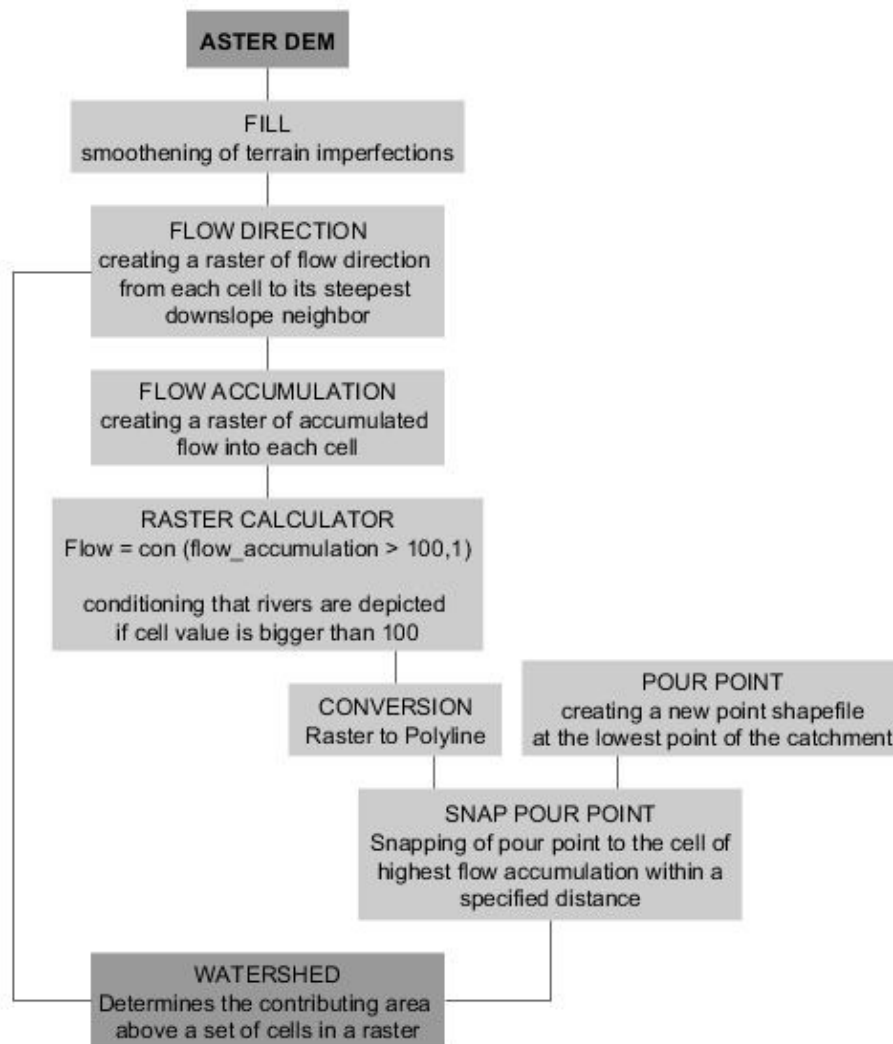
- Service for Hydrometeorology and Environmental Monitoring, Moscow. URL <http://worldweather.wmo.int/107/c01040.htm> (accessed 7.6.12).
- Santoro, M., Strozzi, T., 2012. Circumpolar digital elevation models > 55° N.
- Schirrmeyer, L., Grosse, G., Kunitsky, V., Magens, D., Meyer, H., Dereviagin, A., Kuznetsova, T., Andreev, A., Babiy, O., Kienast, F., others, 2008. Periglacial landscape evolution and environmental changes of Arctic lowland areas for the last 60 000 years (western Laptev Sea coast, Cape Mamontov Klyk). *Polar Research* 27, 249–272.
- Schirrmeyer, L., Grosse, G., Schwamborn, G., Andreev, A.A., Meyer, H., Kunitsky, V.V., Kuznetsova, T.V., Dorozhkina, M.V., Pavlova, E.Y., Bobrov, A.A., others, 2003. Late Quaternary history of the accumulation plain north of the Chekanovsky Ridge (Lena Delta, Russia): a multidisciplinary approach. *Polar Geography* 27, 277–319.
- Schirrmeyer, L., Kunitsky, V., Grosse, G., Wetterich, S., Meyer, H., Schwamborn, G., Babiy, O., Derevyagin, A., Siegert, C., 2011b. Sedimentary characteristics and origin of the Late Pleistocene Ice Complex on north-east Siberian Arctic coastal lowlands and islands—A review. *Quaternary International* 241, 3–25.
- Schirrmeyer, L., Kunitsky, V., Grosse, G., Wetterich, S., Meyer, H., Schwamborn, G., Babiy, O., Derevyagin, A., Siegert, C., 2011. Sedimentary characteristics and origin of the Late Pleistocene Ice Complex on north-east Siberian Arctic coastal lowlands and islands – A review. *Quaternary International* 241, 3–25.
- Schwamborn, G., Meyer, H., Fedorov, G., Schirrmeyer, L., Hubberten, H.W., 2006. Ground ice and slope sediments archiving late Quaternary paleoenvironment and paleoclimate signals at the margins of El'gygytgyn Impact Crater, NE Siberia. *Quaternary research* 66, 259–272.
- Schwamborn, G., Schirrmeyer, L., Frütsch, F., Diekmann, B., 2012. Quartz weathering in freeze-thaw cycles: experiment and application to the El'gygytgyn crater lake record for tracing Siberian permafrost history. *Geografiska Annaler: Series A, Physical Geography*.
- Serreze, M.C., Barry, R.G., 2011. Processes and impacts of Arctic amplification: A research synthesis. *Global and Planetary Change* 77, 85–96.
- Shahgedanova, M., 2003. Climate at Present and in the Historical Past, in: Shahgedanova, M. (Ed.), *The Physical Geography of Northern Eurasia*. Oxford University Press, Oxford, pp. 70–102.
- Shahgedanova, M., Kuznetsov, M., 2003. *The Arctic Environments*. Oxford University Press, Oxford.
- Smith, L.C., Sheng, Y., MacDonald, G.M., Hinzman, L.D., 2005. Disappearing Arctic Lakes. *Science* 308, 1429–1429.
- Smol, J.P., Douglas, M.S.V., 2007. Crossing the final ecological threshold in high Arctic ponds. *PNAS* 104, 12395–12397.
- Stuiver, M., Quay, P.D., 1981. Atmospheric ¹⁴C changes resulting from fossil fuel CO₂ release and cosmic ray flux variability. *Earth and Planetary Science Letters* 53, 349–362.
- Sukhinin, A.I., French, N.H.F., Kasischke, E.S., Hewson, J.H., Soja, A.J., Csiszar, I.A., Hyer, E.J., Loboda, T., Conard, S.G., Romasko, V.I., Pavlichenko, E.A., Miskiv, S.I., Slinkina, O.A., 2004. Burned Areas in Russia. Department of Geography, University of Maryland. URL <http://ftp.glcfc.umd.edu/data/burned/> (accessed 9.9.12).
- Thorn, C.E., Darmody, R.G., Dixon, J.C., Schlyter, P., 2001. The chemical weathering

- regime of Kärkevagge, arctic–alpine Sweden. *Geomorphology* 41, 37–52.
- Tishkov, A., 2003. Boreal Forests, in: Shahgedanova, M. (Ed.), *The Physical Geography of Northern Eurasia*. Oxford University Press, Oxford.
- UArctic Atlas, n.d. Arctic Boundaries. University of the Arctic. URL <http://www.uarctic.org/atlasmaplayer.aspx?m=642&amid=7246> (accessed 7.15.12).
- Ulrich, M., Grosse, G., Chabrillat, S., Schirrmeister, L., 2009. Spectral characterization of periglacial surfaces and geomorphological units in the Arctic Lena Delta using field spectrometry and remote sensing. *Remote Sensing of Environment* 113, 1220–1235.
- UNEP/GRID-Arendal, 1998. Permafrost distribution in the Arctic | UNEP/GRID-Arendal - Maps & Graphics library. URL http://www.grida.no/graphicslib/detail/permafrost-distribution-in-the-arctic_3823# (accessed 8.26.12).
- USDA, 1999. Soil Taxonomy - A Basic System of Soil Classification for Making and Interpreting Soil Surveys. URL ftp://ftp-fc.sc.egov.usda.gov/NSSC/Soil_Taxonomy/tax.pdf
- USGS, 2012. EarthExplorer. URL <http://earthexplorer.usgs.gov/> (accessed 11.21.12).
- Van Everdingen, R., 2005. Frozen Ground Glossary. Multi-language glossary of permafrost and related ground-ice terms. Boulder, CO: National Snow and Ice Data Center. URL <http://nsidc.org/fgdc/glossary/> (accessed 8.27.12).
- Van Geel, B., Aptroot, A., Baittinger, C., Birks, H.H., Bull, I.D., Cross, H.B., Evershed, R.P., Gravendeel, B., Kompanje, E.J.O., Kuperus, P., Mol, D., Nierop, K.G.J., Pals, J.P., Tikhonov, A.N., Van Reenen, G., Van Tienderen, P.H., 2008. The ecological implications of a Yakutian mammoth's last meal. *Quaternary Research* 69, 361–376.
- Van Wagoner, J.C., Mitchum, R.M., Campion, K.M., Rahmanian, V.D., 1990. Siliciclastic sequence stratigraphy in well logs, cores, and outcrops.
- Verardo, D.J., Froelich, P.N., McIntyre, A., 1990. Determination of organic carbon and nitrogen in marine sediments using the Carlo Erba NA-1500 analyzer. *Deep Sea Research Part A. Oceanographic Research Papers* 37, 157–165.
- Vogt, C., 2009. Data report: semiquantitative determination of detrital input to ACEX sites based on bulk sample X-ray diffraction data, in: *Proc. IODP | Volume*. p. 2.
- Walker, H.J., Harris, M.K., 1976. Perched ponds: An arctic variety. *Arctic* 223–238.
- Walter, K.M., Zimov, S.A., Chanton, J.P., Verbyla, D., Chapin, F.S., 2006. Methane bubbling from Siberian thaw lakes as a positive feedback to climate warming. *Nature* 443, 71–75.
- Washburn, A.L., 1979. *Geocryology: a survey of periglacial processes and environments*, 2nd ed. ed. Edward Arnold, London.
- Weise, O.R., 1983. *Das Periglazial*. Gebr. Borntraeger.
- Weninger, B., Jöris, O., 2008. A 14C age calibration curve for the last 60 ka: the Greenland-Hulu U/Th timescale and its impact on understanding the Middle to Upper Paleolithic transition in Western Eurasia. *Journal of Human Evolution* 55, 772–781.
- Werner, K., Tarasov, P.E., Andreev, A.A., Müller, S., Kienast, F., Zech, M., Zech, W., Diekmann, B., Werner, K., Tarasov, P.E., Andreev, A.A., Müller, S., Kienast, F., Zech, M., Zech, W., Diekmann, B., 2010. A 12.5-kyr history of vegetation dynamics and mire development with evidence of Younger Dryas larch presence in the Verkhoyansk Mountains, East Siberia, Russia, A 12.5-kyr history of vegetation dynamics and mire development with evidence of Younger Dryas larch presence in the Verkhoyansk Mountains, East Siberia, Russia. *Boreas*, *Boreas* 39, 39, 56, 56–68,

- 68.
- Wetterich, S., Kuzmina, S., Andreev, A.A., Kienast, F., Meyer, H., Schirrmeister, L., Kuznetsova, T., Sierralta, M., 2008. Palaeoenvironmental dynamics inferred from late Quaternary permafrost deposits on Kurungnakh Island, Lena Delta, northeast Siberia, Russia. *Quaternary Science Reviews* 27, 1523–1540.
- White, J.W.C., Alley, R.B., Brigham-Grette, J., Fitzpatrick, J.J., Jennings, A.E., Johnsen, S.J., Miller, G.H., Steven Nerem, R., Polyak, L., 2010. Past rates of climate change in the Arctic. *Quaternary Science Reviews* 29, 1716–1727.
- Wielgolaski, F.E., Goodall, D.W., 1997. Polar and alpine tundra. Elsevier.
- Wolfe, B.B., Edwards, T.W.D., Aravena, R., 1999. Changes in carbon and nitrogen cycling during tree-line retreat recorded in the isotopic content of lacustrine organic matter, western Taimyr Peninsula, Russia. *The Holocene* 9, 215–222.
- Wolter, J., 2010. Late Holocene development of a polygon mire in NW Yakutia inferred from plant macrofossil and lithological analyses (Diploma thesis).
- Zamotaev, I., 2003. Soils, in: Shahgedanova, M. (Ed.), *The Physical Geography of Northern Eurasia*. Oxford University Press, Oxford.
- Zazula, G.D., Froese, D.G., Elias, S.A., Kuzmina, S., Mathewes, R.W., 2007. Arctic ground squirrels of the mammoth-steppe: paleoecology of Late Pleistocene middens (~24 000–29 450 14C yr BP), Yukon Territory, Canada. *Quaternary Science Reviews* 26, 979–1003.
- Zhang, T., Barry, R.G., Knowles, K., Heginbottom, J.A., Brown, J., 1999. Statistics and characteristics of permafrost and ground-ice distribution in the Northern Hemisphere 1. *Polar Geography* 23, 132–154.
- Zimov, S.A., Schuur, E.A.G., Chapin, F.S., 2006. Permafrost and the Global Carbon Budget. *Science* 312, 1612–1613.

Appendix

Determination of the lake and river catchments using ArcGIS 10.1



Explanations derived from the ESRI ArcGIS online help (<http://resources.arcgis.com/en/help/>, accessed: 15th February 2013)

ASTER DEM data derived from: <http://earthexplorer.usgs.gov/>, accessed at 10th November 2012

Water content, grain size, and mineralogy

Depth (cm)	Water content (wt-%)	Mean grain size (μm)	Clay (vol-%)	Silt (vol-%)	Sand (vol-%)	Grain size sorting (Φ scale)	Grain size skewness	Quartz	Anorthite	Illite
								(1.82 Å) vs. TI	(3.195 Å) vs. TI	(9.997 Å) vs. TI
5-10	51.79	9.30	16.01	74.46	9.53	2.02	0.05	0.549	0.434	0.017
15-20	47.14	14.19	13.73	64.17	22.10	2.42	-0.07	0.556	0.417	0.027
25-30	43.54	10.62	17.06	65.71	17.23	2.39	-0.30	0.556	0.421	0.023
35-40	30.10	7.45	23.75	58.54	17.71	2.44	-0.58	0.546	0.398	0.057
45-50	29.50	5.70	26.46	62.95	10.59	2.16	-0.65	0.539	0.411	0.050
55-60	29.18	5.71	26.25	61.60	12.15	2.22	-0.77	0.522	0.438	0.039
65-70	32.43	7.87	23.21	60.44	16.35	2.39	-0.38	0.487	0.473	0.040
75-80	33.81	6.70	25.41	60.97	13.62	2.32	-0.52	0.520	0.422	0.059
85-90	31.64	6.53	24.72	63.29	11.99	2.28	-0.62	0.511	0.427	0.062
95-100	28.83	8.05	21.04	67.54	11.42	2.21	-0.20	0.475	0.480	0.045
105-110	21.80	23.90	11.82	50.55	37.63	2.25	0.99	0.296	0.684	0.020
115-120	24.20	16.05	15.05	55.37	29.58	2.43	0.34	0.327	0.645	0.029
125-130	21.04	15.58	15.49	52.55	31.96	2.50	0.26	0.393	0.588	0.019
135-140	21.56	14.43	17.01	53.73	29.26	2.49	0.25	0.387	0.592	0.021
145-150	17.12	15.15	14.99	53.57	31.44	2.51	0.16	0.336	0.640	0.023
155-160	16.65	13.70	16.73	54.17	29.10	2.51	0.11	0.296	0.683	0.021
165-170	16.39	15.62	15.70	52.88	31.42	2.48	0.27	0.345	0.631	0.024
175-180	18.40	15.12	16.78	52.68	30.54	2.51	0.26	0.333	0.640	0.027
185-190	20.95	10.36	20.42	57.63	21.95	2.50	-0.14	0.344	0.625	0.032
195-200	19.42	10.82	19.30	58.44	22.26	2.46	-0.07	0.243	0.729	0.028
205-210	18.99	9.36	22.05	58.49	19.46	2.51	-0.26	0.390	0.566	0.044
215-220	20.32	8.28	20.85	64.45	14.70	2.31	-0.29	0.375	0.591	0.034
225-230	18.16	23.67	14.77	40.25	44.98	2.86	0.30	0.431	0.548	0.021
235-240	21.16	17.87	16.54	46.26	37.20	2.64	0.32	0.360	0.620	0.020
245-250	25.43	14.36	17.17	54.73	28.10	2.52	0.20	0.388	0.582	0.031
255-260	18.43	14.92	13.71	58.21	28.08	2.40	0.18	0.326	0.649	0.025
265-270	24.50	9.59	19.96	61.67	18.37	2.36	-0.11	0.380	0.596	0.024
275-280	22.69	15.61	15.55	52.00	32.45	2.53	0.21	0.291	0.688	0.021
285-290	25.73	32.30	8.99	43.39	47.62	2.22	1.10	0.310	0.674	0.015
295-300	22.91	15.83	16.10	52.41	31.49	2.55	0.22	0.318	0.664	0.018
305-310	20.40	20.51	14.49	50.61	34.90	2.59	0.34	0.371	0.603	0.026
315-320	23.55	19.37	12.97	49.60	37.43	2.47	0.43	0.323	0.655	0.022
325-330	21.05	20.43	14.21	48.00	37.79	2.64	0.30	0.275	0.704	0.021
335-340	20.69	21.67	11.36	59.78	28.86	2.20	0.83	0.295	0.680	0.025
345-350	20.03	18.79	15.97	49.22	34.81	2.57	0.44	0.305	0.672	0.023

CNS, TOC, and $\delta^{13}\text{C}$

Depth (cm)	C (wt-%)	N (wt-%)	S (wt-%)	TOC (wt-%)	TIC (wt-%)	Carbonates (wt-%)	TOC/N _{ATOMIC}	$\delta^{13}\text{C}$ vs. PDB
5-10	29.83	1.43	0.33	28.75	1.08	9.01	23.42	-28
15-20	24.81	1.16	0.27	23.80	1.01	8.41	23.98	-28.40
25-30	21.04	1.08	0.23	20.16	0.88	7.31	21.88	-28.23
35-40	4.06	0.32	0.17	3.27	0.79	6.60	11.85	-29.76
45-50	3.87	0.33	0.17	3.21	0.66	5.48	11.22	-30.37
55-60	3.75	0.33	0.17	3.15	0.61	5.05	11.23	-31.40
65-70	3.99	0.31	0.19	3.22	0.77	6.42	11.93	-30.67
75-80	2.57	0.25	0.18	2.36	0.21	1.73	11.02	-29.77
85-90	2.46	0.24	0.17	2.26	0.20	1.64	11.18	-29.29
95-100	2.07	0.19	0.18	1.86	0.21	1.74	11.52	-27.14
105-110	1.33	0.10	0.11	1.17	0.16	1.35	13.35	-26.66
115-120	2.00	0.14	0.11	1.82	0.17	1.44	15.44	-27.00
125-130	1.37	0.11	0.12	1.23	0.13	1.12	13.04	-26.78
135-140	1.89	0.14	0.13	1.77	0.12	1.01	14.89	-27.27
145-150	0.99	0.09	0.11	0.83	0.16	1.31	11.00	-25.66
155-160	1.07	0.09	0.10	0.94	0.13	1.11	12.16	-26.28
165-170	1.20	0.11	0.10	1.06	0.14	1.16	11.56	-26.33
175-180	1.42	0.11	0.09	1.28	0.14	1.18	13.35	-26.35
185-190	1.37	0.10	0.10	1.05	0.32	2.66	12.92	-25.20
195-200	1.34	0.09	0.11	1.04	0.31	2.56	12.87	-25.05
205-210	1.41	0.08	0.14	0.99	0.42	3.48	14.32	-24.72
215-220	1.59	0.09	0.16	1.08	0.51	4.26	13.39	-24.76
225-230	1.12	0.07	0.19	0.84	0.28	2.30	13.26	-25.82
235-240	0.92	0.07	0.13	0.70	0.23	1.88	11.95	-25.92
245-250	2.09	0.13	0.15	1.87	0.22	1.82	16.67	-27.13
255-260	1.17	0.08	0.11	0.99	0.18	1.50	14.67	-26.29
265-270	2.65	0.16	0.15	2.43	0.21	1.78	17.52	-27.48
275-280	1.84	0.12	0.11	1.62	0.22	1.85	16.38	-26.85
285-290	2.88	0.20	0.12	2.62	0.26	2.16	15.09	-27.80
295-300	1.92	0.11	0.12	1.76	0.16	1.33	18.97	-27.05
305-310	2.04	0.13	0.13	1.81	0.24	1.98	16.76	-27.16
315-320	2.81	0.18	0.11	2.63	0.18	1.48	16.95	-27.77
325-330	1.79	0.11	0.11	1.58	0.21	1.75	16.50	-27.00
335-340	1.39	0.10	0.09	1.15	0.24	1.99	13.72	-26.53
345-350	1.28	0.09	0.08	1.07	0.21	1.77	14.67	-26.39

Total plant macrofossil finds

Db (cm)	Plant taxa	Type of macrofossil (& number of finds, if more than one)
15-20	<i>Carex</i> sp. L.	archene (3)
55-60	Characeae	oospores (8)
65-70	<i>Potamogeton</i> cf. <i>vaginatus</i> Turcz.	fruit stone
95-100	<i>Carex</i> sp. L.	archene
105-110	<i>Alnus viridis</i> ssp. <i>fruticosa</i> (Rupr.) Nyman <i>Betula nana</i> L. <i>Betula</i> cf. <i>nana</i> L. Betulaceae <i>Carex</i> sect. <i>Phacocystis</i> Dumort. <i>Larix gmelinii</i> (Rupr.) Rupr. <i>Hippuris vulgaris</i> L.	catkin scale, nutlet (3) leaf (2) nutlet nutlet archene (2) needle (3) seed (2)
115-120	Betulaceae <i>Carex</i> sect. <i>Phacocystis</i> Dumort. <i>Larix gmelinii</i> (Rupr.) Rupr, short shoot <i>Salix</i> sp. L.	nutlet archene seed (2), needle bud
135-140	Betulaceae	nutlet
165-170	<i>Carex</i> sect. <i>Phacocystis</i> Dumort. <i>Eriophorum</i> sp. L. <i>Salix</i> sp. L.	archene archene bud
175-180	<i>Carex</i> sect. <i>Phacocystis</i> Dumort. <i>Cerastium</i> cf. <i>arvense</i> L. <i>Potentilla</i> cf. <i>stipularis</i> L.	archene (2) seed nutlet
195-200	<i>Eriophorum brachyantherum</i> Trautv. & C.A. Mey. <i>Potentilla</i> cf. <i>nivea</i> L. <i>Larix gmelinii</i> (Rupr.) Rupr	archene nutlet seed
205-210	<i>Salix</i> sp. L.	bud (2)
225-230	<i>Larix gmelinii</i> (Rupr.) Rupr. cf. <i>Potentilla</i> sp. L.	needle nutlet
235-240	<i>Larix gmelinii</i> (Rupr.) Rupr <i>Potamogeton filiformis</i> Pers. <i>Potentilla arenosa</i> , (Turcz.) Juz. <i>Potentilla</i> cf. <i>hyarctica</i> Malte <i>Salix</i> sp. L. charcoal pieces	needle (3), seed (3) fruit stone nutlet nutlet bud (2)
245-250	Betulaceae <i>Carex</i> sp. L. cf. <i>Dryas octpetala</i> L. <i>Larix gmelinii</i> (Rupr.) Rupr	nutlet archene leaf fragments (2) needle (6), fascicle (8),

	<i>Potentilla</i> cf. <i>stipularis</i> L. <i>Vaccinium</i> cf. <i>vitis-idaea</i> L.	seed (2) nutlet berry –
255-260	<i>Carex</i> sp. L. <i>Eriophorum brachyantherum</i> Trautv. & C.A. Mey. <i>Larix gmelinii</i> (Rupr.) Rupr.	archene (2) archene needle (4)
265-270	<i>Betula nana</i> L. <i>Carex</i> sect. <i>Phacocystis</i> Dumort. <i>Larix gmelinii</i> (Rupr.) Rupr. fossil rodent excrements	nutlet (2) archene (2) needle (3) (3)
275-280	Betulaceae <i>Carex</i> sect. <i>Phacocystis</i> Dumort. <i>Eriophorum brachyantherum</i> Trautv. & C.A. Mey. <i>Larix gmelinii</i> (Rupr.) Rupr.	nutlet archene archene needle (3)
285-290	<i>Alnus viridis</i> ssp. <i>fruticosa</i> (Rupr.) Nyman <i>Betula</i> cf. <i>pendula</i> Roth <i>Carex</i> sect. <i>Phacocystis</i> Dumort. <i>Epilobium palustre</i> L. <i>Larix gmelinii</i> (Rupr.) Rupr. <i>Potentilla</i> cf. <i>hyarctica</i> Malte cf. <i>Trichophorum uniflorum</i> (Trautv.) Malyshev & Lukitsch. charcoal remain	nutlet nutlet (2), leaf fragment archene seed needles (5) nutlet (2) nutlet -
295-300	<i>Alnus viridis</i> ssp. <i>fruticosa</i> (Rupr.) Nyman <i>Betula</i> cf. <i>pendula</i> Roth. Betulaceae cf. <i>Eriophorum brachyantherum</i> Trautv. & C.A. Mey. <i>Larix gmelinii</i> (Rupr.) Rupr, <i>Potentilla</i> cf. <i>arenosa</i> (Turcz.) Juz. <i>Vaccinium vitis-idaea</i> L.	nutlet catkin scale nutlet (2) archene cone, needles (15), seed nutlet leaf (2)
305-310	cf. <i>Arctous rubra</i> (Rehder & Wilson) Nakai <i>Carex</i> sect. <i>Phacocystis</i> Dumort. <i>Betula</i> cf. <i>pendula</i> Roth <i>Larix gmelinii</i> (Rupr.) Rupr. <i>Papaver</i> sect. <i>Scapiflora</i> Reichenb. <i>Potentilla</i> sp. L.	fruit-stone with remains of epicarp archene nutlet seed, short shoot, needles (12) seed nutlet
315-320	<i>Carex</i> sect. <i>Phacocystis</i> Dumort. <i>Larix gmelinii</i> (Rupr.) Rupr.	archene (3) needles (12), seeds (3)
325-330	<i>Betula</i> cf. <i>pendula</i> Roth <i>Carex</i> sect. <i>Phacocystis</i> Dumort.	nutlet (2) archene

	<i>Cerastium</i> cf. <i>arvense</i> L. <i>Eriophorum brachyantherum</i> Trautv. & C.A. Mey. <i>Larix gmelinii</i> (Rupr.) Rupr.	seed archene needle (6), short shoots (3)
335-340	Betulaceae <i>Carex</i> sect. <i>Phacocystis</i> Dumort. <i>Larix gmelinii</i> (Rupr.) Rupr. <i>Potentilla</i> cf. <i>arenosa</i> (Turcz.) Juz. Charcoal remains	nutlet archene (3) needle (3), seed nutlet (2)
345-350	<i>Larix gmelinii</i> (Rupr.) Rupr. cf. <i>Eriophorum brachyantherum</i> Trautv. & C.A. Mey.	needles (2) archene

Acknowledgements

I would like to show my gratitude to Prof. Bernhard Diekmann and Prof. Christoph Zielhofer for the kind support and the examination of my master's thesis. I owe many thanks to all members of the Lena 2009 and 2010 expeditions to Lake El'gene-Kyuele because of the tough fieldwork. The excavation of the outcrop, the collection and transport of sample material, the taking of photographs, etc. were essential for this study. My deepest gratitude goes to Boris Biskaborn for his tireless support, motivation, and criticism in methodical and thematic issues. I thank my AWI colleagues Ute Bastian and Christin Orfert for the kind support in the sedimentology laboratory, and Lutz Schönicke and Dr. Hanno Meyer in the isotope laboratory. Highly appreciated are the expertise and advice of Dr. Frank Kienast at the Senckenberg Research Station for Quaternary Palaeontology in Weimar, and Juliane Wolter at the AWI during the plant macrofossil analysis, Stefan Schimpf and Rita Fröhlking during the XRD measurement, and Aleksandra Mansfeld and Samuel Stettner during the GIS analyses. I further thank all reviewers of my thesis: Julia Jäger, Boris Radosavljevic, Caroline Noerling, and Boris Biskaborn. After all, I have spent a very pleasant and productive time in company of my mates at the AWI in Potsdam. Lastly, I would like to thank Luise Lützkendorf, who welcomed and hosted me when I first arrived in Potsdam.

большое спасибо!